Encapsulation of Hydrophobic Drugs Using Polymeric Micelles

Completed by :
Tamara Talakesh

First Supervisor :
Dr. Shirin Alexander

Submitted in partial fulfilment of the requirements for the degree of Master of Science in Medical Engineering by research

Swansea University

2026

Abstract (Summary)

Hydrophobic drugs, which are poorly soluble in water, present significant challenges in drug delivery due to their low bioavailability. Nanoparticles, such as micelles, have emerged as effective drug delivery vehicles that enhance the absorption efficiency of these drugs.

Micelles are spherical structures formed by amphiphilic molecules in aqueous environments. They have a hydrophobic core and a hydrophilic shell, making them ideal for encapsulating hydrophobic drugs. This encapsulation improves the solubility and stability of the drugs, facilitating better absorption and bioavailability. Advantages of Micelles: Enhanced Solubility, Controlled Release, and Targeted Delivery.

This project aims to enhance the delivery and efficacy of hydrophobic inflammatory drugs using polymeric micelles encapsulation. The encapsulation process involves dissolving the drugs and polymers in a suitable solvent, followed by self-assembly into micelles. By studying the effects of pH and temperature on drug release, the project seeks to optimize the conditions for controlled and targeted drug delivery, potentially improving therapeutic outcomes for patients.

The micelles will be tested in different pH environments to simulate conditions in various parts of the body, and the effect of temperature on drug release will be studied to understand how body temperature and potential fever conditions might influence drug delivery.

Declarations and Statements

This work has not previously been accepted in substance for any degree and is not being concurrently submitted in candidature for any degree.

Signed Date 02/08/2026
Tamara Talakesh

This work is the result of my own independent study/investigation, except where otherwise stated. Other sources are acknowledged by footnotes giving explicit references. A bibliography is appended.

Signed Date 02/08/2026
Tamara Talakesh

I hereby give my consent for my work, if relevant and accepted, to be available for photocopying and for inter-library loan, and for the title and summary to be made available to outside organisations.

Signed Date 02/08/2026
Tamara Talakesh

Swansea Universities' ethical procedures were followed in this work.

Signed Date 02/08/2026
Tamara Talakesh

Table of Contents

Acknowledgements

I would like to express my sincere gratitude to my supervisor, Dr. Shirin Alexander, for her continuous guidance, support, and encouragement throughout this project. Her expertise and constructive feedback were invaluable in shaping the direction and quality of this thesis.

I am deeply grateful to the staff and researchers at Swansea University who provided technical assistance, laboratory access, and insightful discussions during the experimental stages of this work.

My heartfelt thanks go to my family, specially my husband and my uncle, for their unwavering support, patience, and belief in me throughout my studies. Their encouragement has been essential to the completion of this thesis.

Finally, I would like to thank my friends and colleagues for their motivation, kindness, and companionship during this journey.

Definitions or Abbreviations

API — active pharmaceutical ingredient

ASDs — amorphous solid dispersions

AUC — area under the concentration–time curve

BCS Class II — Biopharmaceutics Classification System, Class II

CD — cyclodextrin

Cmax — maximum concentration

DLC — drug loading capacity

DLS — Dynamic Light Scattering

DMF — dimethylformamide

FDA — Food and Drug Administration

FTIR — Fourier Transform Infrared Spectroscopy

HPMC — hydroxypropyl methylcellulose

IB — isobutylene-based polymers

IB-alt-MA-g-PEG — isobutylene–maleic anhydride alternating copolymer grafted with polyethylene glycol

Ma — maleic acid-based

MA-alt-C_{18}-g-PEG — maleic anhydride–C18 alkyl alternating copolymer grafted with polyethylene glycol

PCL — polycaprolactone

PCS — photon correlation spectroscopy

PEG-g-LIR — PEG-grafted liquid isoprene rubber

PDI — polydispersity index

pHEMA — polyhydroxyethyl methacrylate

PIB — polyisobutylene

PLGA — poly(lactic-co-glycolic acid)

PVP — polyvinylpyrrolidone

PSD — particle size distribution

pKa — acid dissociation constant

SANS — Small-Angle Neutron Scattering

SEM/TEM — scanning electron microscopy / transmission electron microscopy

SLN — solid lipid nanoparticles

THF — tetrahydrofuran

Tmax — time to reach Cmax

UV-Vis — ultraviolet–visible spectroscopy

List of Figures

Chapter 1 – Introduction, Background, and Literature Review

Schemes in Chapter 1

Chapter 2 – Materials and Methods

Schemes in Chapter 2

Chapter 3 – Results and Discussion (Aggregation Structure of Grafted Polymers in Solution without Drug)

Chapter 4 – Results and Discussion (Encapsulation of hydrophobic drugs into core-shell grafted polymer structures)

Schemes in Chapter 4

Appendices

List of Tables

Chapter 1

Introduction, Background, and Literature Review

1.1 Introduction

The delivery of hydrophobic drugs remains a persistent challenge in pharmaceutical science due to their poor aqueous solubility and limited oral bioavailability. Traditional formulations often depend on organic solvents or lipid-based carriers, which can introduce toxicity and instability in physiological environments. To overcome these limitations, innovative approaches such as water-soluble prodrug technologies have been developed, offering enhanced pharmacokinetics and therapeutic efficacy while maintaining safety standards (2). Additionally, the spatial arrangement of hydrophobic and charged molecular regions plays a crucial role in determining the stability and binding behaviour of drug molecules. This molecular architecture influences how drugs interact with biological targets and how stable they remain under physiological conditions(3). Hydrophobic drugs tend to aggregate or precipitate in bodily fluids, making their delivery difficult. To address these limitations, micelles have emerged as promising drug carriers (4, 5).

Micelles are nanoscale, self-assembled structures formed by amphiphilic compounds that contain both hydrophilic (water-attracting) and hydrophobic (water-repelling) segments. In aqueous environments, these molecules spontaneously organise so that their hydrophobic parts cluster inward to form a core, while their hydrophilic parts face outward, creating a shell that interacts favourably with water (Figure 1.1)(6).

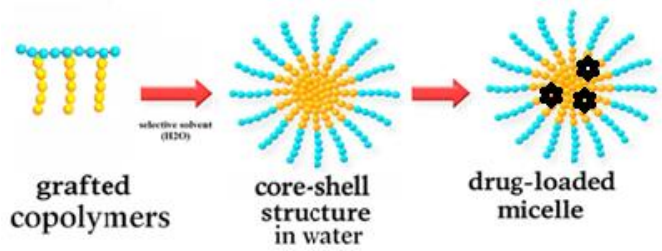

Fig 1.1: Schematic example of drug-loaded micelles[1].

These micelles possess a hydrophobic core capable of encapsulating poorly soluble drugs and a hydrophilic shell that ensures colloidal stability in aqueous media (Figure 1.2). This dual nature allows for improved solubilisation, protection from degradation, and controlled release of therapeutic agents(5, 7). The present study focuses on the design, formulation, and characterisation of micellar systems based on amphiphilic copolymers to enhance drug solubilisation and delivery efficiency.

[1] https://www.cd-bioparticles.net/technology/delivery-vehicles/nanoparticles-for-therapeutic-vehicles-polymer-micelles?srsltid=AfmBOopcLR8Rj6pmjjdhL-ziZb25yxHl1IQckWYgQB3D_HlmzDgeXvUi

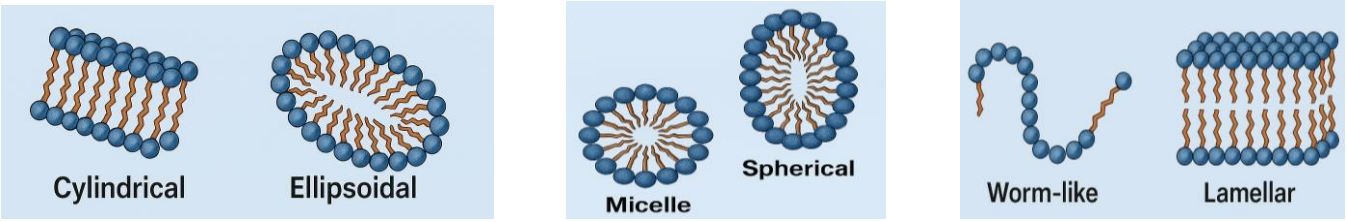

Fig 1.2: different micelle morphologies and their formation[2].

Amphiphilic copolymers such as maleic acid-based (Ma) and isobutylene-based polymers (IB), along with PEG-grafted liquid isoprene rubber (PEG-g-LIR), were selected for their ability to self-assemble into nanoscale structures suitable for encapsulating hydrophobic drugs like ibuprofen and Oxaprozin (scheme 1.1). These polymers exhibit a tunable hydrophilic–hydrophobic ratio, enabling precise modulation of solubility and drug–polymer interactions. Coupled with their biocompatibility and structural versatility, these characteristics make them particularly advantageous for advanced drug delivery applications. The study aims to optimise polymer composition, concentration, and environmental conditions such as pH and temperature to achieve stable, reproducible, and biocompatible micellar formulations.

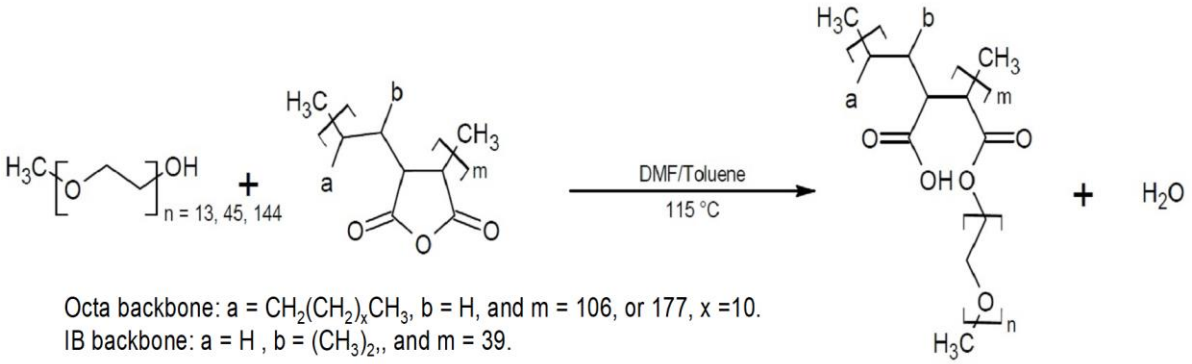

Scheme 1.1: Chemical structures of MA-alt-C_{18}-g-PEG and IB-alt-MA-g-PEG. Typical repeating unit ratios for MA-alt-C_{18}-g-PEG: m ≈ 106, n ≈ 45 (Mn ≈ 2000 g/mol). Reaction conditions: DMF/toluene, 115 °C.

[2] https://link.springer.com/chapter/10.1007/978-3-032-07376-1_1

Several factors, including polymer molecular weight, grafting density, drug-to-polymer ratio, and environmental conditions, influence the physicochemical behaviour of micelles. Understanding these parameters is crucial for designing effective drug delivery systems.

Analytical techniques such as Dynamic Light Scattering (DLS)[3] and Small-Angle Neutron Scattering (SANS)[4] are employed to assess micelle size, dispersity, structural integrity, and encapsulation efficiency. For grafted polymers, Fourier Transform Infrared Spectroscopy (FTIR) is an analytical technique used to identify chemical bonds and functional groups in a material by measuring how it absorbs infrared light. Each type of bond vibrates at a characteristic frequency, producing a unique spectrum that acts like a molecular fingerprint. This makes FTIR widely used for material characterisation, quality control, and confirming chemical composition. These methods provide critical insights into the stability and performance of self-assembled polymeric nanostructure formulations under various conditions. The integration of these techniques ensures a comprehensive evaluation of the micellar systems developed in this study.

This chapter provides a detailed overview of the scientific context, theoretical foundations, and prior research that inform the current investigation. By synthesising insights from the literature and aligning them with experimental objectives, the chapter establishes a robust framework for the development of advanced micellar drug delivery systems.

1.2 Background

1.2.1 Medical Role and Challenges of Ibuprofen and Oxaprozin

Ibuprofen

Ibuprofen ($C_{13}H_{18}O_2$; molecular weight ~206.28 g/mol) is a widely used non-steroidal anti-inflammatory drug (NSAID) with analgesic, antipyretic, and anti-inflammatory properties. It is commonly prescribed for conditions such as arthritis, musculoskeletal pain, and fever. Its mechanism of action involves inhibiting cyclooxygenase (COX-1 and COX-2) enzymes, reducing prostaglandin synthesis and thereby alleviating inflammation and pain (8). Despite its effectiveness, ibuprofen is classified as a Biopharmaceutics Classification System (BCS) Class II drug, characterised by low aqueous solubility and high membrane permeability (9). This means its absorption is primarily limited by its dissolution rate, which can lead to variable bioavailability and delayed therapeutic onset (scheme 1.2). Ibuprofen exhibits distinct chemical characteristics that influence its behaviour in polymer-based nanocapsulation systems. Structurally, it contains a carboxylic acid group and a hydrophobic aromatic ring with an isobutyl side chain, contributing to its amphiphilic nature and enabling interactions with both hydrophilic and

[3] Dynamic Light Scattering (DLS) is a mature biophysical technique that can accurately characterize the particle size in suspensions and emulsions.
[4] Small-Angle Neutron Scattering (SANS) is an experimental technique that uses elastic neutron scattering at small scattering angles to investigate the structure of various substances at a mesoscopic scale of about 1–100 nm.

a) **b)**

hydrophobic domains of polymers like LIR410-g-PEG. Its pKa of approximately 4.9 means that ibuprofen is predominantly deprotonated at physiological and basic pH, enhancing solubility and facilitating ionic interactions with cationic polymers(10). The molecule is chiral, existing as R- and S-enantiomers, with the S-form being pharmacologically active; notably, the R-enantiomer undergoes metabolic inversion in vivo to become the active S-form. In nanocarrier systems, ibuprofen's hydrophobic regions promote encapsulation within micellar cores, while its carboxyl group can form hydrogen bonds with polar polymer segments(11).

Scheme 1.2: Chemical structures of (a) ibuprofen and (b) oxaprozin. Structures are redrawn based on data from ChemSpider [5,6].

Analytical techniques such as FTIR and UV-Vis spectroscopy are commonly employed to characterise ibuprofen's incorporation and interactions within nanocarriers. FTIR reveals characteristic stretches for the carboxylic acid (~1700 cm^{-1}) and aromatic groups, while UV-Vis allows for quantification and monitoring of drug release. These chemical and spectroscopic properties make ibuprofen a valuable model compound for studying pH-dependent encapsulation efficiency, polymer-drug interactions, and release kinetics in advanced drug delivery systems(12).

To overcome these limitations, various formulation strategies have been developed to enhance ibuprofen's solubility and bioavailability. These include nanocarrier systems such as nanocrystals, nanosuspensions, and polymeric nanoparticles(13). Amorphous solid dispersions (ASDs) using polymers like hydroxypropyl methylcellulose (HPMC) and polyvinylpyrrolidone (PVP) have proven effective in maintaining supersaturation and improving dissolution rates(14). Additionally, recent studies by Patel et al. (2021) and Sharma et al. (2022) have demonstrated the potential of PEG-based micelles for sustained ibuprofen release, which not only improves solubility but also reduces gastric side effects and enhances patient compliance(15, 16). In addition to nanotechnology-based carriers, as reported by Petkar et al. (2011) the development of ibuprofen pro-drugs has emerged as an effective chemical strategy to mask the acidic carboxyl group, thereby minimizing direct gastric mucosal irritation. These advancements underscore the promise of polymeric nanocapsulation in optimising the pharmacokinetic and pharmacodynamics profiles of ibuprofen, thereby enhancing its clinical utility.

[5] https://www.chemspider.com/Chemical-Structure.3544.html
[6] https://www.chemspider.com/Chemical-Structure.4453.html

Oxaprozin

Oxaprozin ($C_{18}H_{15}NO_3$; molecular weight ~293.32 g/mol) is a non-steroidal anti-inflammatory drug (NSAID) from the propionic acid class, primarily used for the long-term management of rheumatoid arthritis and osteoarthritis. It features a long half-life of approximately 50–60 hours, allowing for once-daily dosing, and preferentially accumulates in synovial fluid, thereby enhancing its therapeutic effect in joint diseases (17). Like ibuprofen, oxaprozin is classified as a BCS Class II drug, indicating low aqueous solubility but high membrane permeability. However, due to its bulkier structure and the presence of an oxazole ring, oxaprozin is generally less soluble than ibuprofen, posing additional formulation challenges(9, 18).

Oxaprozin exhibits unique chemical properties that influence its behaviour in polymer-based drug delivery systems. Structurally, it contains a carboxylic acid group and a biphenyl moiety, which contribute to its hydrophobic nature and enable strong interactions with lipid-based carriers and hydrophobic polymer domains(19, 20). Its pKa is approximately 4.3, meaning it exists largely in its ionised form at physiological pH, which enhances solubility and facilitates electrostatic interactions with cationic polymers. Oxaprozin binds extensively to plasma albumin (≥99.5%), and its pharmacokinetics are influenced by competitive binding with other drugs and endogenous ligands(21). In nanocarrier systems, oxaprozin has shown high encapsulation efficiency (>95%) and controlled release behaviour, particularly in pH-sensitive hydrogels and lipid nanoparticles, where release is minimised in gastric conditions and enhanced in intestinal environments(22, 23). FTIR analysis confirms successful incorporation into polymer matrices, with characteristic carboxylic acid and aromatic stretches, while UV-Vis spectroscopy is used for quantification and release profiling. Notably, oxaprozin-loaded hydrogels maintain pH and temperature responsiveness, though drug loading slightly reduces swelling capacity. These properties make oxaprozin a valuable candidate for site-specific, controlled drug delivery systems, especially in formulations targeting inflammatory conditions with reduced gastrointestinal side effects(24).

To overcome oxaprozin's limited solubility and bioavailability, various nanocapsulation strategies have been explored, including solid lipid nanoparticles (SLNs), polymeric nanoparticles, and cyclodextrin inclusion complexes(25, 26). These approaches have demonstrated enhanced anti-inflammatory activity, improved pharmacokinetic profiles, and more consistent drug absorption(27). PEGylated nanoparticles have shown promise in targeting inflamed tissues, thereby maximising therapeutic efficacy while minimising systemic exposure. Studies by Gupta et al. (2020) and Mehra have demonstrated the feasibility of using PEG and maleic acid-based polymers for oxaprozin delivery, with favourable outcomes in preclinical models(28, 29). These findings underscore the importance of polymeric nanocapsulation in addressing the formulation challenges associated with oxaprozin and enhancing its therapeutic potential(30).

These two drugs are known for their effectiveness in managing pain and inflammation. However, their therapeutic potential is often limited by poor aqueous solubility, which restricts absorption and bioavailability when administered orally. This poses a significant challenge in pharmaceutical formulation, as conventional delivery systems frequently rely on organic solvents or lipid-based carriers

that may compromise safety and stability. This study aims to explore alternative strategies to improve and enhance the solubility and delivery of these hydrophobic drugs, paving the way for safer and more effective therapeutic options.

1.3 Solutions to Solubility Challenges and Their Applicability

Enhancing the solubility of poorly water-soluble drugs, particularly those classified as BCS Class II, remains a critical challenge in pharmaceutical formulation(31). Over the past few decades, numerous strategies have been developed (Figure 1.3) to address this limitation, including polymeric micelles, solid dispersions, lipid-based carriers, and nanoparticle systems(32, 33). Although these approaches differ in their structural design and delivery mechanisms, they share fundamental chemical principles aimed at improving drug solubilisation.

Fig 1.3: Nanostructured Drug Delivery Platforms for Solubility Enhancement(32, 33).

Most notably, these methods exploit hydrophobic interactions, hydrogen bonding, and amphiphilic carriers to create a favourable microenvironment that stabilises the drug in a dispersed or molecularly mixed state(34). Improving solubility is essential because it directly influences bioavailability, which refers to the proportion of an administered drug that reaches the systemic circulation in an active form. For BCS Class II drugs, bioavailability is primarily limited by the dissolution rate rather than membrane permeability; therefore, strategies that enhance solubility and dissolution can significantly improve therapeutic efficacy(34, 35).

1.3.1. Nanotechnology-Based Formulations

SLNs have emerged as promising nanotechnology-based drug delivery systems designed to overcome the limitations of poorly water-soluble drugs, such as ibuprofen and oxaprozin. These formulations primarily consist of the drug itself, reduced to nanometer-scale particles, without necessarily requiring additional solubilising agents. The dramatic reduction in particle size increases the surface area and dissolution rate, which enhances apparent solubility and, consequently, bioavailability. This significantly increases the surface area available for dissolution, thereby enhancing solubility and absorption. The particle size of nanocrystals and SLNs typically ranges from 50 to 1000 nm and is commonly determined using techniques such as DLS, photon correlation spectroscopy (PCS), laser diffraction, or electron microscopy

(SEM/TEM) for direct visualisation. For ibuprofen, nanocrystal formulations have been shown to markedly improve dissolution rates, leading to a faster onset of therapeutic action compared to conventional formulations. This rapid absorption is particularly beneficial for managing acute pain and inflammation, where timely relief is crucial(36).

Similarly, SLNs have been employed to encapsulate oxaprozin, an NSAID, resulting in improved pharmacokinetic profiles and enhanced anti-inflammatory efficacy in preclinical models (37). A pharmacokinetic profile refers to the pattern of drug concentration in plasma over time, typically described by parameters such as Cmax (maximum concentration), Tmax (time to reach Cmax), AUC (area under the concentration–time curve, representing total drug exposure), and half-life(38). The lipid matrix of SLNs not only protects the drug from degradation but also facilitates controlled release, potentially reducing dosing frequency and minimising gastrointestinal side effects commonly associated with NSAIDs(39). These nanocarrier systems are versatile and suitable for both oral and topical administration, offering flexibility in treatment approaches(40). Notably, studies have reported a marked increase in bioavailability with these advanced formulations, underscoring their potential to significantly improve therapeutic outcomes in inflammatory and pain-related conditions(41, 42).

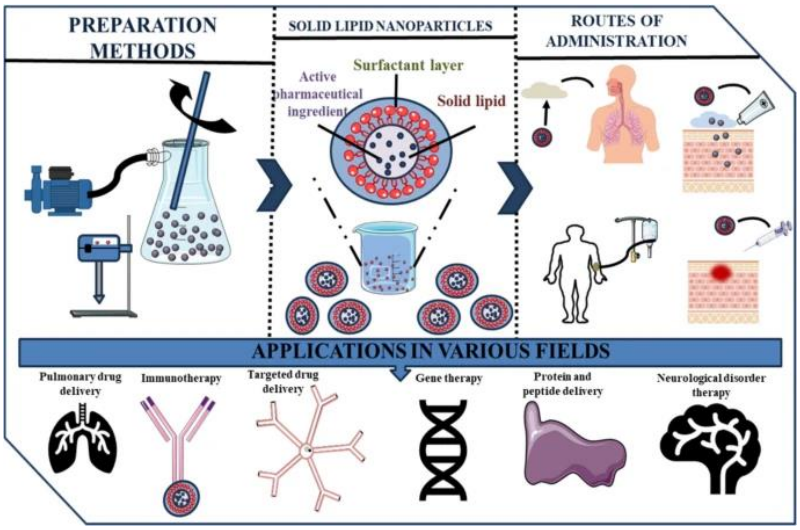

Fig 1.4: SLNPs have demonstrated the ability to enhance bioavailability, improve drug stability, bypass biological barriers, and enable controlled drug release(41).

1.3.2. Cyclodextrin Complexation

Cyclodextrin (CD) complexation is a non-covalent inclusion process in which a drug molecule, or part of it, is incorporated into the hydrophobic cavity of a cyclodextrin. CDs are cyclic oligosaccharides composed of α-(1to 4)-linked glucose units, forming a truncated cone-shaped structure with a hydrophilic exterior and a relatively hydrophobic inner cavity. This cavity accommodates nonpolar regions of drug molecules through hydrophobic interactions, van der Waals forces, and occasionally hydrogen bonding, resulting in an inclusion complex that improves apparent solubility (scheme 1.3). The use of CDs in drug

formulations, however, is limited by factors such as cost, production constraints, and potential toxicity. Additionally, drug bioavailability from CD-based systems can be suboptimal (43).

Incorporating small amounts of water-soluble polymers into the aqueous complexation medium significantly enhances the efficiency of drug–CD complexation(44, 45). These polymers improve both the pharmaceutical and biological performance of the complexes by stabilising the inclusion complex and preventing drug aggregation, leading to better solubility and bioavailability. Notably, this enhancement occurs regardless of the drug's physicochemical properties, as polymers actively participate in the complexation process(46).

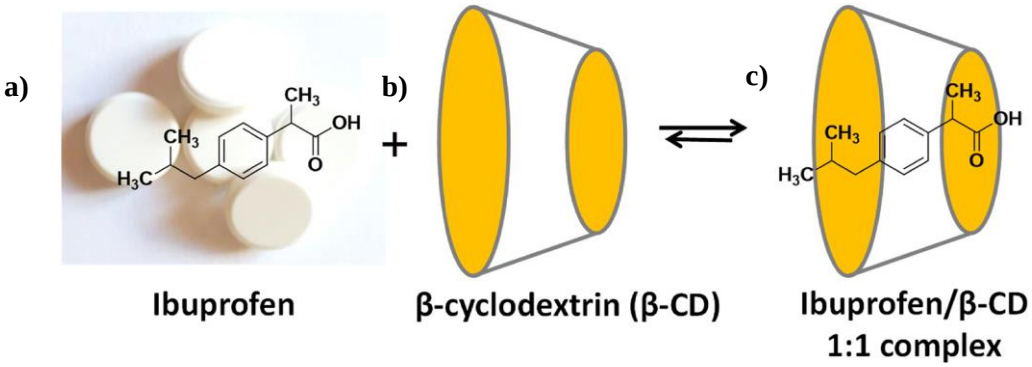

Scheme 1.3: Inclusion Complex Formation Between Ibuprofen and β-Cyclodextrin. (a, left) Chemical structure of ibuprofen overlaid on a tablet image, representing the free drug. (b, centre) Schematic of β-cyclodextrin (β-CD) as a truncated cone, illustrating its hydrophobic cavity. (c, right) Formation of a 1:1 reversible inclusion complex, with ibuprofen encapsulated inside the β-CD cavity, enhancing solubility and stability(47).

1.3.3. Amorphous Solid Dispersions (ASDs)

Amorphous solid dispersions (ASDs) are a widely used formulation strategy to enhance the solubility and bioavailability of poorly water-soluble drugs. In ASDs, the drug is molecularly dispersed within a hydrophilic polymer matrix, commonly polyvinylpyrrolidone (PVP) or hydroxypropyl methylcellulose (HPMC), which stabilises the drug in its amorphous, high-energy state(48). This amorphous form lacks the crystalline structure that typically limits dissolution, resulting in significantly improved solubility and faster dissolution rates. The polymer not only prevents recrystallisation but also enhances wettability and maintains supersaturation in the gastrointestinal tract, leading to improved absorption(49).

ASDs are particularly suitable for oral dosage forms such as tablets and capsules, and they have been successfully applied in commercial products. The enhanced dissolution profile of ASDs often translates into more consistent plasma drug concentrations, reducing variability in therapeutic response and improving overall efficacy(50). Numerous studies have demonstrated that ASDs can lead to several-fold

increases in bioavailability (Figure 1.5) for drugs with poor aqueous solubility, making them a cornerstone in modern pharmaceutical development(48).

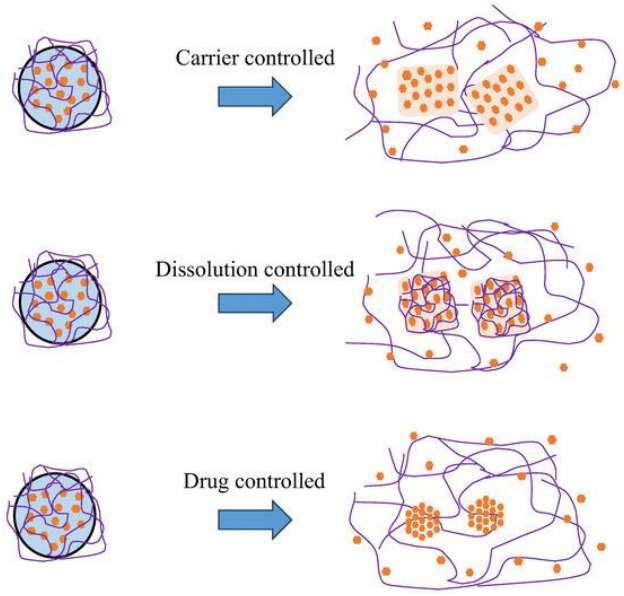

Fig. 1.5: The mechanism of ASD in dissolution media(1)
1) In carrier-controlled release, drug molecules diffuse through the polymer matrix, potentially via a viscous gel layer formed on the surface of ASD particles. If the dissolved drug concentration exceeds its amorphous solubility, amorphous liquid phase separation (ALPS) occurs, leading to the formation of drug-rich particles.
2) In congruent release, both the drug and polymer dissolve together, leading to rapid dissolution and the formation of drug-rich particles. The polymer helps to stabilise the supersaturated solution.
3) In drug-controlled release, the polymer dissolves first, leaving the drug to control the dissolution rate. Supersaturation does not occur if the remaining drug is unstable in its amorphous form without the polymer, which can result in crystallisation{Budiman, 2023 #3}.

1.3.4. Co-crystallization

Co-crystals have emerged as a promising strategy to enhance the solubility and stability of poorly water-soluble drugs without altering their pharmacodynamic properties(51). In particular, co-crystals of ibuprofen with nicotinamide and oxaprozin with caffeine have been explored to improve aqueous solubility and dissolution rates(52). Co-crystals are crystalline materials composed of an active pharmaceutical ingredient (API) and a co-crystal former (such as nicotinamide or caffeine) in a defined stoichiometric ratio, held together by non-covalent interactions like hydrogen bonding(53).

This approach does not alter the drug's pharmacodynamics but modifies its solid-state properties. Co-crystals often exhibit improved aqueous solubility and dissolution rates compared to the pure drug because the new crystal lattice is generally less stable than the original drug crystal, making it easier to break apart in water(54). This enhanced dissolution is the primary reason for using co-crystallisation as a strategy for poorly water-soluble drugs(8, 55). These co-crystals are formed by non-covalent interactions between the API and a suitable co-crystal former, resulting in a new crystalline structure with improved physicochemical properties (Figure 1.6). Importantly, the therapeutic efficacy of the drug remains unchanged, as the API retains its molecular identity. Co-crystals are especially suitable for solid oral dosage forms such as tablets and capsules, offering enhanced manufacturability and shelf-life stability(56). Studies have shown that such formulations can lead to improved bioavailability and more consistent plasma levels, making them a valuable tool in drug development for enhancing performance while maintaining safety and efficacy(53, 57).

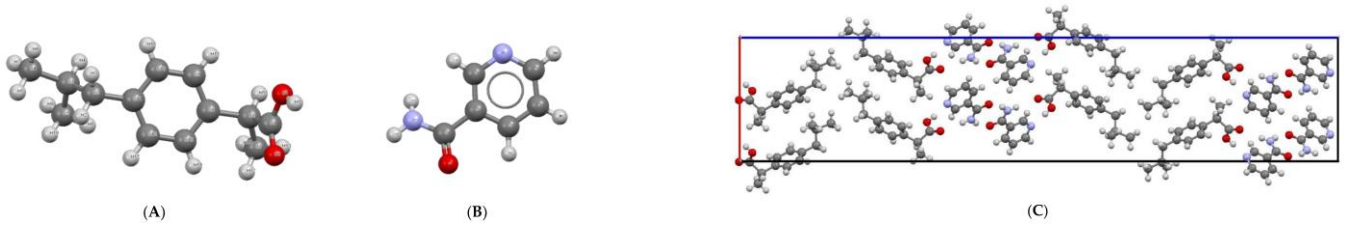

Fig.1.6: Chemical structures of (A) ibuprofen and (B) nicotinamide. (C) Packing structure of an ibuprofen / nicotinamide co-crystal (SODDIZ)(55).

1.3.5. Nanosuspension via Antisolvent Crystallisation Using Porous Hollow-Fibre Membranes

Porous hollow-fibre antisolvent crystallisation (PHFAC) is a continuous, membrane-intensified route to produce drug nanocrystals/nanosuspensions by metering an antisolvent through a microporous fibre wall directly into a flowing API solution, thereby creating controlled supersaturation and uniform nucleation/growth. In the ibuprofen system most relevant here, the module was built around a clinical Hemoflow F60 dialyser (a Fresenius hollow-fibre bundle), operated with ibuprofen in ethanol on the shell side and water (with a trace of Tween-80) in the fibre lumen. Under optimised flow, surfactant concentration, and temperature, the study achieved 300–400 nm particles with narrow PSD (PDI ≈0.1–0.2), complete in-vitro release within ~40 min, and physical size stability for ~3 months—all in a continuous mode of operation. The membrane serves as a contacting/mixing interface; it does not chemically combine with the drug (the drug never enters the bore)(54, 58). The Hemoflow/F-series dialysers are part of Fresenius' polysulfone membrane family (often branded as Fresenius Polysulfone/Helixone in their dialyser portfolio). Thus, in the cited ibuprofen PHFAC setup, hollow fibres can be regarded as polysulfone-based.

In the broader membrane-assisted antisolvent crystallisation literature, polypropylene (PP) membranes (both flat-sheet and hollow-fibre) are also used as the contacting medium for antisolvent dosing, with similar benefits for controlling supersaturation and narrowing crystal size distributions(59). The antisolvent (water) is pumped through the fibre lumen at slightly higher pressure and issues through the fibre pores as micro-jets into the shell-side drug solution (ethanol). This controlled, distributed mass transfer avoids local over-supersaturation, enabling uniform nucleation and growth of nanocrystals rather than broad, polydisperse agglomerates. A small amount of surfactant (e.g., Tween-80, ~0.011 mM in the optimised case) stabilises the newly formed particles and helps fix the size window (here, 300–400 nm at ~30–32 °C). Several groups have shown that residence time and the flow-rate ratio of solvent to antisolvent are decisive levers for pushing sizes below 200 nm in other APIs, including sub-100 nm with

short residence in cross-flow HFM modules (e.g., griseofulvin). Extended-duration studies further demonstrate stable, scalable operation for continuous nanocrystal production(38, 54, 60).

A closely related PHFAC variant can co-feed a polymer with the drug so that, upon antisolvent contact, polymer precipitates onto the crystal surface (or co-precipitates) to yield polymer-coated nanocrystals for stabilisation or modified release, implemented in porous hollow-fibre crystallizers and protected by patent literature(55).

In the 2023 ibuprofen PHFAC study, DLS was used for hydrodynamic size and PDI; SEM confirmed morphology/size; zeta potential assessed colloidal stability; XRD/DSC confirmed crystallinity/purity; and FTIR checked surface chemistry. These measurements are standard for nanosuspensions and align with the broader membrane-assisted crystallisation literature and CFD-aided design studies(54, 61). Relative to batch antisolvent addition, membrane-assisted antisolvent crystallisation offers finer control of supersaturation, typically yielding narrower crystal size distributions and more reproducible particle attributes. Versus top-down routes (high-pressure homogenization, media milling), PHFAC avoids high energy input and media wear while delivering similar or smaller sizes depending on the API and residence time; critically, it operates continuously with straightforward scale-out (more fibres or modules). Contemporary reviews of antisolvent crystallisation(including membrane-intensified variants) consistently highlight these advantages for particle-size control, morphology/polymorph management, and process intensification(62).

This approach leverages the high surface area and controlled environment provided by the membrane system to generate uniform nanosized drug particles, significantly enhancing dissolution and absorption characteristics (63). Furthermore, membrane-based nanonisation techniques are increasingly recognised as scalable and efficient solutions for improving the performance of poorly soluble drugs like ibuprofen, without compromising stability or therapeutic efficacy(58, 64, 65).

1.4 Literature review

Researchers such as Langer and Folkman (1976) pioneered the use of biodegradable polymers for controlled drug release, further cementing the role of polymers in modern medicine(66). Today, polymeric drug delivery systems are integral to the design of advanced therapeutics, particularly in oncology, infectious diseases, and chronic conditions. The historical trajectory of polymer-based drug delivery underscores its foundational importance and sets the stage for contemporary innovations in nanocapsulation(67-70). The application of polymers in drug delivery has evolved significantly since the mid-20th century, marking a transformative era in pharmaceutical sciences(71).

The earliest documented use of polymers for biomedical purposes can be traced back to 1949 with the development of Ivalon, a poly(vinyl alcohol) hydrogel cross-linked with formaldehyde, which was initially used as a surgical implant(72). This innovation laid the groundwork for future exploration into

polymeric materials as drug carriers. In the 1960s, Wichterle and Lim introduced polyhydroxy ethyl methacrylate (pHEMA), a hydrophilic polymer that became a cornerstone for hydrogel-based drug delivery systems(73). These early developments demonstrated the potential of polymers to control drug release rates, enhance bioavailability, and improve patient compliance.

Over the decades, the field has expanded to include a wide array of synthetic and natural polymers, each tailored for specific therapeutic applications. The integration of polymers into drug delivery has enabled the development of systems capable of targeted delivery, sustained release, and reduced toxicity.

1.4.1 Nanocapsulation Techniques

Nanocapsulation involves the entrapment of APIs within nanoscale carriers, typically ranging from 10 to 1000 nm. These carriers are often constructed using biocompatible polymers, which serve as the encapsulating agents that form the matrix or shell around the drug. Common nanocapsulation techniques include nanoprecipitation, emulsion-solvent evaporation, spray drying, and layer-by-layer assembly(74). Each method offers distinct advantages in terms of particle size control, encapsulation efficiency, and scalability. For example, nanoprecipitation is a simple and rapid method suitable for hydrophobic drugs(75), while emulsion-based techniques allow for the encapsulation of both hydrophilic and hydrophobic compounds(76).

Recent advancements have focused on microfluidic-assisted synthesis and supercritical fluid technologies to achieve uniform particle size and high drug loading(77). Surface modification strategies, such as PEGylation and ligand conjugation, are employed to enhance targeting and reduce immunogenicity(78). The choice of polymers such as PLGA, chitosan, or alginate plays a critical role in determining the carrier's biodegradability, drug release profile, and compatibility with the encapsulation method. These techniques and materials are essential for the development of next-generation nanomedicines with improved therapeutic indices.

1.4.2 Polyethylene glycol (PEG)

Polyethylene glycol (PEG) has emerged as one of the most extensively studied and utilised polymers in drug delivery (scheme 1.4) due to its biocompatibility, hydrophilicity, and ability to evade the immune system(79).
PEGylation, the process of attaching PEG chains to drug molecules or carriers, enhances the pharmacokinetic profile of therapeutics by increasing solubility, reducing renal clearance, and minimising immunogenicity. This strategy has been successfully employed in several FDA-approved formulations, including Doxil® and Onpattro®, which utilise PEGylated liposomes and lipid nanoparticles, respectively. In recent years, PEG has been incorporated into micelles, hydrogels, and dendrimers to improve drug loading and release characteristics(80).

For instance, PEG-PCL copolymers have been developed into thermoresponsive injectable hydrogels that provide sustained drug release at physiological temperatures(81). Additionally, PEG-PLA nanoparticles

have demonstrated enhanced ocular drug delivery by improving corneal penetration and retention time(82). The versatility of PEG in forming various nanostructures makes it a valuable tool in the design of targeted and responsive drug delivery systems. Studies by Zhang et al. (2018) and Liu et al. (2020) have highlighted the role of PEG in enhancing the therapeutic efficacy of anticancer agents while minimising systemic toxicity. As research continues, PEG-based nanocarriers are expected to play a pivotal role in the next generation of personalised medicine(75).

PEG-grafted liquid isoprene rubber (PEG-LIR) represents a novel class of amphiphilic polymers that combine the elasticity of rubber with the hydrophilicity of PEG (scheme 1.5). This hybrid structure allows for the formation of soft, deformable nanocapsules capable of encapsulating both hydrophilic and hydrophobic drugs(83). Singh et al. (2024) reported that PEG-LIR nanocapsules exhibited excellent biocompatibility, prolonged circulation time, and enhanced cellular uptake in vitro(84). The grafting of PEG chains onto the rubber backbone reduces protein adsorption and opsonisation[7], thereby improving stealth properties. These nanocapsules have been explored for the delivery of anti-inflammatory drugs, anticancer agents, and vaccines. Their tunable mechanical properties and surface functionality make them suitable for a wide range of biomedical applications, including targeted and stimuli-responsive drug delivery(85-87).

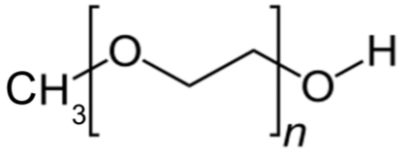

Scheme 1.4: Polyethylene glycol (PEG) chemical structure, n = 45 (88, 89).

1.4.3 Poly (maleic anhydride-alt-1-octadecene) (MA-alt-C_{18}-g-PEG)

Poly(maleic anhydride-alt-1-octadecene), commonly referred to as MA-alt-C_{18}-g-PEG, is a hydrophobic copolymer (scheme 1.6) that has gained attention for its amphiphilic properties and ability to form stable nanocapsules(90). Its alternating structure of maleic anhydride and long-chain alkyl groups allows for self-assembly into micellar and vesicular structures in aqueous environments. Recent studies have demonstrated that MA-alt-C_{18}-g-PEG can be functionalized with hydrophilic moieties or conjugated with targeting ligands to enhance its biocompatibility and specificity. Gupta and Mehra (2022) reported the successful encapsulation of hydrophobic drugs using MA-alt-C_{18}-g-PEG-based nanocapsules, achieving sustained release and improved pharmacokinetics(28). The polymer's anhydride groups also allow for facile chemical modification, enabling the attachment of PEG chains or bioactive molecules. These

[7] https://microbenotes.com/opsonization/

properties make MA-alt-C_{18}-g-PEG a versatile platform for drug delivery, particularly for poorly soluble drugs such as NSAIDs and anticancer agents(91-93).

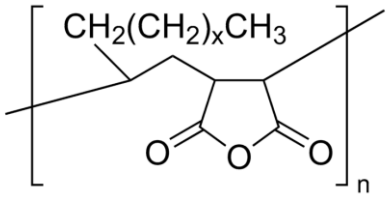

Scheme 1.5: Chemical structure of the pre-PEGylated poly (maleic anhydride-alt-1-octadecene) (MA-alt-C_{18}) backbone[8] , x = 10, n = 106.

1.4.4 Poly (isobutylene-alt-maleic anhydride) (IB-alt-MA-g-PEG)

Poly (isobutylene-alt-maleic anhydride) (IB-alt-MA-g-PEG) is a copolymer known for its mechanical stability, hydrophobicity, and the presence of reactive anhydride groups, which enable further chemical modification (scheme 1.6). These properties make IB-alt-MA-g-PEG a promising material for nanocapsule formulation in both oral and transdermal drug delivery(94). Its alternating structure provides a balance between rigidity and flexibility, facilitating the formation of stable nanostructures. For instance, Zhang et al. (2023) demonstrated that IB-alt-MA-g-PEG-based nanocapsules could encapsulate hydrophobic drugs with high efficiency and release them in a pH-responsive manner, making them suitable for gastrointestinal targeting(95). Moreover, IB-alt-MA-g-PEG can be functionalized with hydrophilic polymers such as PEG to enhance solubility and prolong systemic circulation. Its compatibility with various fabrication techniques, such as nanoprecipitation and emulsion polymerisation, further enhances its utility in drug delivery systems (39, 96, 97).

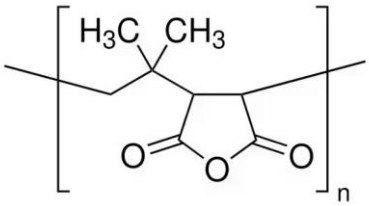

Scheme 1.6: Chemical structure of the pre-PEGylated poly isobutylene-alt-maleic anhydride (IB-alt-MA-g-PEG) backbone [9] , n = 39 .

[8] https://www.sigmaaldrich.cn/CN/zh/product/aldrich/419117
[9] https://www.sigmaaldrich.com/GB/en/product/aldrich/531278

In contrast, polyisobutylene (PIB) is a homopolymer valued for its excellent barrier properties, flexibility, and chemical resistance. It is widely used in transdermal patches due to its impermeability to moisture and gases, which helps maintain drug stability. However, PIB lacks functional groups like anhydrides, limiting its ability to undergo chemical modification or respond to environmental stimuli. As a result, PIB is primarily used as a passive matrix or adhesive rather than an active, responsive carrier(98). The anhydride groups in IB-alt-MA-g-PEG offer a distinct advantage over PIB by enabling post-polymerisation functionalization, such as conjugation with targeting ligands, pH-sensitive moieties, or hydrophilic chains. This allows IB-alt-MA-g-PEG-based systems to be tailored for stimuli-responsive release, targeted delivery, and enhanced bioavailability capabilities that PIB alone cannot provide. While MA-alt-C_{18}-g-PEG (poly(maleic anhydride-alt-alkene)) shares some structural similarities with IB-alt-MA-g-PEG and also contains reactive anhydride groups, its performance depends heavily on the specific alkene used in the copolymer(99). IB-alt-MA-g-PEG, with isobutylene as the co-monomer, offers a unique combination of hydrophobicity, mechanical strength, and modifiability, which may not be matched by all MA-alt-C_{18}-g-PEG variants. Therefore, the choice between IB-alt-MA-g-PEG, PIB, or MA-alt-C_{18}-g-PEG should be guided by the desired drug release profile, route of administration, and need for functionalisation(100).

1.4.5 Applications to Ibuprofen and Oxaprozin

Ibuprofen and oxaprozin are NSAIDs with poor aqueous solubility, limiting their bioavailability and therapeutic efficacy. Nanocapsulation using polymers such as MA-alt-C_{18}-g-PEG, IB-alt-MA-g-PEG, and LIR410-g-PEG has shown promise in overcoming these limitations. Wang et al. (2023) developed ibuprofen-loaded nanocapsules using hollow fibre membrane crystallisation, achieving rapid dissolution and enhanced bioavailability(58, 101). Similarly, oxaprozin has been encapsulated in solid lipid nanoparticles and polymeric carriers to improve its solubility and reduce gastrointestinal side effects(23). PEGylated nanocapsules have demonstrated prolonged circulation and targeted delivery to inflamed tissues, enhancing anti-inflammatory efficacy while minimising systemic exposure(39, 68, 70). These findings underscore the potential of polymeric nanocapsulation in optimising the pharmacokinetics and therapeutic outcomes of NSAIDs (Figure 1.7).

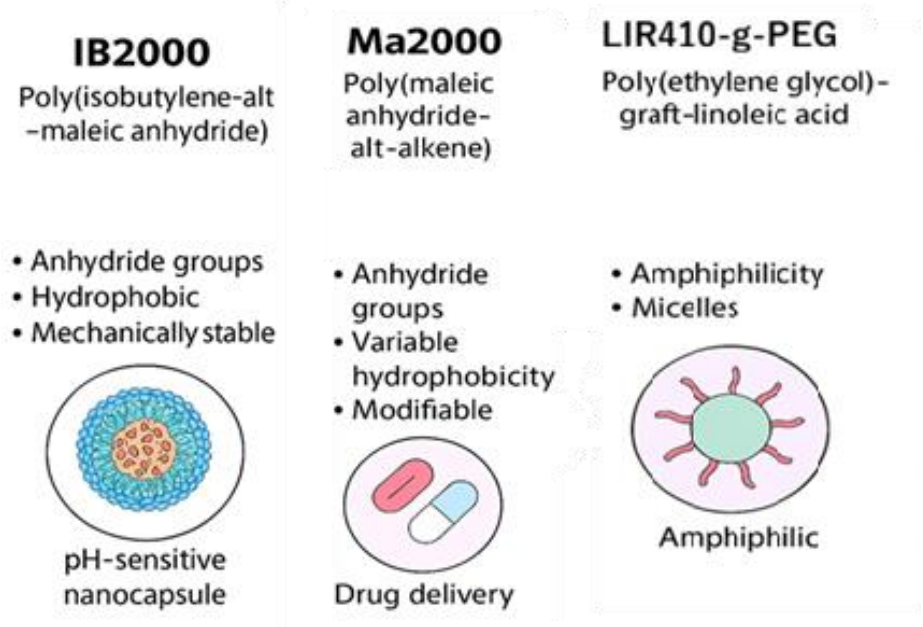

Fig.1.7: Comparative Overview of Three Grafted Polymers Used in Drug Delivery{Herdiana, 2022 #4}{Raffa, 2021 #5}.

1.5 Research Rationale, Novelty, and Comparative Advantages

Hydrophobic drugs such as ibuprofen and oxaprozin present a persistent formulation challenge due to their poor aqueous solubility, which limits their absorption and therapeutic performance despite high membrane permeability. Existing strategies, including lipid-based carriers, solid dispersions, and nanocrystals, often suffer from drawbacks such as instability, toxicity, or limited control over release profiles.

This study introduces a polymer-based nanocapsulation approach using amphiphilic systems (MA-alt-C_{18}-g-PEG, IB-alt-MA-g-PEG, and LIR410-g-PEG) that self-assemble into micelles in aqueous and deuterated environments. These micelles encapsulate hydrophobic drug molecules within their core, enhancing solubility, stability, and bioavailability. The polymers' tunable hydrophilic–hydrophobic balance enables precise control over micelle formation under varying pH and temperature conditions, offering potential for stimuli-responsive drug delivery.

The novelty of this work lies in its direct comparison of three structurally distinct polymer systems under identical experimental conditions, supported by advanced characterisation techniques including FTIR, DLS, and SANS. The use of D_2O further enhances structural resolution in neutron scattering studies. Among the tested systems, IB-alt-MA-g-PEG demonstrated superior performance in forming stable, uniform nanocapsules. This integrated approach not only provides deeper insight into micelle behaviour

and drug–polymer interactions but also establishes a versatile platform for designing next-generation delivery systems for poorly soluble therapeutics.

1.6 Aim and Objectives of the Study

The overarching aim of this project is to characterise the pH-responsive behaviour of LIR410-g-PEG, IB-alt-MA-g-PEG, and MA-alt-C_{18}-g-PEG copolymers and assess their ability to encapsulate ibuprofen and oxaprozin. The specific objectives are:

1. To investigate the effect of pH on the hydrodynamic size and polydispersity of LIR410-g-PEG, IB-alt-MA-g-PEG, and MA-alt-C_{18}-g-PEG micelles using DLS across a defined pH range.
2. To examine internal structural features and pH-dependent morphological changes using SANS, applying appropriate models to extract quantitative parameters.
3. To compare the encapsulation tendencies of ibuprofen and oxaprozin, relating differences to their molecular properties.
4. To evaluate polymer–drug interactions under acidic, neutral, and alkaline conditions, identifying any trends relevant to drug delivery applications.

1.7 Thesis Structure

- Chapter 1**:** Provides the scientific context for amphiphilic polymers and nanocapsulation, reviews relevant literature on drug delivery systems, and outlines the research objectives.
- Chapter 2: describes in detail the materials, preparation protocols, and experimental methods used, including DLS and SANS procedures.
- Chapter 3: presents the experimental results, alongside discussions of how pH and polymer concentration influence micellar behaviour.
-Chapter 4: presents the experimental results, alongside discussions of how pH, drug type and concentration influence micellar behaviour.
- Chapter 5: Conclusions, limitations, and recommendations for future work

Chapter 2

Materials and Methods

2.1 Materials

All reagents and solvents were of analytical grade and used as received unless otherwise stated. A detailed list of materials is provided in Table 2.1.

Table 2.1: List of materials used in this study.

Material	**Supplier / Source**	**Specification / Details**	**Chemical Structure**
Ibuprofen (≥98%)	Sigma-Aldrich, UK	–	
Oxaprozin (≥98%)	Sigma-Aldrich, UK	–	
Poly (maleic anhydride-alt-1-octadecene) (MA-alt-C_{18}-g-PEG)	Synthesised by Dr Wafaa Al Shatee (previous PhD student)	a=CH2(CH2)xCH3, b=H, m=106 or 177 and x=10	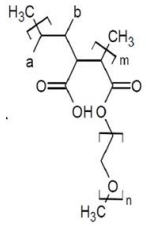
Poly (isobutylene-alt-maleic anhydride) (IB-alt-MA-g-PEG)	Synthesised by Dr Wafaa Al-Shatee (previous PhD student)	a=H, b=(CH3)2 and m=39	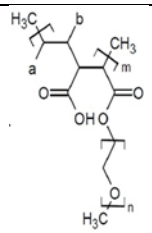
PEG-grafted liquid isoprene rubber (LIR410-g-PEG)	Kindly provided by Dr Donald Hill (collaborator)	LIR backbone ≈ 41,000 g/mol; PEG side chains ≈ 10,000 g/mol; grafting density ≈ 45–50%	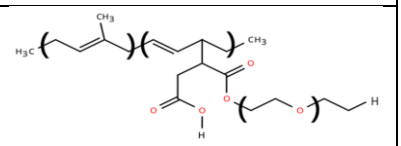
Deuterium oxide (D_2O, 99.9 atom % D)	Sigma-Aldrich, UK	–	
DCl (35 %w/w in D_2O) and NaOD (40 %w/w in D_2O)	Sigma-Aldrich, UK	–	
Tetrahydrofuran (THF), Ethanol (HPLC grade)	Merck / Fisher Scientific	–	

2.1.1 Polymer synthesis and Molecular Weight Optimization

To construct amphiphilic polymer systems suitable for nanoscale self-assembly, we selected MA-alt-C_{18}-g-PEG, LIR410-g-PEG, and IB-alt-MA-g-PEG as the primary components (scheme 2.1). These polymers were commercially sourced and pre-synthesised and were not synthesised as part of this study. MA-alt-C_{18}-g-PEG, a hydrophilic dicarboxylic acid-based polymer, contributes to aqueous solubility and potential

hydrogen bonding interactions. IB-alt-MA-g-PEG, a hydrophobic isobutylene-based copolymer, provides flexibility and hydrophobic character, supporting core formation in nanostructures. LIR410-g-PEG, a graft copolymer composed of a liquid isoprene rubber backbone and polyethylene glycol side chains, offers amphiphilic balance, enabling self-assembly into stable nanocapsules with enhanced solubility and prolonged circulation. The combination of these polymers allows for tunable nanocapsulation behaviour, responsive to environmental conditions such as pH and temperature.

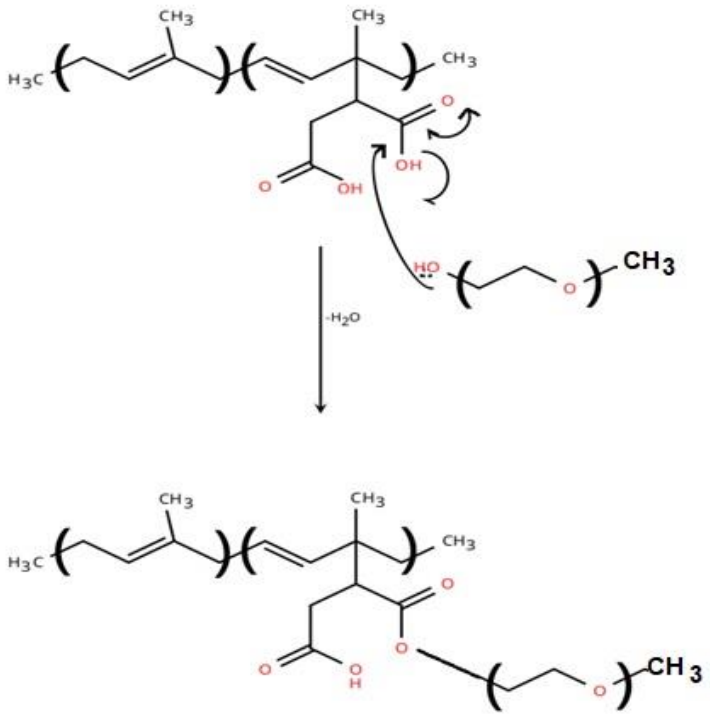

Schema 2.1: Synthetic route, "graft onto" polymerisation between poly (ethylene glycol) methyl ether and Poly (maleic anhydride-alt-1-octadecane) backbone.

To enhance amphiphilicity and promote nanostructure formation, PEG-grafted Liquid Isoprene Rubber (LIR410-g-PEG) was incorporated as a surfactant. This copolymer consists of a hydrophobic LIR backbone (MW ~410 g·mol^{-1}) grafted with hydrophilic PEG chains[1] (MW ~10,000 g·mol^{-1}).

2.1.2 Synthesis of LIR410-g-PEG

[1] https://www.elastomer.kuraray.com/us/wp-content/uploads/sites/2/2021/07/7_Article_RFP_4_2015s.pdf

LIR410-g-PEG was used as a surfactant and stabiliser during nanoprecipitation and emulsion-based nanocapsulation procedures. It was dissolved in deionised water or D_2O and mixed with drug solutions to facilitate nanostructure formation.

To prepare the graft copolymer, LIR 410 (1.7 g, 0.056 mmol, 1.0 equivalent) was first dissolved in 150 mL of toluene under magnetic stirring at elevated temperature until a clear solution was obtained. Methoxy polyethylene glycol ($mPEG_{10000}$) (5.6 g, 0.56 mmol, 10.0 equivalents) was then added, and the reaction mixture was heated under reflux conditions for seven days to promote complete grafting.

Upon completion, the reaction mixture was cooled to room temperature, and the solvent was removed under reduced pressure (in vacuo). The crude product was then dispersed in deionised water and transferred into dialysis tubing with a molecular weight cut-off of 12–14 kDa. Dialysis was performed against deionised water for seven days, with the water being replaced at least once daily to remove unreacted species and low-molecular-weight impurities. Finally, the purified LIR410-g-PEG was recovered from the tubing and dried on a hot plate under controlled conditions to yield the final solid product.

2.2 Preparation of Blank and Drug-Loaded Polymeric Micelles

Polymer solutions were prepared by dissolving MA-alt-C_{18}-g-PEG, IB-alt-MA-g-PEG, and LIR410-g-PEG in deionised water at defined weight ratios. Each polymer was treated as an individual system. The initial polymer concentration was set at 5% w/w in 10 mL of solvent. Additional concentrations of 2%, 1%, 0.5%, 0.25%, and 0.1% w/w were also prepared to study the effect of polymer concentration on micelle formation and drug encapsulation. These systems were characterised using DLS to measure particle size and distribution, and SANS to investigate structural features and aggregation behaviour. Fourier-Transform Infrared Spectroscopy (FTIR) was also employed to confirm the chemical structure and successful grafting of PEG onto the LIR backbone in LIR410-g-PEG.

The polymer solutions were first subjected to ultrasonic stirring for 30 minutes at 37 °C, followed by overnight magnetic stirring at the same temperature to ensure complete dissolution and homogeneity. After this step, stock solutions were prepared and used for drug loading.

Model hydrophobic drugs (ibuprofen and oxaprozin) were added to the polymer solutions at concentrations of 0.1%, 0.25%, and 0.5% w/w relative to the total solution volume. After the drug addition, the mixtures were treated with ultrasonic stirring for 30 minutes at 37 °C, followed by overnight magnetic stirring to promote encapsulation and prevent aggregation.

To evaluate the effect of pH, selected formulations were prepared using:

- 0.25%w/w Ibuprofen in 5%w/w polymer solutions

- 0.5%w/w Oxaprozin in 5%w/w polymer solutions

These concentrations were chosen based on DLS results, which indicated optimal particle sizes in the nanoscale range at these drug-to-polymer ratios.

Additionally, to investigate the influence of polymer concentration on micelle formation, formulations with fixed drug concentrations were prepared using varying polymer concentrations (2%, 1%, 0.5%, 0.25%, and 0.1% w/w). This allowed for a systematic study of how polymer content affects micelle size, stability, and drug encapsulation efficiency.All formulations were stirred overnight before DLS measurements to ensure equilibrium and minimise aggregation.

2.2.1 Drug-to-Polymer Ratio Studies

Understanding the relationship between drug and polymer concentrations is critical for optimising micelle formation, drug encapsulation efficiency, and colloidal stability. This section explores how varying the drug-to-polymer ratio influences the physicochemical properties of micellar systems, particularly particle size and polydispersity.

2.2.2 Fixed Drug Concentration, Varying Polymer Concentration

In this approach, the drug concentration was held constant at 0.25% w/w, while the polymer concentration was systematically varied across 0.1%, 0.25%, 0.5%, 1%, and 2% w/w. This design allowed for the identification of the minimum polymer concentration required to form stable micelles capable of encapsulating the drug effectively.

The goal was to determine the critical micelle concentration (CMC), the threshold at which amphiphilic polymers self-assemble into micelles. Below this concentration, micelle formation is incomplete or unstable, leading to poor encapsulation and larger, polydisperse aggregates. Above the CMC, micelles are more uniform and stable, which is essential for drug delivery applications.

2.2.3 Fixed Polymer Concentration, Varying Drug Concentration

In the second set of experiments, the polymer concentration was fixed at 5% w/w, and the drug concentration was varied at 0.1%, 0.25%, and 0.5% w/w. This setup was used to evaluate the drug-loading capacity of the micelles and to observe how increasing drug content affects micelle size, encapsulation efficiency, and colloidal stability. Higher drug concentrations can lead to micelle swelling or destabilisation, especially if the drug exceeds the solubilisation capacity of the micellar core. These experiments helped define the optimal drug loading range for each polymer system.

After preparation, samples were subjected to 30 minutes of ultrasonic stirring at 37 °C, followed by overnight magnetic stirring at the same temperature. Before DLS analysis, samples were equilibrated for 10 minutes to ensure thermal and structural stability.

2.3 pH-Dependent Studies

To evaluate the impact of pH on micelle formation, structural stability, and particle size, polymer solutions were prepared at a fixed concentration of 2% (w/w) in either deionised water or deuterated water (D_2O). The pH was adjusted to 3, 5, 8, or 12 using deuterium chloride (DCl, 35% in D_2O) or sodium deuteroxide (NaOD, 40% in D_2O) to simulate a range of physiological and pathological conditions, including acidic tumour microenvironments and alkaline intestinal fluids. For drug-loaded formulations, the polymer concentration was increased to 5% (w/w) to facilitate adequate micelle formation and drug encapsulation capacity.

Ibuprofen (0.25% w/w) and oxaprozin (0.5% w/w) were selected for these studies based on preliminary dynamic light scattering (DLS) results, which demonstrated favourable particle size profiles and good compatibility with the polymer systems.

All preparations and pH adjustments were carried out using micropipettes to ensure precise volumetric control and high reproducibility, particularly in small-volume samples. The pH of each formulation was verified using pH indicator paper (range 1–14), selected for its practicality in low-volume and deuterated systems where conventional electrode-based pH meters are less suitable.

Following pH adjustment, samples were subjected to ultrasonic stirring for 30 minutes at 37°C, followed by overnight magnetic stirring at room temperature, to achieve complete dissolution, homogeneity, and equilibration prior to DLS analysis. This approach enabled systematic assessment of pH effects on micelle behaviour, providing data essential for understanding performance in pH-variable biological environments and potential applications in stimuli-responsive drug delivery.

2.4 Temperature Control and Thermosensitivity Studies

Temperature control was maintained using a temperature-controlled water bath covering the range 15–45°C to ensure reproducible conditions during polymer dissolution, drug loading, and micelle formation. For sub-ambient temperatures, a cold-water bath with chilled water was employed.

Thermosensitivity studies evaluated the impact of temperature on micelle hydrodynamic diameter, polydispersity index (PDI), and stability using dynamic light scattering (DLS). Measurements were performed at 15°C, 25°C, 35°C, and 45°C to encompass storage, ambient, physiological (37°C), and hyperthermic conditions. Samples were equilibrated in the water bath for 10 minutes at each temperature prior to analysis. Increases in size or PDI at higher temperatures would indicate destabilisation, aggregation, or potential drug leakage, whereas stable profiles suggest thermoresilient formulations.

These protocols were particularly optimised for IB-alt-MA-g-PEG formulations, which exhibited superior DLS performance (smaller, more uniform particle sizes) compared to MA-alt-C_{18}-g-PEG and LIR410-g-PEG. Consequently, IB-alt-MA-g-PEG was prioritised for detailed studies.

The standard preparation protocol for all polymers involved:

1. Ultrasonic stirring for 30 minutes at 37°C to promote initial dispersion and minimise aggregation.
2. Overnight magnetic stirring at room temperature to facilitate complete micelle formation and stabilisation.

This two-step process was repeated after drug addition to ensure efficient encapsulation and prevent drug-induced aggregation. All samples underwent overnight stirring prior to DLS analysis to reach equilibrium and reduce measurement variability. Similar procedures were applied to the other polymers, but with focused optimisation on IB-alt-MA-g-PEG due to its formation of stable nanoscale assemblies.

2.5 Methods (Characterisation Techniques)

2.5.1 Dynamic Light Scattering (DLS)

Particle size and distribution were determined using a Malvern Zetasizer Nano ZS (633 nm He–Ne laser, 173° backscatter detection). Samples were diluted in deuterated water, transferred to disposable polystyrene or quartz cuvettes, and equilibrated for 10 minutes at room temperature to ensure thermal stability. Each sample was measured ten times, and average values were calculated for reproducibility. Zetasizer Software v7.13 was used for data acquisition and analysis, with water refractive index and viscosity manually entered for each temperature. The polydispersity index (PDI) was used to assess size uniformity; values below 0.2 indicated monodisperse micelles. Samples showing multimodal distributions or abnormal scattering were re-prepared to maintain data integrity.

Measurements confirmed nanoscale particle formation for MA-alt-C_{18}-g-PEG/IB-alt-MA-g-PEG and LIR410-g-PEG systems, while Ma5000/IB5000 systems exhibited larger aggregates.

For this study, as it is mentioned above, all samples after stirred with an ultrasonic and magnetic stirrer, stored in glass bottles with a tight lid to keep the content away from any vaporize or additional components from the environment. They were transferred to the DLS lab, where, before preparing the DLS and reaching the demand temperature, samples were kept stirring on the magnetic stirrer to avoid any interference with the sample formation. Then, by using a pipette, samples were transferred to the cuvette (wearing gloves was necessary to avoid any fingerprints on the cuvette). After confirmation of the volume in the cuvette with guidelines, the sample was left in the DLS and started the experiment.

2.5.2 Small Angle Neutron Scattering (SANS)

Small-Angle Neutron Scattering (SANS) measurements were performed on the SANS2D beamline at the ISIS Neutron and Muon Source (UK) to characterise the internal structure of micellar formulations. Samples were prepared in quartz cells with a path length of 1–2 mm and measured at 298K. Deuterated water (D_2O) was used as the solvent to enhance contrast between micellar components and the

background. SANS detector ranges cover momentum transfers (Q) from 0.0035 to 1 $Å^{-1}$, probing particle or structure sizes from ~1 nm to several hundred nanometers[1] .
A collimated beam of cold neutrons was directed through the samples, and scattering was detected at small angles to probe differences in scattering length density (SLD) between the hydrophobic core, hydrophilic shell, and solvent. Multiple detector distances and neutron wavelengths were employed to cover a broad q-range, enabling resolution of both core and shell regions.
Raw scattering data were corrected for background, transmission, and detector efficiency, and subsequently reduced to one-dimensional scattering profiles (intensity vs. q) for model fitting and structural analysis.

2.5.3 SANS data analysis (SasView)

This study analysed SANS data in **SasView (v6.0.1)** to extract size and shape information and to select physically consistent models for each polymer system. The workflow combined a Guinier check, manual estimates of contrast and a flat incoherent background (estimated from the high-q tail, typically q~0.3 – 0.9 Å), and systematic model testing (Guinier–Porod/Beaucage, Debye/Gaussian coil, flexible cylinder, homogeneous sphere, core–shell, and two-Lorentzian/correlation-length). For each dataset, we inspected appropriate q subranges (low q for Guinier, mid q for form-factor features, high q for Porod/background), fixed or tightly bounded the background during fits, and used initial parameter guesses consistent with the Guinier bounds. Model selection was based on reduced χ^2, residual structure, parameter stability and covariance, and physical plausibility; when no clear Guinier knee was present, we reported a lower bound on $R_g$using $R_g \gtrsim 1.3/q_{\min}$. Full fit reports, covariance matrices, exact q-ranges, and the SasView project files are provided in Appendix A for reproducibility.

2.5.4 Data Import and Preprocessing

Raw SANS data files (in .txt or. hd5 format) were imported into SasView. Each dataset included scattering intensity (I) as a function of the scattering vector (q). Before fitting, background subtraction and data normalisation were performed as needed.

Model Selection and Fitting

Appropriate form factor models were selected based on the expected micelle morphology. The most used models included:

- Core–Shell Sphere Model: to describe micelles with a hydrophobic core and hydrophilic shell

[1] https://www.isis.stfc.ac.uk/Pages/SANS_Q-range.aspx

- Polydisperse Sphere Model: to account for size distribution within the micelle population
- Guinier–Porod Model: for systems with less-defined or hierarchical structures
- Cylinder Model: systems like worm-like micelles, nanorods, or polymer fibrils.
- Poly-micelle Model: Suitable for systems where micelles form clusters or networks, such as in polymer-surfactant complexes.

Initial parameter estimates (e.g., core radius, shell thickness, scattering length densities) were input based on DLS data and literature values. The Levenberg–Marquardt algorithm was used for non-linear least squares fitting.

2.5.5 Parameter Extraction

From the fitted models, key structural parameters were extracted:

- Radius of gyration (Rg)
- Core radius and shell thickness
- Volume fraction and SLD contrast
- Chi-squared (χ^2) and residuals to assess goodness-of-fit

These parameters provided detailed information about the size, shape, and internal structure of the micelles, complementing the hydrodynamic size data obtained from DLS.

2.5.6 Visualisation and Reporting

SasView's built-in plotting tools were used to visualise the experimental data alongside the fitted model curves. Fit quality was evaluated based on residual plots and reduced chi-squared values. Final plots and parameter tables were exported for inclusion in figures and supplementary materials (for more information, see Appendix A, B).

2.5.7 Fourier transform infrared (FTIR) spectroscopy

Fourier Transform Infrared (FTIR) spectroscopy is a widely used analytical technique for confirming chemical structure and functional group modifications in surfactants and polymer systems. The Thermo Scientific Nicolet™ iS10 FTIR spectrometer (often referred to as i510 in shorthand) is a mid-infrared Fourier Transform Infrared instrument designed for routine material characterization, and when paired with an ATR (Attenuated Total Reflectance) accessory, it enables rapid, preparation-free analysis of

solids, powders, and liquids[1] . In the case of PEG-grafted surfactants, FTIR provides a molecular fingerprint by detecting characteristic vibrational bands associated with specific bonds. For example, the presence of strong C–O–C stretching vibrations (typically around 1100 cm^{-1}) confirms the PEG backbone(102), while ester or amide linkages formed during grafting appear as distinct carbonyl (C=O) absorption bands near 1730–1750 cm^{-1}. These spectral features allow verification of successful grafting and assessment of chemical integrity without destroying the sample. FTIR is particularly advantageous because it is rapid, non-destructive, and capable of distinguishing between hydrophilic PEG segments and hydrophobic domains in amphiphilic copolymers. For detailed interpretation of PEG-related FTIR spectra, readers are referred to specialised literature on polymer characterisation and PEG-based graft copolymers(103)**.**

2.6 Polymer and Drug Stock Preparation

Polymer stock solutions were prepared by dissolving each polymer (LIR410-g-PEG, IB-alt-MA-g-PEG, or MA-alt-C_{18}-g-PEG) in deionised or deuterated water at the desired concentrations immediately after the overnight stirring step. This approach ensured that the solutions remained homogeneous and minimised the risk of aggregation before drug loading.

Model hydrophobic drugs (Ibuprofen and Oxaprozin) were added directly to the freshly prepared polymer solutions at concentrations of 0.1%, 0.25%, or 0.5% w/w, depending on the experimental design. After the drug addition, the mixtures were subjected to 30 minutes of ultrasonic stirring at 37 °C, followed by overnight magnetic stirring at the same temperature to ensure complete encapsulation and stability. In this study, only aqueous solvents (deionised or deuterated water) were used for all formulation steps to maintain biocompatibility and avoid solvent-related interference. However, THF and ethanol were used separately in control experiments to dissolve the pure drugs and measure their baseline particle sizes via DLS and SANS, serving as a reference for evaluating encapsulation efficiency.

All stock solutions were stored at ambient laboratory temperature and used immediately after preparation to ensure consistency and reproducibility across all formulations.

2.7 Additional Characterisation Techniques

To complement DLS and provide a more holistic understanding of micelle behaviour, several additional techniques were employed:

[1] https://www.thermofisher.com/order/catalog/product/IQLAADGAAGFAHDMAPC

- UV-Vis Spectroscopy: Used to quantify drug loading and release by measuring absorbance at the drug's characteristic wavelength (e.g., 220 nm for Ibuprofen). Calibration curves were prepared in triplicate for each drug to ensure accuracy.
- Visual Inspection and Turbidity Scoring: Samples were visually assessed for clarity, turbidity, and phase separation. A qualitative turbidity scale was applied:

0 = clear, 1 = slightly turbid, 2 = opaque. This provided a quick visual indicator of micelle stability.

These complementary techniques helped validate DLS findings and provided deeper insight into the physical stability, encapsulation efficiency, and environmental responsiveness of the micellar systems.

2.8 Sample Handling and Storage

Proper sample handling and storage are essential to preserve micelle integrity and prevent degradation. All micellar formulations were prepared fresh and analysed within 24 hours unless otherwise specified. For temperature-dependent studies, samples were equilibrated at the target temperature for 10 minutes before analysis.

All formulations were prepared using the same stock solutions and under identical stirring and filtration conditions to minimise batch-to-batch variability. Equipment was thoroughly cleaned between batches to prevent cross-contamination.

2.9 Controls and Replicates

To ensure the reliability and reproducibility of results, all experiments were conducted in triplicate. The following controls were included:

- Blank controls: Polymer-only micelles (without drug) were used to assess the baseline size and stability of the micellar system.
- Negative controls: Drug solutions prepared without polymer were used to confirm that micelle formation was essential for solubilization. These typically showed visible precipitation or large particle sizes (>1 µm), confirming the stabilising role of the polymer.

For each experimental condition, pH, temperature, polymer concentration, and drug loading, at least three independent batches were prepared and analysed.

2.10 Data Processing and Statistical Analysis

All raw DLS and SANS data were processed using Python (v3.10) for statistical evaluation and SasView for structural modelling. Descriptive statistics, including mean, standard deviation, and coefficient of variation, were calculated with NumPy and Pandas, and results were reported as mean ± SD. No inferential statistical tests were applied; interpretation relied on trend analysis, data quality assessment, and model fitting.

SANS profiles were fitted in SasView using appropriate form-factor models such as core–shell spheres, polydisperse spheres, and Guinier–Porod functions to extract parameters including radius of gyration, core radius, shell thickness, and scattering length density contrast. Linear regression in Python was used when examining relationships between micelle behaviour and variables such as temperature, pH, or concentration. Outliers were removed only when justified by clear technical artefacts.

All figures were generated using Matplotlib and Seaborn, with error bars representing standard deviation. This combined computational workflow ensured transparent, reproducible, and consistent analysis across all datasets.

2.11 Method Validation and Reproducibility

To ensure the reliability, accuracy, and reproducibility of all experimental results, a series of method validation procedures were implemented:

- Instrument Calibration:

  The Zetasizer was calibrated weekly using 100 nm polystyrene latex standards to verify particle size accuracy.

- Inter-Day Variability:

  Selected samples were measured on three consecutive days to assess reproducibility. Results were expressed as relative standard deviation (RSD), with values below 5% considered acceptable.

- Intra-Batch Consistency:

  For each formulation, three independent batches were prepared and analysed to confirm consistency in micelle size, PDI, and drug loading.

All instruments were operated by the same trained user to minimise operator variability. Data was recorded in laboratory notebooks and cross-checked for consistency and traceability.

These precautions ensured that the data collected reflected the true behaviour of the micellar systems under controlled and reproducible conditions, supporting the validity of the experimental findings.

Chapter 3

Results and Discussion

(Aggregation Structure of Grafted Polymers in Solution without Drug)

Overview

This chapter presents the experimental findings obtained using the three amphiphilic polymers described in Chapter 2: poly (maleic anhydride-alt-1-octadecene) (MA-alt-C_{18}-g-PEG), poly (isobutylene-alt-maleic anhydride) (IB-alt-MA-g-PEG), and PEG-grafted liquid isoprene rubber (LIR410-g-PEG). These polymers were used as received and were not synthesised or modified during this project.

The work focused on two principal aspects: (i) the self-assembly behaviour and stability of blank (drug-free) polymeric micelles in aqueous media as a function of polymer concentration, pH, and temperature, and (ii) the encapsulation of two model hydrophobic NSAIDs, ibuprofen and oxaprozin, into the resulting core–shell nanostructures, with emphasis on the influence of pH and drug-to-polymer ratio. These investigations addressed the research objectives introduced in Chapter 1 by examining how polymer chemistry and formulation conditions determine micelle size and colloidal stability; by evaluating the extent to which the systems exhibit pH- and temperature-responsive behaviour suitable for stimuli-sensitive drug delivery; and by comparing the relative performance of MA-alt-C_{18}-g-PEG, IB-alt-MA-g-PEG, and LIR410-g-PEG as nanocarriers for ibuprofen and oxaprozin in terms of encapsulation behaviour, particle size, and environmental stability.

Results are presented according to the principal characterisation techniques employed: Dynamic Light Scattering (DLS) and Small-Angle Neutron Scattering (SANS) in D_2O. Structural modelling and interpretation were performed using SasView software and custom Python scripts, which enabled extraction of parameters such as radius of gyration (Rg), core–shell dimensions, and aggregation number (Nagg). DLS provided intensity-weighted Z-average hydrodynamic diameters (Dh) via cumulants analysis, serving as a rapid screening tool and reference for the more detailed nanoscale structural information subsequently obtained by SANS. Together, these complementary datasets and modelling approaches provide an integrated interpretation of polymer responsiveness and suitability for drug delivery applications.

This chapter is structured as follows: Section 3.1 covers aggregation structure without drug, including concentration, pH, and comparative summaries; Section 3.2 examines temperature effects; and Section 3.3 provides overall conclusions and future work recommendations. A unique contribution of this study is the direct, side-by-side comparison of the three polymers using both DLS and SANS, with novel SANS insights on IB-alt-MA-g-PEG highlighting its distinct shape-shifting response.

3.0 Aggregation Structure of Grafted Polymers in Solution without Drug

3.1 Overview of Experimental Conditions

This section examines the self-assembly behaviour of the three amphiphilic graft copolymers (MA-alt-C_8-g-PEG, IB-alt-MA-g-PEG, and LIR410-g-PEG) in the absence of drug.

Polymer solutions were prepared by dissolution in D_2O, enabling spontaneous aggregation of the hydrophobic graft segments under the conditions described in Chapter 2. Concentrations of 0.1, 0.25, and 0.5 % w/w were investigated, with additional pilot screening at higher levels where solubility permitted. Concentrations varied between techniques: lower for DLS (1–2 %w/w) to optimise solubility and avoid multiple scattering artifacts, and higher for SANS (2–5 %w/w) to ensure sufficient scattering intensity. pH was adjusted from 3 to 12 to simulate physiological ranges, and temperatures from 15–45 °C to assess thermoresponsiveness.

Pilot measurements at 2 %w/w and 5 %w/w revealed clear concentration-dependent trends, as summarised in Table 3.1. IB-alt-MA-g-PEG formed assemblies in the 333–584 nm range, with the substantial size increase at higher concentration consistent with ionic repulsion between partially hydrolysed maleic anhydride groups and the relatively low grafting density, both of which promote inter-micellar association and secondary aggregation. MA-alt-C_8-g-PEG generated moderately sized particles at 2 %w/w but became highly polydisperse and oversized at 5 %w/w, which is attributed to bridging between its long hydrophobic C18 grafts, facilitating loose and unstable higher-order aggregates. In contrast, LIR410-g-PEG produced the smallest and most uniform particles (162–227 nm), indicating that the dense PEG corona provides effective steric stabilisation that suppresses inter-micellar association and limits aggregate growth.

Table 3.1: Effect of polymer concentration on micelle size in D_2O (pilot screening).

Polymer	Concentration (%w/w)	Particle size (nm)
IB-alt-MA-g-PEG	2	333 ± 20
IB-alt-MA-g-PEG	5	395 ± 20
MA-alt-C_8-g-PEG	2	215 ± 10
MA-alt-C_8-g-PEG	5	653 ± 74
LIR410-g-PEG	2	162 ± 3
LIR410-g-PEG	5	227 ± 10

These pilot data indicate that LIR410-g-PEG provides the most favourable size control, consistent with steric stabilisation from its PEG grafts. In contrast, MA-alt-C_8-g-PEG and IB-alt-MA-g-PEG exhibit pronounced concentration-dependent enlargement due to stronger hydrophobic or inter-micellar

interactions at higher loadings. These observations informed the selection of polymer–concentration ranges used in the subsequent DLS and SANS analyses.

To evaluate the effect of polymer type and concentration on micelle formation, poly (maleic anhydride-alt-1-octadecene) (Ma) grafted with different molecular weights of PEG was first screened. The Ma5000 variant produced aggregates exceeding 1000 nm, consistent with excessive hydrophobic chain length promoting inter-particle association and flocculation. Since particles above ~200 nm typically exhibits limited circulation and reduced cellular uptake, Ma5000 was excluded from further investigation. Consequently, MA-alt-C_{18}-g-PEG was selected for a more detailed study.

At 2 %w/w, MA-alt-C_{18}-g-PEG produced particles of approximately 215 nm, whereas increasing the concentration to 5 %w/w resulted in significantly larger and more polydisperse aggregates (653 ± 74 nm). This concentration-dependent enlargement is attributed to hydrophobic bridging between the long C_{18} grafts at higher polymer densities, leading to unstable higher-order aggregates. These findings suggest that 2 %w/w is closer to the concentration range supporting effective micelle formation, whereas 5 %w/w exceeds the threshold at which inter-micellar association becomes dominant. Although the critical micelle concentration (CMC) was not directly measured, the observed behaviour is consistent with 2 %w/w approaching the CMC and 5 %w/w exceeding it.

In contrast, LIR410-g-PEG generated the smallest and most uniform assemblies across both concentrations tested (162–227 nm). This improved stability is consistent with the steric stabilisation provided by the dense PEG corona, which suppresses inter-micellar association and limits aggregate growth even at higher polymer loadings. These favourable size characteristics were also maintained under additional experimental conditions, including variations in temperature and pH.

Overall, all three polymers formed measurable nanoscale assemblies; however, only LIR410-g-PEG consistently achieved particle sizes within the optimal range for drug delivery (<200 nm at 2 %w/w). These findings, summarised in Table 3.2, support the selection of LIR410-g-PEG as the lead candidate for further optimisation and subsequent drug-loading experiments.

When characterizing drug-free micelles, the limitations of Dynamic Light Scattering (DLS) must be considered. DLS Z-average values are intensity-weighted and, consequently, highly sensitive to even trace populations of large aggregates or impurities. Therefore, DLS data alone cannot provide definitive structural confirmation. For a rigorous physical characterization, Z-average diameters must be interpreted alongside the polydispersity index (PDI) and -potential.

Furthermore, morphology should be validated using complementary techniques such as Small Angle Neutron Scattering (SANS), Size Exclusion Chromatography (SEC), or cryo-TEM. In the absence of a drug payload, mapping the Critical Micelle Concentration (CMC) remains essential to establish the thermodynamic stability of the self-assembled structures and to provide a baseline for understanding their subsequent performance in biological environments (99, 159).

Table 3.2: Comparative assessment of polymer systems for nano drug delivery based on particle size and stability.

Polymer system	Key findings	Suitability for drug delivery
IB-alt-MA-g-PEG	Particle sizes 333–584 nm; strong concentration-dependent enlargement.	**Unsuitable** — high risk of aggregation and rapid clearance.
MA-alt-C_8-g-PEG	~215 nm at 2 %w/w; becomes oversized and highly polydisperse at 5 %w/w.	**Borderline** — acceptable only near lower concentrations; unstable at higher loadings.
LIR410-g-PEG	162 nm (2 %w/w) and 227 nm (5 %w/w); narrow size distribution; stable under multiple conditions.	**Promising candidate** — good size control; suitable for optimisation and drug loading.

As summarised in Table 3.2, LIR410-g-PEG exhibited the most favourable particle sizes and stability across all tested concentrations, consistently remaining within or near the ideal nanoscale range for drug delivery applications. In contrast, IB-alt-MA-g-PEG and MA-alt-C_8-g-PEG displayed concentration-dependent particle enlargement and reduced stability, limiting their suitability for systemic use. These comparative results therefore justified the selection of LIR410-g-PEG as the lead polymer for subsequent optimisation and drug-loading studies, while IB-alt-MA-g-PEG and MA-alt-C_8-g-PEG were retained solely for limited comparative purposes.

3.2 Effect of Polymer Concentration

3.2.1 Effect of concentration on Particle Characteristics (DLS)

The effect of polymer concentration on particle size was evaluated using Dynamic Light Scattering (DLS). Measurements were performed at three concentrations (0.1%, 0.25%, and 0.5% w/w) for the alternating copolymers MA-alt-C_8-g-PEG and IB-alt-MA-g-PEG. This analysis aimed to assess how increasing polymer concentration affects the hydrodynamic diameter, providing insight into concentration-dependent aggregation behaviour.

Small-Angle Neutron Scattering (SANS) complemented the DLS measurements by offering detailed information on the internal structure of polymeric micelles. While DLS provides the hydrodynamic diameter in solution, SANS allows determination of parameters such as core radius, shell thickness, radius of gyration (Rg), and aggregation number. These parameters are crucial for understanding the spatial organisation and density distribution within micelles, which cannot be accessed by DLS alone.

Figure 3.1 presents the DLS results for all three amphiphilic polymer systems (IB-alt-MA-g-PEG, MA-alt-C_8-g-PEG, and LIR410-g-PEG) at 0.10, 0.25, and 0.50 % w/w. Error bars indicate the reported variability (± values for each data point). Displaying all datasets on a single axis allows direct, like-for-like comparison of the concentration-dependent changes in hydrodynamic particle size for each polymer.

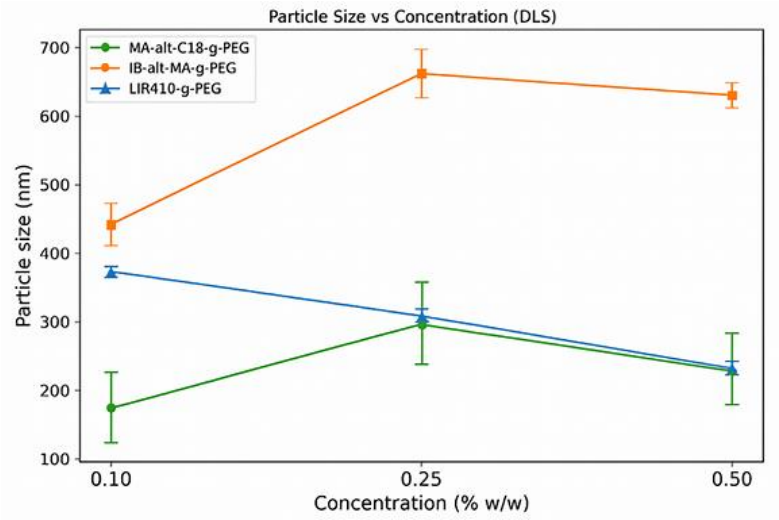

Fig 3.1: Effect of polymer concentration on hydrodynamic diameter measured by DLS. Mean particle sizes were measured at 0.10%, 0.25%, and 0.50% w/w for three amphiphilic polymers: MA-alt-C_{18}-g-PEG (green), IB-alt-MA-g-PEG (orange), and LIR410-g-PEG (blue). Error bars represent standard deviation across triplicate measurements. IB-alt-MA-g-PEG exhibited a peak in particle size at 0.25% w/w (≈663 nm) followed by a slight decrease. LIR410-g-PEG showed a consistent decrease in size with increasing concentration, while MA-alt-C_{18}-g-PEG displayed a shallow maximum at 0.25% w/w (≈298 nm), indicating moderate concentration-dependent aggregation.

Detailed Analysis of Polymer Systems

IB-alt-MA-g-PEG. Increasing concentration from 0.10% to 0.25% w/w caused a marked rise in mean particle size (445 nm to 662.6 ± 35.3 nm), followed by a modest decrease to 630.7 ± 18.5 nm at 0.50% w/w. This sharp increase suggests crossing of a critical aggregation threshold, beyond which micelle–aggregate formation becomes thermodynamically favourable (104). The slight reduction at 0.50% w/w may reflect structural rearrangement or compaction. Practically, ≥0.25% w/w yields >600 nm aggregates, which risk turbidity and sedimentation, although viscosity effects were not measured here.

MA-alt-C_{18}-g-PEG. Mean sizes were 175.8 ± 51.2 nm (0.10% w/w), 298.1 ± 59.7 nm (0.25% w/w), and 231.4 ± 52.2 nm (0.50% w/w). This profile suggests initial growth followed by compaction, but large error bars indicate substantial variability. Within the tested range, MA-alt-C_8 -g-PEG shows weak and inconsistent concentration dependence. Further characterisation (PDI, zeta potential, time resolved stability) is required to confirm structural transitions(105, 106).

LIR410-g-PEG. In contrast, LIR410-g-PEG exhibited a clear monotonic decrease in size with concentration: 373 ± 8 nm (0.10% w/w), 311 ± 10 nm (0.25% w/w), and 237 ± 10 nm (0.50% w/w). This inverse relationship aligns with PEG-based amphiphilic systems, where higher polymer availability promotes more efficient self-assembly and tighter packing, reducing hydrodynamic diameter through thinner hydration shells and steric interactions (107, 108).

Comparative Summary

At matched concentrations, IB-alt-MA-g-PEG consistently formed the largest aggregates (≥445–663 nm), LIR410-g-PEG the smallest (373–237 nm), and MA-alt-C_8-g-PEG intermediate but variable (~176–298–231 nm). These differences highlight the role of polymer chemistry and architecture in governing association, packing, and hydration.

From a delivery perspective, LIR410-g-PEG at 0.50% w/w yields compact particles (~237 nm) favourable for systemic or targeted applications requiring sub-300 nm carriers. IB-alt-MA-g-PEG at ≥0.25% w/w produces large aggregates (>600 nm), potentially useful for depot or sustained-release formulations but requiring attention to syringeability and stability. MA-alt-C_8-g-PEG remains a candidate pending optimisation to reduce variability.

3.2.2 Effect of concentration on the aggregation structure of grafted and co-polymers (SANS)

The Guinier–Porod (GP) model combines a low-q Guinier regime with a high-q Porod regime, yielding size information such as the radius of gyration (Rg) and a dimensionality parameter *s* (0 for spheres, 1 for rods, 2 for lamellae). This model is widely applied to compact aggregates and micelles, where shape and surface characteristics dominate scattering behaviour (109).

In contrast, the two-Lorentzian model is shape-independent and describes scattering in terms of correlation lengths (ξ_1, ξ_2), which capture hierarchical or diffuse structures (Figure 3.2)[1] . Each Lorentzian term[3] corresponds to an Ornstein–Zernike-type decay of correlations, making this model particularly suitable for systems characterised by short-range order or clustering rather than discrete, well-defined particles (109).

In practice, the GP model is most appropriate for micellar systems such as MA-alt-C_8-g-PEG and LIR410-g-PEG, where Rg and the Porod exponent provide meaningful information on size and morphology. Conversely, the two-Lorentzian model is better suited to IB-alt-MA-g-PEG, which exhibits broad scattering features and concentration-dependent low-q intensity, indicative of correlated domains rather than discrete micelles (Table3.3).

[1] Chapter 32: Empirical Models (NIST SAŃS Toolbox)

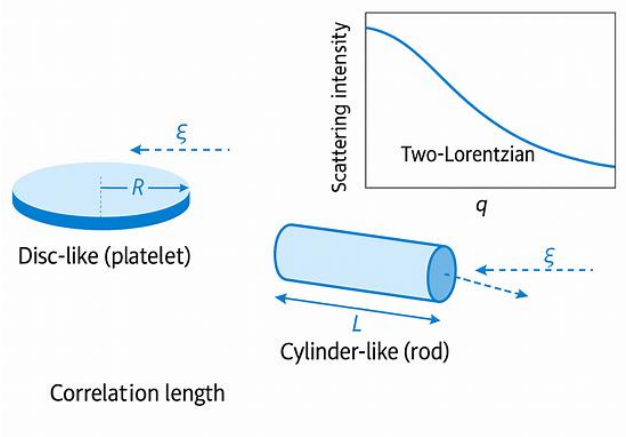

Fig.3.2: Schematic of Disc-Like and Cylinder-Like Aggregates with Correlation Lengths. Disc-like aggregates (left) are defined by radius R and thickness T; cylinder-like aggregates (right) by length L and radius a. Dashed arrows represent correlation lengths ξ, indicating short-range structural ordering. The inset shows a two-Lorentzian scattering profile, where each term reflects a distinct correlation scale. This model captures hierarchical or diffuse structures beyond the scope of Guinier–Porod analysis.

Table 3.3: Comparison of scattering models applied to polymer systems.

Model	**Key Parameters**	**Best suited for**	**Applied to**	**Interpretation**
Guinier–Porod	Radius of gyration (Rg), Porod exponent, dimensionality (s)	Compact micelles with defined shape	MA-alt-C_8 -g-PEG, LIR410-g-PEG	Provides size and morphology; suitable for spherical or rod-like aggregates
Two-Lorentzian	Correlation lengths (ξ_1, ξ_2)	Diffuse or hierarchical domains	IB-alt-MA-g-PEG	Captures short-range order and clustering; indicates network-like or loose packing

Figure 3.3 shows representative SANS intensity profiles for co-polymer IB-alt-MA-g-PEG at three different concentrations in D_2O and in deuterated THF as a good solvent.

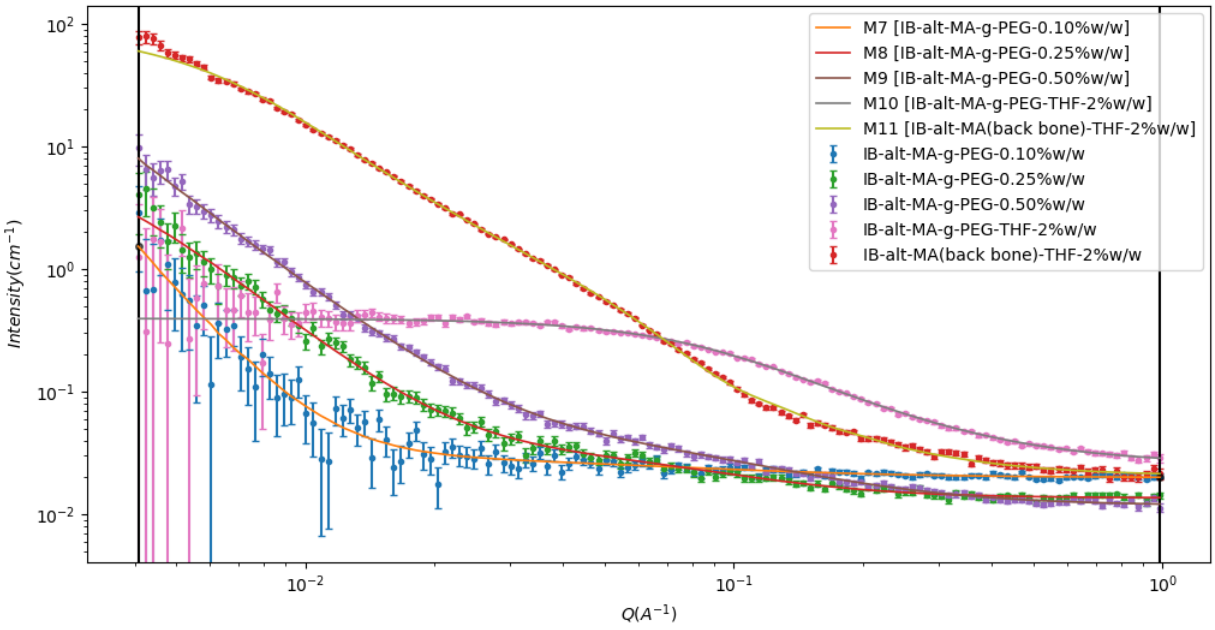

Fig.3.3: Small-angle neutron scattering (SANS) profiles of IB-alt-MA-g-PEG at varying concentrations. Scattering intensity (cm^{-1}) is plotted against the scattering vector Q ($Å^{-1}$) on a log–log scale. Data sets correspond to IB-alt-MA-g-PEG at 0.10%, 0.25%, and 0.50% w/w in D_2O, alongside 2 %w/w sample in d-THF, and IB-alt-MA 2 %w/w back bone in d-THF. Error bars denote measurement uncertainty. The curves illustrate concentration-dependent low-q upturns and broad features, consistent with correlated domains rather than discrete micelles. Fitted lines represent the applied scattering models, highlighting differences in structural interpretation across conditions.

Table 3.4: a) The combined Two-Lorentzian analysis confirms that the IB-alt-MA-g-PEG samples at 0.1–0.5 %w/w, **b)** IB-alt-MA-g-PEG 2%w/w in d-THF, **c)** IB-alt-MA 2%w/w in d-THF, the applied models for fitting are Two-Lorentzian, polymer-exclude-volume, and polymer-micelle respectively.

a)

concentration	**Lorentz length1(Å)**	**Lorentz length2(Å)**	**Lorentz exp1**	**Lorentz exp2**	**χ^2**
0.10	1818.2 ± 3.6	14.6 ± 8.8	3.6 ± 0.6	1.6 ± 0.6	0.9
0.25	345. 7 ± 15.4	11.6 ± 2.1	2.8 ± 0.2	2.2 ± 0.3	0.8
0.50	4687.6 ± 4.7	9. 6 ± 1.3	2.6 ± 0.1	1.9 ± 0.2	0.7

b)

System	Rg (Å)	Porod-exp	χ^2
IB-alt-MA 2%w/w in d-THF	462.5 ± 20.2	1.9 ± 0.03	0.8

c)

System	radius Core (Å)	Rg (Å)	N_{agg}	χ^2
IB-alt-MA Backbone 2%w/w in d-THF	41.5± 3.2	173.5± 5.1	5.7± 0.3	2.5

The SANS profiles of IB-alt-MA-g-PEG at 0.10–0.50% w/w reveal a biphasic structural response consistent with the DLS trends. At 0.10% w/w, the scattering curve shows a smooth decay with minimal low-q upturn, indicating compact micelles with limited clustering. The Two-Lorentzian model provided stable fits across all concentrations (Table 3.4a), capturing both short-range internal structure ($L_1 \approx 9$–15 Å) and longer-range inter-aggregate correlations (L_2 ranging from 346 to 4688 Å). The initial decrease in L_2 from 1818 Å to 346 Å between 0.10 and 0.25% w/w suggests tighter packing or reduced spacing between aggregates. At 0.50% w/w, the sharp increase in L_2 to 4688 Å reflects the onset of swelling or loose clustering, consistent with the DLS-observed size expansion (110, 111).

The Lorentzian exponents (2.6–3.6) fall within the expected range for polymeric micelles and swollen domains, supporting the use of a Two-Lorentzian model to resolve overlapping structural features. This approach is particularly useful for systems exhibiting both intra-aggregate and inter-aggregate scattering, where unified models often suffer from parameter coupling and instability (112).

To contextualise the aqueous behaviour, SANS data from IB-alt-MA-g-PEG in d-THF (2% w/w) were fitted using a polymer-excluded-volume model (Table 3.4b). The extracted Rg of 462 Å and Porod exponent of 1.9 are characteristic of flexible polymer coils in good solvent conditions, justifying the use of this model (109). The excluded-volume model is appropriate for describing scattering from polymer chains where solvent quality leads to chain expansion and deviation from ideal Gaussian behaviour.

In contrast, the IB-alt-MA backbone in d-THF (Table 3.4c) was best described by a polymer-micelle model, yielding a core radius of 41.5 Å, Rg of 173.5 Å, and aggregation number of 5.7. These parameters indicate micelle-like clustering even in organic solvent, consistent with amphiphilic backbone behaviour(113, 114). The polymer-micelle model is well-suited for systems with a dense hydrophobic core and diffuse corona, and has been widely applied to amphiphilic block copolymers in both aqueous and organic media(115).

Model selection was guided by reduced χ^2 values, residual randomness, and physical plausibility. The Two-Lorentzian model was optimal for IB-alt-MA-g-PEG in water, where both intra- and inter-aggregate scattering features were present(116). The polymer-excluded-volume and polymer-micelle models were

applied only where justified by solvent conditions and molecular architecture(117). Reported uncertainties were derived from covariance matrices and Porod slope regressions, with propagated errors summarised in Table 3.4. A caveat remains that Rg estimates assume the Guinier knee lies within the measured q-range; where this was not fully accessible, values should be considered conservative(118).

Characterization of the Ungrafted IB-alt-MA Backbone in d-THF

To provide a baseline for understanding the role of PEG grafting, the ungrafted poly (isobutylene-alt-maleic anhydride) backbone was characterised in deuterated tetrahydrofuran (d-THF), a good solvent for the anhydride functional groups. The structure is different in THF as the solvent is the good solvent for both the backbone and PEG and therefore there is no aggregation, while polymer is in theta state (119, 120).

These findings complement the DLS results: while LIR410-g-PEG exhibited concentration-dependent size reduction due to tighter packing and more efficient self-assembly, IB-alt-MA-g-PEG displayed a biphasic trend with initial compaction followed by swelling, and MA-alt-C_{18}-g-PEG showed variable aggregation behaviour. SANS confirmed these trends by quantifying changes in aggregation number and core dimensions, particularly for MA-alt-C_{18}-g-PEG, where higher concentrations produced more compact micelles with increased aggregation numbers.

Robustness of the analysis was ensured by treating the low-q Guinier region and the high-q Porod region independently, thereby reducing parameter coupling and avoiding instability common in unified multiregime fits. Reported uncertainties derive from covariance matrices of the Guinier fits and linear regression of the Porod slopes, with propagated errors presented in Table 3.4. A caveat remains that inferred Rg values assume the Guinier knee lies within the measured q-range; where the plateau was not fully accessible, values should be considered conservative estimates. Model selection was guided by reduced χ^2, residual randomness, and physical plausibility. Alternative fits (Guinier–Porod, Debye coil, flexible cylinder, Two-Lorentzian) were tested, with Two-Lorentzian providing the most stable and interpretable parameters for IB-alt-MA-g-PEG in this concentration range.

DLS is highly sensitive to large, loosely associated clusters and diffuse coronas that dominate light scattering and therefore yield large apparent sizes. In contrast, SANS primarily resolves the dense internal cores at higher q, where form-factor scattering dominates, and contributions from low-density outer regions are minimal. Together, these complementary observations support a hierarchical aggregation model in which compact nanoscale cores coexist within larger, dynamic superstructures that govern the hydrodynamic sizes detected by DLS. Full fitting details and q-range specifications are provided in Appendix A and B.

3.3 Effect of pH on Particle Characteristics[1]

Systematic adjustment of pH produced clear and reproducible changes in hydrodynamic size and dispersity across all formulations, demonstrating a measurable pH-dependence of colloidal behaviour. Variations in protonation state altered polymer ionisation, hydration, and interparticle interactions, leading to shifts in micelle packing, aggregation tendency, and overall dispersion stability. In general, acidic conditions favoured smaller and more compact particles, whereas alkaline conditions promoted larger, more polydisperse aggregates, indicating the onset of weak clustering. This pH responsiveness is highly relevant for predicting in-vivo performance, as physiological environments such as the gastrointestinal tract or tumour microenvironments exhibit substantial pH heterogeneity. Understanding these transitions is therefore essential for designing formulations with controlled stability, release behaviour, and site-specific performance(6, 121).

3.3.1 pH-Responsive Behaviour Across Polymer Systems (DLS)

The three polymer systems, IB-alt-MA-g-PEG, MA-alt-C_8-g-PEG, and LIR410-g-PEG, displayed distinct pH-dependent behaviours, confirming that protonation–deprotonation equilibria strongly influence colloidal structure (Figure 3.4).

IB-alt-MA-g-PEG (2% w/w) showed moderate sensitivity: particle size decreased under mildly acidic conditions and increased sharply at alkaline pH, consistent with reduced solubility and enhanced interparticle association at high ionisation levels (122). MA-alt-C_8-g-PEG (2% w/w) exhibited a pronounced maximum in size around pH 8, reflecting competition between hydrophobic C18 segments and ionisation of maleic anhydride groups; structural rearrangement at higher pH accounted for the subsequent decrease (105, 106). LIR410-g-PEG (5% w/w) demonstrated the strongest pH-driven expansion, increasing from ~200 nm in acidic media to >850 nm at pH 12, attributable to enhanced hydration and electrostatic repulsion within the PEG-rich corona (123).

These divergent responses suggest that LIR410-g-PEG is well suited for stimuli-responsive applications, whereas IB-alt-MA-g-PEG and MA-alt-C_8-g-PEG may offer more controlled behaviour in environments with narrower physiological pH ranges(124, 125). Because DLS is dominated by scattering from large, loosely associated clusters, these trends do not necessarily reflect changes in the underlying nanoscale core structure.

[1] Because each polymer exhibits unique structural responses to pH, detailed data tables are presented separately to avoid misleading comparisons. A combined schematic graph is included at the end of this section to provide a visual overview of size trends across polymers, but interpretation should consider the distinct chemistry of each system.

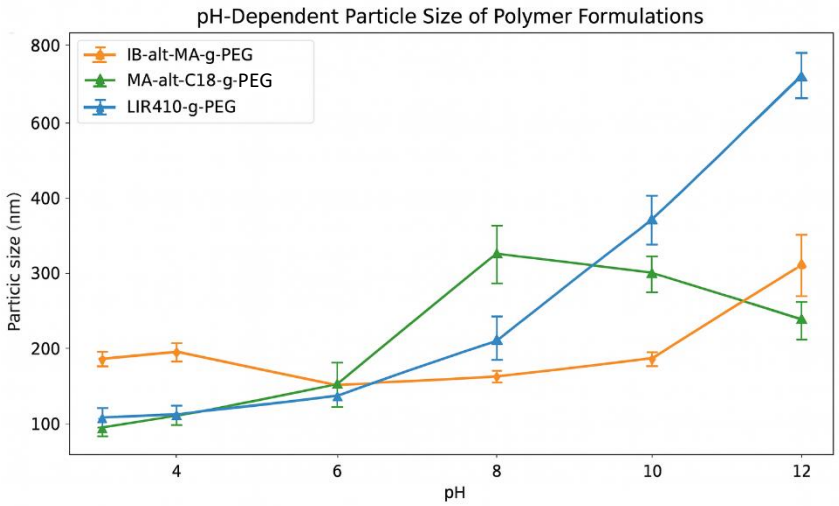

Fig 3.4: pH-Dependent Particle Size of Polymer Formulations (DLS). Particle size variation of IB-alt-MA-g-PEG (2% w/w), MA-alt-C_{18}-g-PEG (2% w/w), and LIR410-g-PEG (5% w/w) as a function of pH, measured by dynamic light scattering. LIR410-g-PEG shows pronounced swelling under alkaline conditions, MA-alt-C_{18}-g-PEG peaks near pH 8, and IB-alt-MA-g-PEG exhibits moderate pH sensitivity. Error bars indicate standard deviation across replicates.

3.3.1.1 IB-alt-MA-g-PEG pH-sensitivity (DLS)

To resolve the structural origin of the pH-dependent behaviour, IB-alt-MA-g-PEG (2% w/w) was further examined using SANS at pH 3, 6, 8, and 12. The polymer contains alternating isobutylene and maleic anhydride units; upon hydrolysis, the anhydride converts to maleic acid, which possesses two carboxylic groups with pKa values of ~1.9 and ~6.1(126). At low pH, these groups remain largely protonated, resulting in minimal electrostatic repulsion and favouring compact micellar structures (127, 128).

At intermediate pH, partial ionisation introduces negative charges that expand the micelles. At high pH, full ionisation produces strong repulsion, leading to micelle swelling and the appearance of secondary aggregation, consistent with the increase in hydrodynamic size observed by DLS(108). Overall, the DLS results confirm that IB-alt-MA-g-PEG exhibits moderate but distinct pH-responsive behaviour, driven primarily by the ionisation dynamics of maleic acid groups. This controlled responsiveness suggests its suitability for applications operating within physiologically relevant pH windows (126).

Figure 3.5 shows the pH-responsive behavior of maleic acid-functionalised polymers, highlighting their structural transitions across acidic, neutral, and alkaline environments. At low pH, protonated carboxylic groups minimize electrostatic repulsion, resulting in compact micelle formation. As pH increases toward neutrality, partial deprotonation stabilizes the structure, balancing hydrophobic and hydrophilic interactions. Under alkaline conditions, full deprotonation of maleic acid groups generates negatively charged carboxylates, inducing electrostatic repulsion and pronounced swelling. These transitions underpin tunable micelle morphology and responsiveness, critical for controlled release, solubility modulation, and adaptive material design.

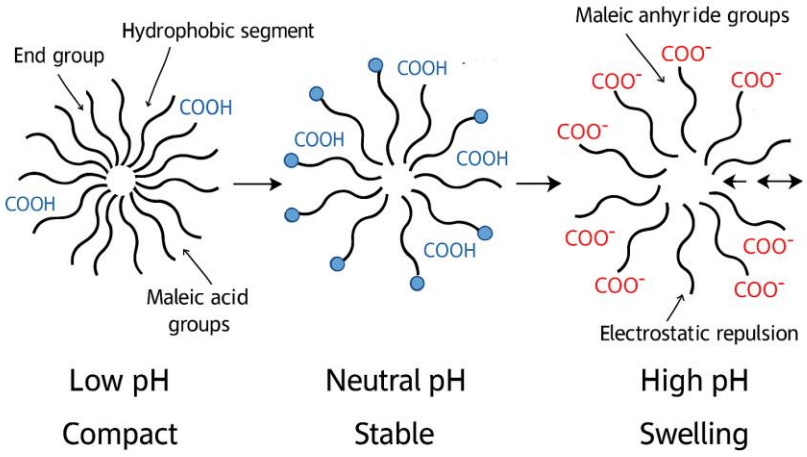

Fig. 3.5: Schematic illustration of pH-dependent micelle behaviour. At low pH, protonated maleic acid groups (–COOH) promote compact micelles with minimal electrostatic repulsion. Partial ionisation at intermediate pH stabilises the structure through a balance of hydrophobic and electrostatic interactions. At high pH, full ionisation to carboxylate groups ($–COO^-$) induces strong repulsion, leading to micelle swelling and increased particle size(105).

3.3.1.2 IB-alt-MA-g-PEG pH effect on characterisation (SANS)

Small-angle neutron scattering (SANS) was employed to examine the structural response of IB-alt-MA-g-PEG micelles to pH variation. As shown in Figure 3.6, the scattering intensity profiles change appreciably across pH 3, 6, 9, and 12, demonstrating that ionisation of maleic anhydride-derived groups strongly influences micellar architecture.

At pH 3, the maleic acid groups are predominantly protonated and hydrophobic, favouring compact micellar assembly. The broad peak likely originates from correlations within the swollen, hydrated PEG-rich corona, where Gaussian-like chain fluctuations create diffuse inhomogeneities. Polydispersity in micelle size and shape smears out expected form factor oscillations (e.g., minima from perfect spheres), rendering rigid geometric models less effective and making the empirical broad_peak approach suitable for capturing these features(129).

The scattering profiles in Figure 3.6 were fitted using a Two-Lorentzian model, as described in Table 3.5. This model does not assume a core–shell geometry; rather, it separates the scattering into two characteristic regimes. The short-range Lorentzian term yields a correlation length (ξ) associated with local density fluctuations within polymer-rich domains, while the long-range term captures inter-aggregate correlations. The Porod exponent extracted from the high-q region reflects the smoothness of the polymer–solvent interface and the compactness of the scattering objects (4). Although the model does not explicitly impose a core–shell structure, the combination of a stable short-range correlation length and Porod exponents approaching 4 suggests the presence of compact internal domains surrounded by more diffuse

polymer regions. This interpretation is qualitative and consistent with micelle-like assemblies, but it should not be taken as a direct morphological fit.

Collectively, these pH dependent changes in the SANS curves demonstrate that ionisation state governs internal organisation and packing density within the aggregates. SANS therefore serves as a crucial complement to DLS, providing access to nanoscale features such as radius of gyration (Rg), correlation lengths, and interfacial characteristics, all of which are highly sensitive to electrostatic and hydration driven rearrangements (105, 108).

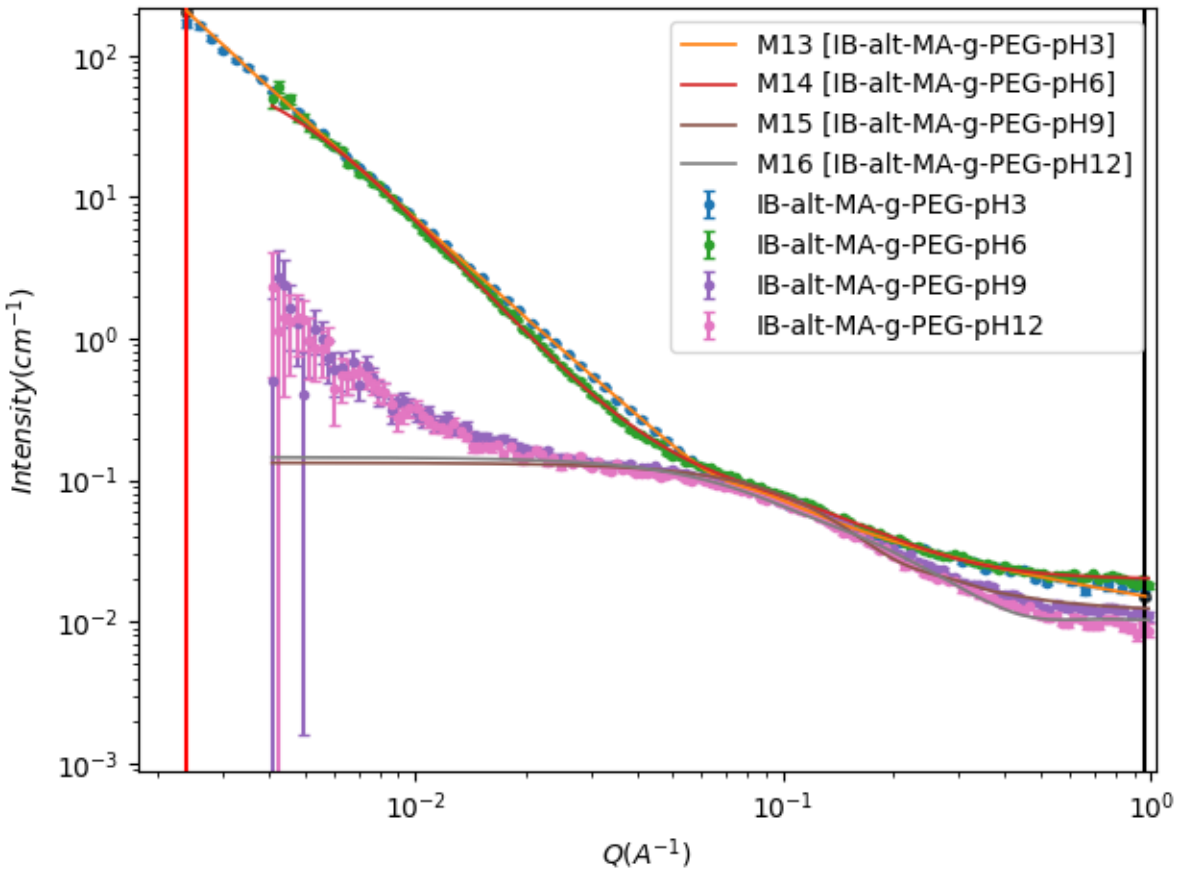

Fig 3.6: SANS intensity profiles of IB-alt-MA-g-PEG (2 %w/w) at pH 3, 6, 9, and 12, plotted as log–log intensity versus scattering vector Q(Å^{-1}). Each curve represents a distinct pH condition, revealing how ionisation of maleic anhydride groups modulates aggregation. At pH 3, high and low-q intensity and steep decay indicate compact micelles with strong interchain correlations. The graph illustrates a significant pH-dependent structural transition.

Table 3.5: Summary of SANS fits for IB-alt-MA-g-PEG at different pH values (2 %w/w).

pH	Best model	lorentz_len_1 (Å)	lorentz_len_2 (Å)	lorentz_exp _1	lorentz_exp _2	X^2
3	Two-Lorentzian	686.7 ± 30.4	4.1 ± 0.2	2.4 ± 0.0	3.3 ± 0.4	3.3
6	Two-Lorentzian	251.7 ± 8.1	7.2 ± 0.2	2.8 ± 0.0	2.7 ± 0.1	2.1
		Length (Å)	**Radius (Å)**			X^2
9	solid cylinder	65.7 ± 1.0	6.8 ± 0.1			4.5
12	solid cylinder	62.6 ± 1.1	6.7 ± 0.1			4.7

The Small-Angle Neutron Scattering (SANS) analysis of the IB-alt-MA-g-PEG samples demonstrates a clear structural transition driven by the pH-dependent ionization of the maleic acid (MA) backbone. The experimental scattering profiles were fitted using two distinct theoretical frameworks, the Two Lorentzian model and the solid cylinder model, to accurately reflect the changing mesoscopic organization of the polymer in solution[1] [,1] [5] [6] .

At pH 3 and 6, the system exhibits a hierarchical structure best captured by the Two Lorentzian model. In this regime, the primary length scale (lorentz_length_1) is notably large, reaching 686.7 Å at pH 3. This indicates the presence of large-scale aggregates or clusters, likely formed by hydrogen bonding between the PEG side chains and the protonated carboxylic acid groups of the IB-alt-MA backbone. The observed intensity upturn at low values, particularly at pH 3 and 6, is primarily attributed to the formation of these large-scale aggregates. However, it should be noted that such features can also arise from slight attractive interactions between polymer chains as the system approaches a phase boundary. Additionally, considering the relatively large error bars in the low-region for some samples, a potential contribution from slight under-subtraction of the background during data reduction cannot be entirely ruled out, which might artificially enhance the scattering intensity at these scales. The secondary, much smaller length scale (4.1–7.2 Å) corresponds to local segment-level fluctuations or the "mesh size" within these larger domains. As the pH increases to 6, the contraction of the primary length scale to 251.7 Å marks the onset of deprotonation, which introduces electrostatic repulsion[1] [7] and begins to disrupt these massive clusters (130, 131).

At highly alkaline conditions (pH 9 and 12), the data is most effectively described by the Correlation Length model. The disappearance of the large-scale Lorentzian component confirms that the aggregates have dissolved into a more homogeneous, well-solubilised network of expanded polymer chains. The resulting correlation length of ~9.7 Å reflects a uniform distribution of polymer segments in the solvent, where the ionized backbone provides sufficient charge repulsion to prevent cluster formation. The stability

[1] SANS Course, Chapter 23: "Scattering from Polymers", available at: sciencetopics.net
[1] NIST Center for Neutron Research, "SANS Model Documentation v4.10", [Online]. Available: www.nist.gov
[1] https://www.sasview.org/docs/user/models/two_lorentzian.html

of the Porod and Lorentz exponents in this range further indicates that the network has reached a steady-state conformation with consistent fractal characteristics(132, 133).

Visually, the SANS figures would show a pronounced high-intensity "upturn" at low scattering vectors (q) for acidic pH, which is the signature of the large lorentz_length_1 clusters. At pH 9 and 12, the polymer no longer forms an amorphous network; instead, it has self-assembled into well-defined cylindrical structures (likely rod-like micelles). The "Length" of ~65 Å and "Radius" of ~6.7 Å provide specific physical dimensions for these carriers.

At highly alkaline conditions (pH 9 and 12), the scattering data is most effectively described by a Cylinder-Cylinder model. The transition from the Two Lorentzian model used at lower pH to a discrete geometric model confirms that the disordered aggregates have reorganized into well-defined, elongated cylindrical micelles. The resulting structures exhibit a consistent length of ~63–66 Å and a radius of ~6.7–6.8 Å. This shift indicates that the fully ionized backbone, while providing charge repulsion, does not simply lead to a homogeneous solution but rather drives the formation of stable, anisotropic assemblies with highly uniform dimensions.

Implications for drug delivery:

The pH-responsive structural transitions of IB-alt-MA-g-PEG copolymers observed via SANS offer versatile mechanisms for advanced pharmaceutical applications. These implications extend beyond simple release, touching on stability, localization, and bioavailability:

- pH-Dependent "Switch" from Aggregates to Rods: The transition from a bulk aggregated state (Two Lorentzian) to a discrete cylindrical geometry provides a clear structural "switch." This morphological change, from large, loose clusters to compact, rigid rods, can be exploited for precision drug release. Such a transition is ideal for biological trigger points, such as the pH increase encountered when moving from the acidic environment of the stomach to the alkaline small intestine(134).
- Dual-Cargo Encapsulation and Protection: The hierarchical architecture at lower pH, containing both long-range aggregates and local segment fluctuations, can potentially house different types of therapeutic agents simultaneously(135). Large-scale clusters can sequester hydrophobic drugs, while the smaller mesh-like regions within the network can protect hydrophilic peptides or proteins from enzymatic degradation in the gastric environment.
- pH-Dependent "Switch" from Aggregates to Rods: The transition from a bulk aggregated state (Two Lorentzian) to a discrete cylindrical geometry provides a clear structural "switch." This morphological change, from large, loose clusters to compact, rigid rods, can be exploited for precision drug release. Such a transition is ideal for biological trigger points, such as the pH increase encountered when moving from the acidic environment of the stomach to the alkaline small intestine.

- Avoidance of "Burst Release": By forming stable, inter-polymer aggregates in the "off" state (acidic pH), the system can effectively minimize the common "burst release" effect where a drug is released prematurely before reaching the target. The high lorentz_length_1 values indicate a dense matrix that physically entraps the payload until deprotonation occurs((134).
- Tunable Pharmacokinetics via PEG Grafts: The PEG segments not only facilitate the structural transition but also provide essential "stealth" properties, reducing protein adsorption and renal clearance(136). This extends the systemic circulation time of the nanocarriers, allowing them more opportunity to accumulate at disease sites through the enhanced permeability and retention (EPR) effect before the pH-triggered release is activated(137).

3.3.1.3 MA-alt-C_{18}-g-PEG pH-sensitivity (DLS)

MA-alt-C_8 -g-PEG is an amphiphilic copolymer composed of alternating hydrophobic octadecene units and reactive maleic anhydride groups, which strongly dictate its pH-dependent behaviour. In aqueous environments, the anhydride groups hydrolyse to form carboxylic acids.

At low pH, these groups remain protonated, minimising electrostatic repulsion and favouring compact micelle structures. As pH increases, ionisation of the carboxyl groups introduces negative charges along the polymer backbone, enhancing electrostatic repulsion, micelle swelling, and larger particle sizes (106) .

The DLS data reveal substantial variability (Figure 3.4), particularly at higher pH values. Large standard deviations and overlapping error margins between pH 6, 8, and 12 suggest that the apparent peak at pH 8 may not be statistically significant. Additional replicates and statistical analysis are required to confirm whether these changes represent genuine structural transitions or experimental uncertainty. Mechanistically, the behaviour aligns with the expected pH-triggered ionisation of maleic anhydride groups:

- **Low pH:** Protonated carboxyl groups allow hydrophobic interactions to dominate, producing tightly packed micelles.
- **Intermediate pH (~8):** Partial ionisation increases hydration and repulsion, leading to micelle expansion and the observed peak in particle size.
- **High pH (≥12):** Full ionisation generates strong electrostatic forces, which may cause further swelling or secondary aggregation due to disrupted micelle packing (138).

This pH-responsive behaviour is consistent with previous studies on poly(maleic anhydride-alt-1-octadecene), where the degree of ionisation directly influences water retention, particle dispersion, and micelle morphology (106).

The observed trend reflects the interplay between hydrophobic interactions from the long octadecene chains and the ionisation of maleic anhydride groups. At low pH, limited ionisation permits hydrophobic interactions to dominate, yielding compact micelles. As pH rises, hydrolysis and ionisation into

carboxylate anions introduce electrostatic repulsion and hydration, causing micelles to swell and become more loosely aggregated. Beyond pH 8, further ionisation may lead to partial disassembly or rearrangement of micelle structures, explaining the slight reduction in particle size at pH 12 (138, 139).

Such pH-responsive behaviour suggests that MA-alt-C_8-g-PEG can be tuned for controlled drug delivery, particularly in environments where pH varies, such as the gastrointestinal tract or tumour microenvironments. The ability to swell or disassemble in response to pH changes could be exploited for site-specific drug release. Future studies may explore how modifying hydrophobic chain length or copolymer ratio influences this sensitivity and stability(124, 140).

3.3.1.4 MA-alt-C_{18}-g-PEG pH effect on characterisation (SANS)

To further investigate the structural behaviour of MA-alt-C_8-g-PEG under aqueous conditions, small-angle neutron scattering (SANS) measurements were performed at 5% w/w in D_2O at 298 K. The resulting scattering profile, shown in Figure 3.7, was fitted using a poly-micelle model. The fit yielded a radius of gyration (R_g) of 85.5 Å, a core radius of 63.7 Å, and an aggregation number of 11.2, indicating moderately sized micellar assemblies.

Guinier–Porod analysis supported these findings, with a dimensionality parameter consistent with spherical micelles. The presence of a well-defined core–shell architecture suggests that MA-alt-C_8-g-PEG forms stable aggregates under these conditions, with hydrophobic octadecene segments forming the core and grafted PEG groups contributing to the hydrated shell.

These structural parameters align with the amphiphilic nature of MA-alt-C_8-g-PEG and its pH-responsive behaviour observed in DLS. The spherical morphology and moderate aggregation number suggest a balance between hydrophobic packing and electrostatic repulsion, which may be tuned by environmental pH. This supports MA-alt-C_8-g-PEG's potential as a responsive carrier system, particularly in physiological environments where pH fluctuations can modulate micelle stability and drug release dynamics.

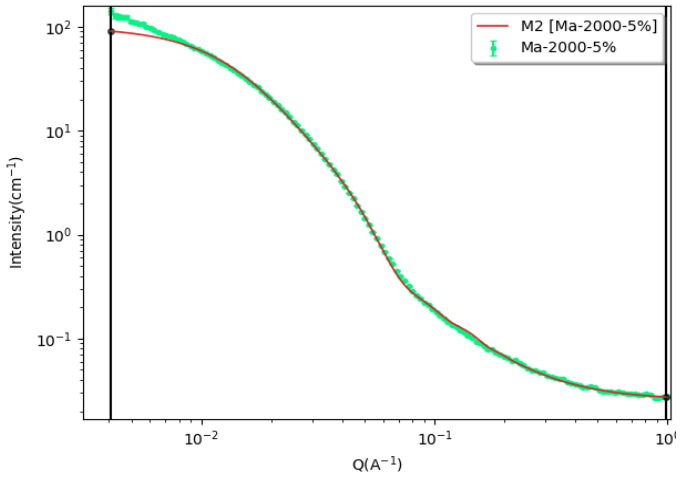

Fig.3.7: SANS profile of MA-alt-C18-g-PEG (5% w/w in D_2O, 310 K).

Experimental data (green points) are fitted with the poly micelle model (red line), yielding Rg = 85.5 Å, core radius = 63.7 Å, and aggregation number = 11.2.

Guinier–Porod analysis confirms spherical micelles with core–shell

To investigate the pH-responsive aggregation of MA-alt-C_{8} -g-PEG, small-angle neutron scattering (SANS) measurements were also performed at 2 % w/w in D_2O across pH 3, 6, 8, and 12 at 298 K. The alternating hydrophobic octadecene segments and ionisable maleic anhydride-derived carboxyl groups confer pronounced pH sensitivity: at low pH, protonated carboxyl groups minimise electrostatic repulsion and promote compact micelle formation; with increasing pH, progressive ionisation enhances hydration and repulsion, ultimately leading to aggregate swelling or disassembly. In the context of styrene-maleic acid (SMA) or octadecene-maleic anhydride copolymers, swelling occurs due to a transition in the polymer's conformation and hydration state as pH increases(141, 142).

Probable reasons of swelling:

- Electrostatic Repulsion: As pH rises above the pKa of the carboxyl groups (~4.5–6.0), the groups deprotonate to form negatively charged carboxylates (COO^-). These fixed negative charges along the polymer backbone repel each other, forcing the previously compact "hypercoil" or micelle to expand and increase its volume.
- Hydrophilicity: The charged carboxylate groups are significantly more hydrophilic than neutral carboxylic acids, which increases the polymer's affinity for water(143).

The proposed core–shell micellar architecture, with a hydrophobic octadecene-rich core and a hydrated shell composed of ionised maleic acid and PEG chains, is illustrated schematically in Figure 3.8, highlighting the expected structural changes with pH.

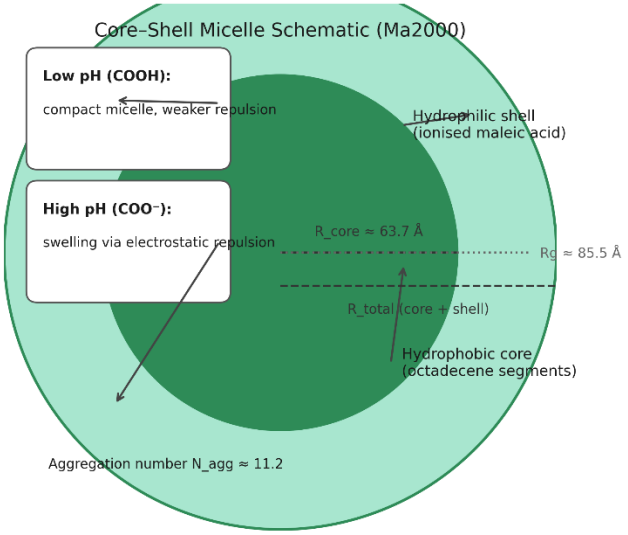

Fig.3.8 Core–shell micelle schematic for MA-alt-C_{18}-g-PEG. The hydrophobic core (octadecene) is surrounded by a hydrophilic shell of ionised maleic acid groups. Annotated dimensions include core radius, total radius, radius of gyration, and aggregation number. pH-dependent behaviour is illustrated: compact micelles at low pH (COOH) and swollen structures at high pH (COO^-), consistent with SANS and DLS findings.

Previous studies support this behaviour. Salamanca et al. (2018) reported pH-dependent swelling and rearrangement in MA-alt-C_{8} -g-PEG micelles (not grafted like our samples), with particle size peaking near pH 8 due to partial ionisation (106). Popescu et al. (2014) observed that electrostatic repulsion at alkaline pH disrupts micelle packing, resulting in smaller, more dispersed aggregates. Technical datasheets

(Sigma-Aldrich, 2022) also highlight that hydrolysis of maleic anhydride to maleic acid introduces pH-sensitive carboxyl groups, directly modulating micelle stability and dispersity(105).

This mechanistic understanding complements the core–shell schematic shown in Figure 3.8 and provides context for the scattering profiles presented in Figure 3.9, which illustrate how micelle structure evolves with pH.

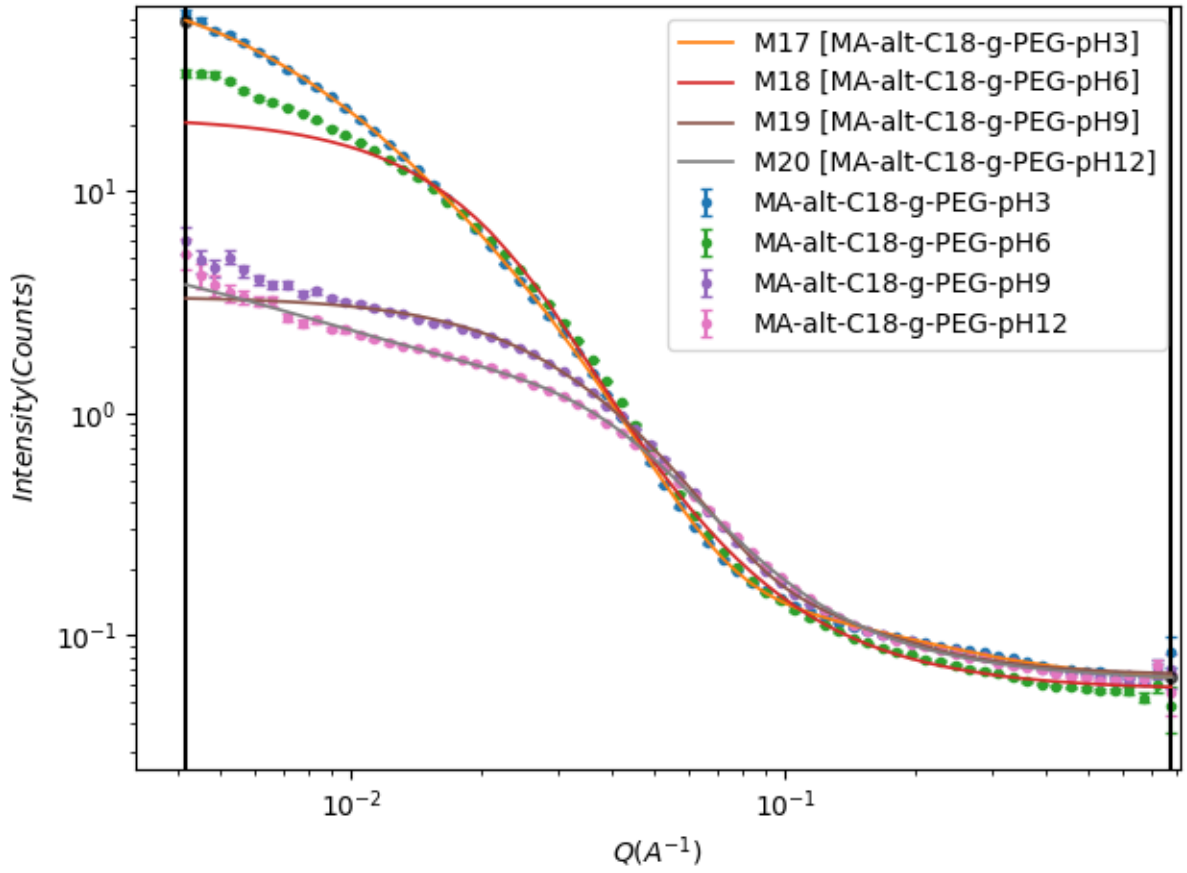

Fig 3.9: SANS profiles of MA-alt-C$_8$-g-PEG (2% w/w in D_2O) at pH 3, 6, 9, and 12. Experimental data (coloured markers) and fitted curves (solid lines) reveal pH-dependent changes in scattering intensity and aggregate structure.

At acidic pH (3), the high low-q intensity and Rg values (of around 100 nm) indicate compact micelles with strong hydrophobic packing. This agrees with Salamanca et al. (2018), who reported that MA-alt-C$_8$-g-PEG micelles are most stable and compact under acidic conditions due to protonated maleic acid

groups. At near-neutral pH (6)[1], partial ionisation introduces electrostatic repulsion, producing hierarchical domains with multiple correlation lengths, and Salamanca et al. (2018) observed similar swelling behaviour near pH 8, where micelles expand but remain stable. At alkaline pH (9), full ionisation reduces interchain attraction, shortening correlation length and dispersing aggregates; Popescu et al. (2014) described this as a disruption of hydrophobic packing by electrostatic forces, leading to smaller, less correlated micelles. At strongly alkaline pH (12), repulsion dominates, further shortening ξ and flattening the low q profile, while mid q curvature suggests rod-like motifs consistent with semiflexible chain behaviour (144). Popescu et al. (2014) noted that ionised maleic acid groups destabilise micelles, producing dispersed or elongated structures (145). Across all pH values, Porod exponents remain ~3.3–3.6, close to the theoretical value of 4 for smooth interfaces, indicating that while aggregate size and correlation change with pH, the micelles maintain compact, smooth surfaces, a finding consistent with several studies (146-149).

Table 3.6: Summary of SANS analysis for MA-alt-C_8-g-PEG (2 %w/w) at different pH values. The applied models for pH 3,6 was fractal core-shell and for pH 9,12 was spherical polymer-micelle.

pH	Fractal Dimension	Correlation Length(Å)	Core-shell radius(Å)	X^2
3	2.8 ± 0.0	78.4 ± 0.3	8.2 ± 0.1	74.0
6	2.9 ± 0.0	53.5 ± 0.2	9.3 ± 0.1	34.0
	N_{agg}	Rg (Å)	radius_core(Å)	X^2
9	3.4 ± 2.5	31.1 ± 3.3	34.5 ± 1.8	10.5
12	1.3 ± 2.1	42.5 ± 18.2	37.8 ± 0.8	8.3

The SANS fitting results, summarized in the table, provide strong quantitative evidence for the pH-responsive structural transition of the MA-alt-C_8-g-PEG copolymer. At low pH values (pH 3 and 6), the material forms large, dense fractal aggregates characterized by a high fractal dimension (approximately 2.8-2.9), indicating a compact structure resulting from the protonated, hydrophobic state of the carboxyl groups. These aggregates exhibit significant correlation lengths (between 53-78 Å). As the pH is increased to 9 and 12, the system undergoes a profound reorganization: the large aggregates disassemble into smaller, individual polymer micelles (indicated by the shift in models and much lower X^2 values), driven by the electrostatic repulsion of the deprotonated carboxylate groups. This transition involves a significant increase in the individual particle's core radius (from ~9 Å in the aggregates to ~35-38 Å in the micelles), a morphological change consistent with the swelling and hydration of the system as water penetrates the core region(150, 151).

Implications for Drug Delivery

MA-alt-C_{18}-g-PEG exhibits an unusually sharp, pH-triggered burst disassembly around physiological-to-alkaline pH, in contrast to the gradual swelling/elongation seen with IB-alt-MA-g-PEG. This makes it an

[1] This analysis was performed specifically for IB-ALT-MA-G-PEG and MA-alt-C_{18}-g-PEG. While other graft copolymer (LIR410-g-PEG) was studied in separate experiments, they were not included in this study.

excellent candidate for oral drug delivery (stable large micelles in gastric acid, rapid release in intestinal pH > 7) or tumour extracellular pH-triggered release applications.

3.3.1.5 LIR410 pH-sensitivity (DLS)

Dynamic light scattering (DLS) was used to evaluate the pH-responsive behaviour of LIR410-g-PEG at 5 % w/w in deionised water. The hydrodynamic diameter increased progressively with pH: ~228 nm at pH 3, ~275 nm at pH 5, ~374 nm at pH 8, and ~856 nm at pH 12 (Figure 3.4).

The compact size observed under acidic conditions reflects protonation of ionisable groups, minimising electrostatic repulsion and favouring hydrogen-bonded, collapsed structures. As pH rises, deprotonation introduces negative charges, enhancing hydration and chain repulsion, which drives marked swelling and, at pH 12, possible secondary aggregation or network formation.

This monotonic, pronounced expansion is characteristic of PEG-grafted polyelectrolytes and is consistent with literature reports on pH- and thermo-responsive PEG-based micelles and nanogels(107, 108, 125). The large size change (>3-fold) positions LIR410-g-PEG as a highly sensitive candidate for stimuli-responsive delivery, particularly in environments exhibiting significant pH gradients such as the gastrointestinal tract (pH 1–8) or the tumour extracellular space (pH 6.5–7.2). Unlike IB-alt-MA-g-PEG and MA-alt-C_8-g-PEG, SANS data were not acquired for this polymer; however, the DLS trend provides clear evidence of strong pH responsiveness.

3.4 Thermoresponsive Behaviour

The temperature-dependent hydrodynamic diameter of the three graft copolymers was investigated by DLS over the range 15–45 °C (Figure 3.10). Due to differences in solubility and colloidal stability, measurements were performed at different polymer concentrations: LIR410-g-PEG at 1 % w/w, and IB-alt-MA-g-PEG and MA-alt-C_8-g-PEG at 5 % w/w. Consequently, the comparison below is qualitative and focuses on general trends rather than absolute values.

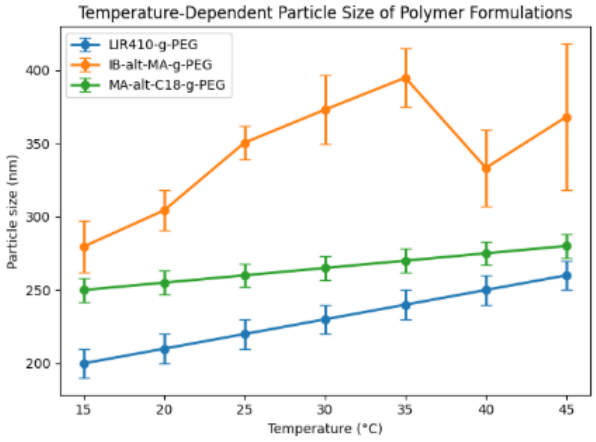

Fig.3.10: Temperature-dependent particle size of LIR410-g-PEG (1%), MA-alt-C_{18}-g-PEG (5%), and IB-alt-MA-g-PEG (5%) formulations. Mean particle size (±SD) is plotted against temperature (15–45 °C). IB-alt-MA-g-PEG shows consistently larger aggregates, while LIR410-g-PEG and MA-alt-C_{18}-g-PEG exhibit moderate size increases with temperature, reflecting general thermoresponsive behaviour.

LIR410-g-PEG (1 % w/w): displayed clear thermoresponsive behaviour, with particle diameter increasing steadily from 162 ± 3 nm at 15 °C to 227 ± 10 nm at 45 °C (152). This gradual expansion is consistent with temperature-induced dehydration of PEG chains and enhanced chain mobility commonly observed in PEGylated systems (153, 154).

MA-alt-C_{18}-g-PEG (5 % w/w): showed it is not basically temperature sensitive, with size rising from 244 ± 8 nm at 15 °C to 278 ± 7 nm at 45 °C. The increase may reflect partial dehydration of the PEG corona or secondary aggregation driven by the highly hydrophobic C18 side chains (155).

IB-alt-MA-g-PEG (5 % w/w): exhibited moderately large particle sizes (280–395 nm) with a clear temperature-dependent trend. The particle size increased steadily from 279.6 nm at 15 °C to a peak of 394.7 nm at 35 °C, followed by a dip at 40 °C and partial recovery at 45 °C. This non-monotonic behaviour suggests a balance between thermal expansion and possible partial disassembly or reorganisation at higher temperatures. The observed variation, supported by substantial standard deviations (±11.4 to ±50.1 nm), indicates that the aggregates are structurally responsive rather than rigid. The data imply moderate chain flexibility and dynamic rearrangement, likely influenced by the alternating backbone and hydrophilic–hydrophobic balance. These features enhance the formulation's potential for temperature-triggered drug delivery, where controlled expansion or dispersion can modulate release kinetics (156).

Overall, LIR410-g-PEG displayed the most pronounced and predictable thermoresponsiveness, whereas MA-alt-C_8-g-PEG appeared essentially thermoresistant within the studied range, and IB-alt-MA-g-PEG showed a moderate temperature-dependent increase in particle size up to 35 °C followed by a decrease and partial recovery at higher temperatures, indicating intermediate rather than fully thermoresistant behaviour. These differences highlight the dominant influence of backbone hydrophobicity and graft architecture on thermal behaviour (155). While the concentration discrepancy precludes direct quantitative comparison, the trends are sufficiently distinct to guide polymer selection: LIR410-g-PEG for applications

requiring thermal modulation (e.g., hyperthermia-triggered release), MA-alt-C_8-g-PEG for systems demanding high thermal stability, and IB-alt-MA-g-PEG for cases where an intermediate, partially temperature-responsive behaviour is advantageous.

Drug Delivery Perspective

From a drug delivery standpoint, LIR410-g-PEG demonstrates the most favourable characteristics, offering small, stable particles suitable for systemic applications and enhanced permeability and retention (EPR) effects. In contrast, IB-alt-MA-g-PEG and MA-alt-C_{18}-g-PEG may be better suited for localised or depot-based delivery systems, where larger particle sizes and slower release profiles are acceptable.

3.5 Conclusion

This study has systematically characterised the self-assembly behaviour of three amphiphilic graft copolymers, IB-alt-MA-g-PEG, MA-alt-C_{18}-g-PEG, and LIR410-g-PEG, using dynamic light scattering (DLS) and small-angle neutron scattering (SANS). The combination of hydrodynamic size data and detailed model-dependent structural analysis in SasView has revealed distinct concentration-, pH-, and temperature-responsive profiles, each conferring specific advantages and limitations for drug delivery applications. (Table 3.6, 3.7)

IB-alt-MA-g-PEG exhibits a sophisticated pH-dependent structural evolution, transitioning from disordered, multi-scale clusters to discrete cylindrical assemblies. While DLS suggests an increase in overall hydrodynamic size under alkaline conditions due to the progressive ionisation of maleic acid groups, SANS analysis reveals a fundamental morphological shift. At pH 3 and 6, the system is characterised by a Two Lorentzian profile, reflecting internal packing density and long-range correlations within loose aggregates. However, at pH 9 and 12, the system undergoes a discrete transition to a Cylinder-Cylinder morphology, forming rigid, rod-like structures with a consistent radius of ~6.7 Å and a length of ~65 Å. This shift from large-scale aggregates to defined nano-cylinders, combined with high thermal stability and predictable swelling, makes the polymer highly promising for localised delivery systems. The ability to trigger a transition into compact, uniform cylindrical units provides a unique mechanism for sustained release depots, where structural robustness and a defined geometric environment are advantageous for consistent drug elution.

MA-alt-C_{18}-g-PEG forms large, compact aggregates under acidic-to-neutral conditions, driven by strong hydrophobic interactions between C18 side chains. Above pH ~8, these aggregates undergo sharp, near-catastrophic disassembly, producing a pronounced burst-release profile. This switch-like behaviour aligns well with oral drug-delivery requirements: stability in gastric acid followed by rapid release in the more alkaline intestinal environment. Although some batch-to-batch variability is observed in DLS, the overall pH-triggered transition is robust and reproducible.

LIR410-g-PEG exhibits the most predictable and monotonic pH-responsive swelling of the three systems. Compact micelles (~160–250 nm) at low pH expand steadily with increasing alkalinity, reaching >800 nm

at high pH. Despite the absence of SANS data, the DLS results indicate a highly responsive, PEG-rich architecture capable of large, reversible volume transitions. This behaviour, combined with stable nanoscale dimensions under acidic and physiological conditions, makes LIR410-g-PEG particularly attractive for systemic nanomedicine, including prolonged circulation, EPR-mediated tumour accumulation, and pH-triggered release in acidic tumour or endosomal environments.

Table 3.6: Overview of pH-responsive structural changes in the three copolymers

Polymer	**Low pH (≤6)**	**Intermediate pH (~7–9)**	**High pH (≥10)**	**Most promising application**
IB-alt-MA-g-PEG	Compact core–shell spheres	Morphological transition to elongated units	Discrete nano-cylinders R~ 6.7Å , L~ 65 Å)	Precision depot release (pH-triggered rod formation)
MA-alt-C_8 -g-PEG	Very large compact aggregates	Onset of disassembly	Near-complete disruption	Burst release (oral delivery)
LIR410-g-PEG	Compact (~230 nm)	Moderate swelling (~370 nm)	Extreme swelling (>850 nm)	Large volume-transition systems (GI tract)

Table 3.7: Comparative summary of stimulus-responsive behaviour and drug-delivery implications.

Polymer	**Typical size (nm)**	**pH response**	**Temperature response**	**Primary drug-delivery implication**
IB-alt-MA-g-PEG	280–395	Cluster-to-Cylinder transition	Moderate increase up to 35 °C, then partial decrease and recovery (intermediate behaviour)	Intermediate responsiveness; pH-triggered structural release
MA-alt-C18-g-PEG	244–278	Sharp disassembly above pH ~8	Minimal change (thermally stable)	Oral burst-release (gastric → intestinal)
LIR410-g-PEG	160–250	Pronounced, reversible swelling	Clear, predictable expansion	Systemic nanomedicine, EPR effect, tumour targeting

Future work should incorporate structure-factor modelling and explicit polydispersity in SANS analysis, complemented by orthogonal techniques such as cryo-TEM, zeta-potential measurements (to quantify surface charge and address observed stability issues in large aggregates), and in vitro release studies under physiologically relevant conditions. These refinements will enable precise tailoring of polymer architecture for specific therapeutic applications, ranging from oral burst-release systems to injectable, tumour-targeted nanocarriers.

Chapter 4

Results and Discussion

(Encapsulation of hydrophobic drugs into core-shell grafted polymer structures)

4.0 Encapsulation of hydrophobic drugs into core-shell grafted polymer structures (effects of pH and concentrations)

This chapter investigates the encapsulation behaviour of two hydrophobic drugs, ibuprofen and oxaprozin, within self-assembled nanostructures formed by three polymer systems with distinct architectures: the grafted copolymer IB-alt-MA-g-PEG, the modified amphiphilic polymer MA-alt-C_8-g-PEG, and the PEG-grafted LIR410. Although these systems differ in chemical composition and branching architecture, all can form core–shell micellar assemblies (except IB-alt-MA-g-PEG) in aqueous media. Understanding how each polymer's structural features influence drug loading and colloidal stability is essential for identifying optimal formulation conditions.

Two complementary formulation strategies were therefore applied:

1. **Fixed drug concentration with varying polymer concentration**, to determine the minimum polymer content required for stabilising drug-loaded micelles and to assess how polymer availability influences particle size and aggregation behaviour.
2. **Fixed polymer concentration with varying drug concentration**, to identify the maximum drug-loading capacity of each system and to evaluate dispersion stability as a function of hydrophobic cargo.

Together, these strategies provide complementary insights: the first defines polymer efficiency in encapsulating a fixed amount of drug, while the second establishes the upper limits of drug loading. These results ultimately guide the identification of optimal formulation conditions for producing stable, reproducible micellar drug-delivery systems.

4.1 Drug–Polymer Compatibility Considerations

Ibuprofen and Oxaprozin are both hydrophobic, non-steroidal anti-inflammatory drugs (NSAIDs) of the propionic acid derivative class; however, their molecular characteristics differ significantly, influencing their compatibility with polymeric carriers (scheme 4.1, Table 4.1).

- **Ibuprofen**
  - Small, compact molecule with a simple aromatic ring and a single carboxylic acid group.
  - Facilitates hydrogen bonding and hydrophobic association with amphiphilic polymers.
  - Structural simplicity makes it more amenable to encapsulation within polymeric matrices or micellar systems, enabling formation of particles in the micron or submicron range.
- **Oxaprozin**
  - Bulkier, elongated structure with an extended aromatic system and additional functional groups.
  - Increased steric hindrance and reduced flexibility limit efficient accommodation within hydrophobic polymer domains.

- Disrupts packing and self-assembly processes, preventing stable microparticle formation with LIR410-g-PEG, IB-alt-MA-g-PEG, or MA-alt-C_{18}-g-PEG.

This structural incompatibility underscores the importance of drug–polymer molecular complementarity in designing polymer-based drug delivery systems. For example, IB-alt-MA-g-PEG (5% w/w) + Oxaprozin (0.01% w/w) yielded particles of 1109 ± 10 nm, while the same concentration with MA-alt-C_{18}-g-PEG produced 1217 ± 68 nm, both significantly larger than those observed with ibuprofen under similar conditions.

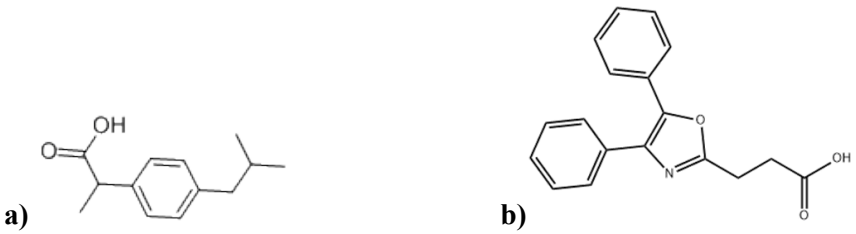

Scheme 4.1 a) Ibuprofen[1] and b) Oxaprozin[2] chemical structures.

Table 4.1: Drug–Polymer Compatibility Summary

Drug	**Molecular Features**	**Encapsulation Behaviour**	**Observed Particle Sizes (examples)**	**Compatibility with Polymers**
Ibuprofen	Small, compact; single aromatic ring; one carboxylic acid group	Favourable interactions (hydrogen bonding, hydrophobic association); stable nanoscale micelles	IB-alt-MA-g-PEG (5% + 0.25% drug): 363 ± 28 nm; LIR410-g-PEG (5% + 0.25% drug): 332 ± 17 nm	High compatibility; reproducible encapsulation across IB-alt-MA-g-PEG, MA-alt-C_8-g-PEG, LIR410-g-PEG
Oxaprozin	Bulkier, elongated; extended aromatic system; multiple functional groups	Steric hindrance disrupts micelle packing; poor encapsulation efficiency	IB-alt-MA-g-PEG (5% + 0.01% drug): 1109 ± 10 nm; MA-alt-C_8-g-PEG (5% + 0.01% drug): 1217 ± 68 nm	Low compatibility; unstable, oversized aggregates with all tested polymers

[1] Ibuprofen | 15687-27-1
[2] Oxaprozin | 21256-18-8

4.1.1 System A (polymer 5% w/w): effect of ibuprofen concentration

Overview of the Experimental Conditions

Dynamic Light Scattering (DLS) was employed to monitor the Z-average hydrodynamic diameter of three polymer systems, IB-alt-MA-g-PEG, MA-alt-C_{18}-g-PEG, and LIR410-g-PEG, across controlled ranges of polymer concentration (0.1–2.0% w/w), ibuprofen concentration (0.1–0.5% w/w), temperature (20–37 °C), and pH (3, 5, 8, 12). Complementary Small-Angle Neutron Scattering (SANS) measurements were used to characterise nanoscale organisation under varying pH and drug-loading conditions, providing structural insight beyond the size-only information obtainable from DLS.

Two complementary formulation systems were designed:

System A – Loading Window

Polymer concentration fixed at 5% w/w; ibuprofen varied (0.10–0.75% w/w) to identify the maximum loading that maintains nanoscale size and acceptable dispersion stability (Table 4.1; Figure 4.2).

System B – Polymer Sufficiency

Ibuprofen fixed at 0.25% w/w; polymer varied (0.1–2.0% w/w) to determine the minimum polymer concentration required to fully solubilise the drug and form stable assemblies.

Concentration ranges were selected based on pilot screens that yielded the most promising combinations for size stability and solubilisation. For ibuprofen, the loading window was intentionally chosen to steer particle sizes into the ~100–300 nm range favoured for systemic circulation and EPR-mediated tumour accumulation (4, 107).

Drug–Polymer Complementarity (Ibuprofen vs Oxaprozin)

Oxaprozin, owing to its bulkier and more rigid aromatic structure, showed poor compatibility with all three polymers at screening points. Even at extremely low drug levels (0.01% w/w), large particles were observed, e.g.:

- **IB-alt-MA-g-PEG 5% + oxaprozin 0.01% → 1109 ± 10 nm**
- **MA-alt-C_{18}-g-PEG 5% + oxaprozin 0.01% → 1217 ± 68 nm**

These sizes are drastically higher than those obtained with ibuprofen, indicating that oxaprozin disrupts polymer packing and does not integrate effectively into hydrophobic domains. This contrast highlights the importance of molecular complementarity for achieving compact, stable nanostructures. Although definitive proof of core encapsulation typically requires spectroscopy or microscopy, the coherent trends across DLS size reduction, SANS-derived micellar features, and visual solubilisation support effective ibuprofen incorporation into the polymeric cores (5).

Unless otherwise stated, subsequent sections focus on ibuprofen-loaded systems because ibuprofen demonstrated favourable encapsulation behaviour across all polymers (Table 4.2).

Table 4.2: Effect of Polymers and ibuprofen Concentration on Micelle Size in D_2O.

Formulation(%w/w)	**Particle Size (nm)**
IB-alt-MA-g-PEG 2 + drug 0.05	289 ± 10
IB-alt-MA-g-PEG 5 + drug 0.1	298 ± 10
IB-alt-MA-g-PEG5 + drug 0.25	363 ± 28
IB-alt-MA-g-PEG 5 + drug 0.5	537 ± 26
IB-alt-MA-g-PEG 5 + drug 0.75	817 ± 89
MA-alt-C_{18}-g-PEG 2 + drug 0.05	839 ± 38
MA-alt-C_{18}-g-PEG 5 + drug 0.1	248 ± 14
MA-alt-C_{18}-g-PEG 5 + drug 0.25	290 ± 15
MA-alt-C_{18}-g-PEG 5 + drug 0.5	422± 25
MA-alt-C_{18}-g-PEG 5 + drug 0.75	304 ± 94
LIR410-g-PEG 2 + drug 0.05	201 ± 8
LIR410-g-PEG 5 + drug 0.1	360 ± 26
LIR410-g-PEG 5 + drug 0.25	332 ± 17
LIR410-g-PEG 5 + drug 0.5	334 ± 7
LIR410-g-PEG 5 + drug 0.75	354 ± 15

Screening at 2% w/w polymer

The 2% data emphasise the importance of polymer sufficiency for effective micelle formation:

- **MA-alt-C_{18}-g-PEG 2% w/w + 0.05%w/w ibuprofen** produced very large particles (839 ± 38 nm), indicating inadequate polymer content to stabilise compact micelles.
- **IB-alt-MA-g-PEG 2% w/w+ 0.05% w/w ibuprofen** produced 289 ± 10 nm, showing more efficient micelle formation.
- **LIR410-g-PEG 2% w/w + 0.05% w/w ibuprofen** yielded the smallest size (201 ± 8 nm), consistent with strong steric stabilisation from PEG grafts and its ability to maintain nanoscale structure even at low polymer levels.

These results provide early evidence that LIR410-g-PEG is the most robust system under polymer-limited conditions, whereas MA-alt-C_{18}-g-PEG requires higher polymer content to produce stable nanostructures.

4.1.2 Effect of concentration on Particle Characteristics (DLS)

To quantify the influence of drug loading on micelle formation, ibuprofen concentration was systematically increased while polymer content was maintained at 5% w/w for all three grafted polymer systems. This design isolates the effect of drug incorporation from polymer sufficiency, allowing identification of the maximum ibuprofen loading compatible with stable nanoscale assemblies.

Maintaining particle diameters within the 100–400 nm window is widely considered optimal for systemic administration, ensuring favourable circulation half-life, reduced risk of uptake by the mononuclear phagocyte system, and effective EPR-mediated accumulation in tumour tissue (4, 107). Deviations beyond this range typically reflect overloaded micellar cores, partial aggregation, or compromised shell integrity.

Across all three polymers, DLS data (Table 4.2; Figure 4.1) showed a clear loading-dependent increase in hydrodynamic diameter, consistent with progressive incorporation of ibuprofen into the hydrophobic core. However, the polymers exhibited distinct tolerances to increased drug concentration.

• **IB-alt-MA-g-PEG** displayed a steady diameter increase from 298 ± 10 nm at 0.10% w/w drug to 537 ± 26 nm at 0.50% w/w, and further to 817 ± 89 nm at 0.75% w/w, indicating that beyond 0.25–0.50% w/w the system approaches its structural limit and begins to lose colloidal compactness.

• **MA-alt-C_{18}-g-PEG** maintained nanoscale size up to 0.25% w/w (290 ± 15 nm) but showed less predictable growth at higher loadings, suggesting a narrower encapsulation window and greater sensitivity to core-swelling effects.

• **LIR410-g-PEG** showed the highest resistance to ibuprofen-induced expansion: sizes remained within 330–360 nm across the full 0.10–0.75% w/w range, reflecting the strong steric stabilisation provided by its PEG corona and more efficient spatial accommodation of hydrophobic cargo.

Overall, these results indicate that while ibuprofen successfully integrates into the micellar cores of all three systems, the degree of structural tolerance is polymer dependent. LIR410-g-PEG supports the broadest loading range without excessive size inflation, whereas IB-alt-MA-g-PEG and MA-alt-C_{18}-g-PEG exhibit more defined upper thresholds beyond which micelles become increasingly swollen or potentially unstable. These DLS trends align with SANS-derived structural parameters (Sections 4.2–4.3), reinforcing that micellar swelling with increasing drug concentration corresponds to genuine core loading rather than aggregation artefacts.

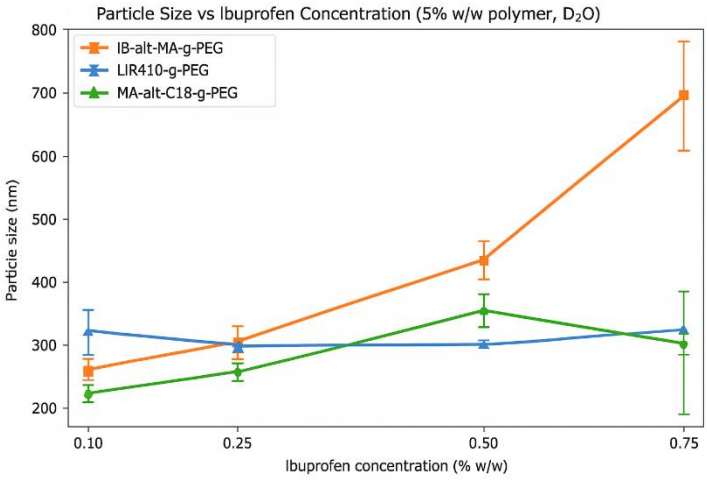

Fig.4.1: Particle size vs ibuprofen concentration for IB-alt-MA-g-PEG (orange), MA-alt-C_{18}-g-PEG (green), and LIR410-g-PEG (blue) at 5% w/w polymer. IB-alt-MA-g-PEG shows continuous size increase, MA-alt-C_{18}-g-PEG displays variable behaviour, and LIR410-g-PEG maintains stable nanoscale dimensions. LIR410-g-PEG is the most suitable for systemic delivery due to consistent particle size within the 200–400 nm range.

In the IB-alt-MA-g-PEG 5% w/w formulation, the particle size at 0.10% w/w ibuprofen was ~260 nm, suggesting efficient incorporation of drug molecules into the hydrophobic cores and tighter packing of the micelle structure. This compaction is consistent with favourable Gibbs free energy of solubilisation, where enthalpy gain from drug–core interactions outweigh entropic (4-6, 105) . At 0.25% w/w, the size increased to 323 nm, consistent with partial saturation of the cores and drug partitioning closer to the interfacial region. At 0.50% w/w, a sharp increase to 431 nm was observed, which may indicate the onset of aggregation or micelle fusion as the optimal drug-to-polymer ratio was exceeded. Comparable transitions in micelle morphology at high drug loading have been reported in polymeric micelle systems (157-159).

At 0.50 % w/w ibuprofen, the sharp increase in particle size may reflect a transition in micelle behaviour, potentially due to saturation of the hydrophobic core and changes in inter-micellar interactions. As drug loading exceeds the optimal drug-to-surfactant ratio, excess ibuprofen may localise near the micelle interface, disrupting surfactant packing and increasing hydrodynamic diameter. While this could suggest the onset of aggregation or micelle fusion, such conclusions require further evidence beyond DLS alone. Similar trends have been reported in polymeric micelle systems, where high drug loading alters corona hydration and micelle morphology (158, 159). This behaviour highlights the concentration-dependent swelling of IB-alt-MA-g-PEG micelles and suggests that systemic suitability is limited to lower drug loadings.

For MA-alt-C_8-g-PEG 5% w/w, the baseline particle size at 0.10% w/w ibuprofen was around 221 nm, indicating a critical concentration at which ibuprofen promotes micelle formation or disrupts aggregation. At 0.25% w/w, particle size increased to approximately 245 nm, reflecting partial re-expansion of the micelles. Beyond this point, particle size rose further, reaching roughly 350 nm at 0.50% w/w, with large error bars reflecting variability and poor reproducibility. This non-linear behaviour is consistent with reports of amphiphilic copolymers exhibiting unstable packing and re-aggregation at higher drug loads (159).

Overall, the data show that only IB-alt-MA-g-PEG exhibits pronounced concentration-dependent swelling and instability, whereas MA-alt-C_8-g-PEG and LIR410-g-PEG remain structurally stable across all ibuprofen concentrations tested.

In contrast, LIR410-g-PEG 5% w/w displayed a stable and narrow size profile across drug concentrations. The formulation measured ~318 nm at 0.10% w/w, decreased to ~298 nm at 0.25% w/w, and rebounded slightly to ~305 nm at 0.50% w/w. These modest changes suggest that PEG chains provide steric stabilisation, limiting structural disruption even as drug loading increases. Notably, the coefficient of variation was lowest at 0.50% w/w, indicating a more uniform dispersion at higher loading. This consistency aligns with previous findings that PEG grafting enhances dispersion stability and reproducibility in micellar systems (5, 158). Moderate ibuprofen loading (0.25–0.5% w/w) therefore produced smaller and more uniform particles than the drug-free baseline, positioning LIR410-g-PEG as the most reliable carrier among the three systems.

Taken together, IB-alt-MA-g-PEG shows compaction at low drug load but rapid swelling beyond 0.25%, MA-alt-C_8-g-PEG exhibits highly variable behaviour with only transient stability, and LIR410-g-PEG maintains a consistent nanoscale profile across concentrations. These findings reinforce LIR410-g-PEG as the most promising candidate for systemic delivery, where reproducible particle size within the 200–400 nm range is critical for circulation stability and EPR-based targeting (4, 107).

4.1.3 Methodological notes and limitations

Dynamic Light Scattering (DLS) Z-average values are intensity-weighted and therefore highly sensitive to small populations of large species. As a result, DLS alone cannot provide definitive structural information. For rigorous claims, DLS should be paired with complementary parameters such as the polydispersity index (PDI) and ζ-potential, while morphology should be validated using techniques such as Small-Angle Neutron Scattering (SANS), Size-Exclusion Chromatography (SEC), or cryo-TEM (Table 4.3). Furthermore, mapping the critical micelle concentration (CMC), encapsulation efficiency, and drug release kinetics is essential to establish causal links between drug loading, micelle structure, and in-vitro/in-vivo performance (99, 159).

Table 4.3: Complementary techniques for validating micelle characterisation and performance

Technique	**Clarifies**
DLS (Z-average, PDI, ζ-potential)	Size distribution, polydispersity, surface charge stability
SANS / SEC	Micelle morphology, aggregation state, and structural uniformity
Cryo-TEM	Direct visualisation of micelle shape and size
CMC mapping	Threshold for micelle formation and drug loading capacity
Encapsulation efficiency	Drug incorporation effectiveness
Release kinetics	Correlation between micelle structure and in-vitro/in-vivo performance

4.1.4 Effect of concentration on Particle Characteristics (SANS)

Understanding how polymer and ibuprofen concentrations influence nanoscale structure is essential for optimising micelle-based delivery systems. Variations in concentration can modify micelle formation, drug encapsulation, aggregation number, and colloidal stability. To assess these effects, SANS was used to examine structural changes in IB-alt-MA-g-PEG, MA-alt-C_8-g-PEG, and LIR410 micelles at different drug loadings. Particular focus was given to changes in low-q scattering, core radius, and indications of clustering, as these parameters directly relate to drug incorporation and potential release behaviour.

IB-alt-MA-g-PEG (5% w/w) with Increasing Ibuprofen Concentration

SANS analysis was used to examine how ibuprofen incorporation modifies the micellar architecture of IB-alt-MA-g-PEG at 5% w/w in D_2O at 37 °C. IB-alt-MA-g-PEG, forms amphiphilic assemblies due to its hydrophobic isobutylene segments and ionisable maleic anhydride groups grafted with hydrophilic PEG chains (Sigma Aldrich, 2022; ChemicalBook, 2025). Previous studies have shown that maleic anhydride-based copolymers can accommodate ibuprofen via hydrophobic partitioning, thereby altering micelle size and aggregation behaviour (100).

At 5% w/w polymer, drug-free IB-alt-MA-g-PEG generates compact micelles with smooth interfaces, evidenced by Porod exponents close to 4. Upon ibuprofen addition (Figure 4.4), a substantial increase in low-q intensity is observed, most prominently at 0.1% w/w ibuprofen, where I (q = 0.004 $Å^{-1}$) increases from ~150 to ~256 cm^{-1}. This rise indicates the formation of larger aggregates or weakly clustered micelles, consistent with hydrophobic interactions that enhance aggregation number.

The mid- and high-q regions (I (q = 0.010 $Å^{-1}$) ≈ 13.5–14.5 cm^{-1}) remain nearly identical across all drug loadings. This stability demonstrates that local chain conformation and surface smoothness are not disrupted by ibuprofen incorporation. Porod exponents of 3.3–3.6 further confirm the persistence of compact micelles, aligning with observations by Jin et al. (2019), who reported size enlargement without changes to surface character in similar copolymer systems.

A notable feature of IB-alt-MA-g-PEG is its non-monotonic clustering behaviour. The most pronounced low-q increase occurs at 0.1% w/w ibuprofen; at higher loadings (0.25–0.5%w/w), low-q intensity decreases slightly (to ~214–235 cm^{-1}). This suggests a threshold effect: small amounts of ibuprofen may bridge or associate multiple micelles, while higher drug loadings distribute more uniformly among cores, reducing cluster formation. Similar non-linear loading effects have been reported in amphiphilic copolymers with hydrophobic drug incorporation.

Across all drug concentrations, Two-Lorentzian model indicates the emergence of weak hierarchical clustering while preserving micelle integrity. These observations are consistent with previous studies reporting that maleic anhydride copolymers maintain their micellar framework while tuning aggregate size in response to additives or pH (105, 106).

Figure 4.4 presents the corresponding SANS profiles. The pronounced increase in low-q scattering at 0.1%w/w ibuprofen highlights enhanced clustering, while the overlapping mid- and high-q regions confirm structural stability at the micellar level. These profiles support the model selection and structural interpretation described above and reinforce literature reports of drug-induced aggregation behaviour in maleic anhydride copolymers.

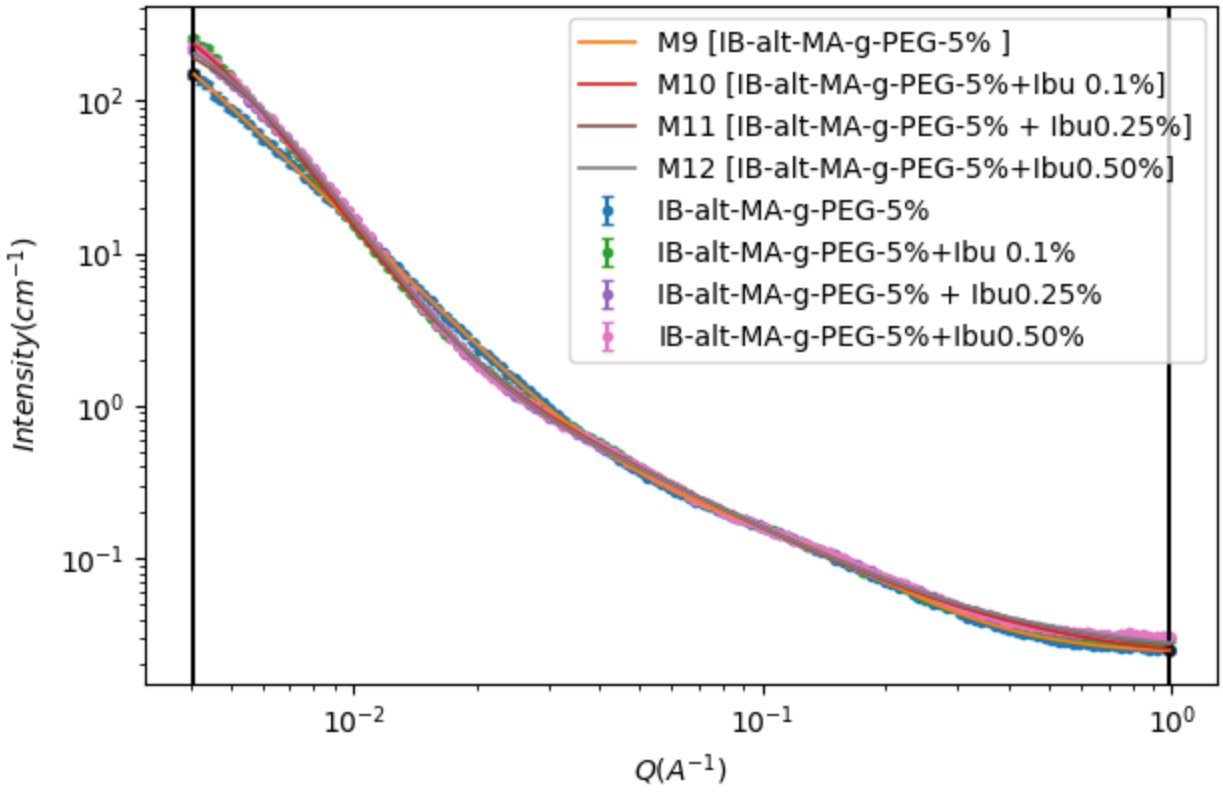

Fig.4.4: SANS intensity profiles of IB-alt-MA-g-PEG (5% w/w) at 37 °C with increasing ibuprofen concentrations (0–0.5% w/w). Experimental data (markers) and fitted model curves (lines) are shown. Low-q intensity rises most at 0.1% w/w, indicating weak micelle clustering, while mid- and high-q regions remain consistent, confirming preserved micelle interface character.

Table 4.4: Comparative SANS observables for IB-alt-MA-g-PEG (5% w/w, 37 °C) with varying ibuprofen concentrations(%w/w). The applied model is Two-Lorentzian model.

Ibuprofen	Lorentz length1(Å)	Lorentz length2(Å)	Lorentz exp1	Lorentz exp2	χ^2
0.00	462.5 ± 20.2	7.7 ± 0.1	2.7 ± 0.00	2.4 ± 0.03	1.4
0.1	272. 7 ± 5.5	79. 2 ± 7.9	3.8 ± 0.03	1.5 ± 0.01	8.7
0.25	224.5 ± 2.7	49. 7 ± 2.9	3.8 ± 0.02	1.5 ± 0.01	7.8
0.5	232.5 ± 3.0	50.7 ± 2.9	3.8 ± 0.02	1.5 ± 0.01	8.0

Summary of Suggested Morphology:

Because the exponents change from 2.7/2.4 (likely a loose, network-like structure) to 3.8/1.5 upon adding Ibuprofen, it can be concluded: Phase Separation/Aggregation: The shift to 3.8 suggests the Ibuprofen is causing the formation of particles with distinct, sharp surfaces (rather than a diffuse network). Elongation: The shift to 1.5 suggests these particles or the network segments between them are becoming more rod-like or elongated{Cao, 2022 #2}[2] .

Effect of Ibuprofen Concentration on MA-alt-C_{18}-g-PEG Micelle Architecture (SANS)

MA-alt-C_{18}-g-PEG is an amphiphilic alternating copolymer composed of hydrophobic octadecene units and ionisable maleic anhydride groups, which hydrolyse to maleic acid in aqueous solution. This dual character enables micelle formation and pH-responsive behaviour, making MA-alt-C_{18}-g-PEG a promising candidate for drug delivery systems (105, 106). Previous studies (145, 160-164)have shown that ibuprofen can partition into hydrophobic domains of maleic anhydride copolymers, altering micelle size and aggregation number.

The mid- and high-q regions (I (q=0.010 $Å^{-1}$) ~55–78 cm^{-1}) remain largely unchanged across all drug loadings, confirming preservation of local chain conformation and interface smoothness. Porod exponents near 3–4 further support the presence of compact micelles with smooth surfaces, consistent with reports showing that ibuprofen alters micelle size but not surface character in dual-responsive copolymer nanoparticles (100).

Unlike IB-alt-MA-g-PEG, where clustering peaked at 0.1% w/w ibuprofen, MA-alt-C_{18}-g-PEG exhibits a more monotonic increase in low-q intensity with drug concentration. This suggests that MA-alt-C_{18}-g-

[2] https://doi.org/10.1016/j.matdes.2022.110583

PEG micelles can accommodate higher drug loadings without destabilisation, in agreement with Salamanca et al. (2018), who reported pH-dependent swelling and rearrangement, and Popescu et al. (2014), who highlighted the stabilising role of electrostatic repulsion in aggregate dispersion.

Figure 4.5 shows the SANS intensity profiles of MA-alt-C18-g-PEG (5% w/w) at 37 °C with increasing ibuprofen concentrations (0–0.5% w/w). Visually, all curves for the different drug loadings are nearly superimposed. All samples display the characteristic decrease in scattering intensity with increasing Q, which is consistent with hierarchical micellar or poly-micellar structures. Compared with the drug-free polymer, the ibuprofen-loaded formulations exhibit only negligible visual differences in low-Q intensity. This observation suggests that the addition of ibuprofen does not drastically alter the overall scattering behaviour or structural length scales of the system within this concentration range. The curves largely overlap across all Q regions, indicating that the internal micellar conformation remains largely consistent across all ibuprofen loadings.

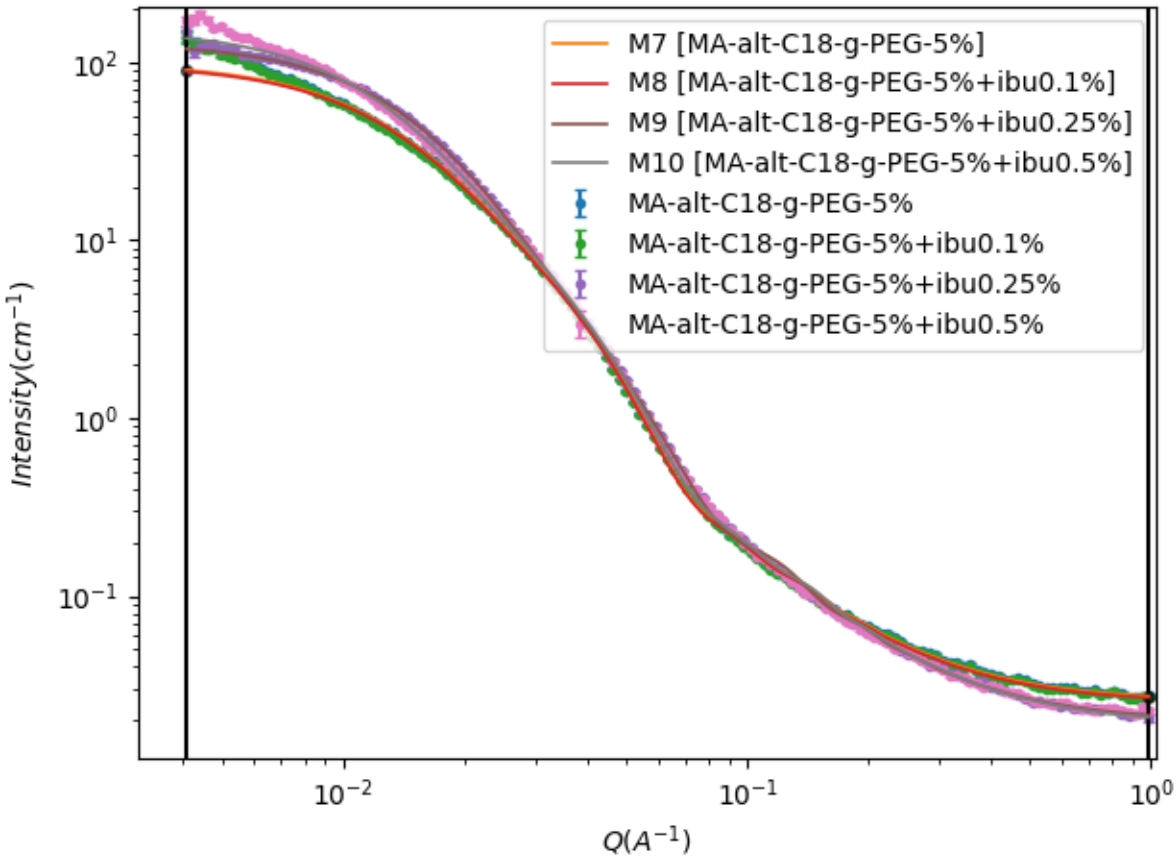

Fig.4.5: SANS intensity profiles of MA-alt-C_8 g-PEG (5% w/w) at 37 °C with increasing ibuprofen concentrations (0–0.5% w/w). Experimental data (markers) and fitted model curves (lines) are shown. A progressive increase in low-q intensity is observed with drug loading, consistent with the presence of larger-scale structures or enhanced micelle association, while mid- and high-q regions show minimal change.

Subtle slope changes in the mid-Q region at higher drug loadings imply the development of denser domains, while the High-Q region remains largely unchanged, indicating that local chain conformation is unaffected by ibuprofen. These observations align with the poly-micelle model fits (Table 4.5), which provide quantitative insight into structural transitions.

Table 4.5: Comparative SANS observables for MA-alt-C_8-g-PEG (5% w/w, 37 °C) with varying ibuprofen concentrations(%w/w). The applied model for this data set is Ploymer_micelle from Sphere.

Ibuprofen	**Radius_core(Å)**	**Rg(Å)**	**n_aggreg**	**χ2**
0.00	63.7 ± 0.2	85.4 ± 0.3	11.2 ± 0.1	20.7
0.10	63.7 ± 0.2	85. 3 ± 0.48	11.2 ± 0.5	21.7
0.25	47.1 ± 0.9	74.8 ± 8.2	21.0 ± 4.8	8.5
0.50	62.6 ± 0.2	94. 4 ± 0.4	14.5 ± 0.3	25.7

In the absence of ibuprofen, MA-alt-C_8-g-PEG micelles exhibit a core radius of approximately 63.7 Å and an aggregation number of ~11, characteristic of small, stable aggregates with smooth interfaces. At 0.1% w/w ibuprofen, both the core radius and aggregation number remain nearly unchanged, and no substantial increase in low-q intensity is observed. This indicates that micelle architecture is effectively preserved at low drug loading, consistent with reports that maleic anhydride copolymers can accommodate small amounts of hydrophobic drug without major structural disruption.

A pronounced transition occurs at 0.25% w/w ibuprofen, where the core radius decreases to ~47 Å while the aggregation number almost doubles (~21). This points to significant micellar reorganisation, likely involving the formation of more numerous, smaller micelles or partial fragmentation of larger aggregates. The corresponding SANS profile shows a clear enhancement in low-q intensity, supporting the interpretation that ibuprofen loading drives redistribution of hydrophobic domains within the polymer and promotes a higher aggregation number, in agreement with observations in dual-responsive copolymer systems.

At the highest concentration examined (0.5% w/w), the core radius increases again to ~62.6 Å, while the aggregation number remains elevated (~14) and the radius of gyration rises notably to ~94 Å. These changes point to the formation of larger, loosely associated clusters, accompanied by a marked low-q upturn in the scattering profile. Such behaviour indicates that high ibuprofen loading promotes partial inter-micelle association, potentially enhancing colloidal stability but also suggesting a denser network that may slow subsequent drug release.

Taken together, these results demonstrate that MA-alt-C_8-g-PEG micelles undergo a concentration-dependent structural response to ibuprofen loading. Moderate drug levels (0.25% w/w) induce substantial micellar restructuring that enhances drug accommodation by increasing the aggregation number and decreasing core size. Higher loading (0.5% w/w) triggers partial clustering, which may stabilise the micellar network but could compromise release efficiency. This dual behaviour highlights the need to optimise drug-to-polymer ratios to balance encapsulation capacity with desirable release profiles in MA-alt-C_8-g-PEG-based delivery systems.

Effect of Ibuprofen Concentration on LIR410-g-PEG Micelle Architecture (SANS)

In Figure 4.6, shape-predicting analysis is shown for LIR410-g-PEG 2%w/w in deuterated D_2O and 5%w/w in D_2O. As previously, first trying to find the most probable model by applying Guinier-Porod with Rg = 13.1Å, s = 0.23 and porod-exp = 1.6, which suggested the sphere category. Again, for this polymer, some of the auto-fitting values, such as sld-core, were not meaningful. Therefore, by using the Multimodal option, it could be possible to mix different models that, for this study, polymer-micelle and Guinier were mixed (Figure 4.6). The polymer micelle model explains the mid-Q region (core–corona structure), and the Guinier term accounts for the low-Q upturn (large-scale clustering or intermicellar associations).

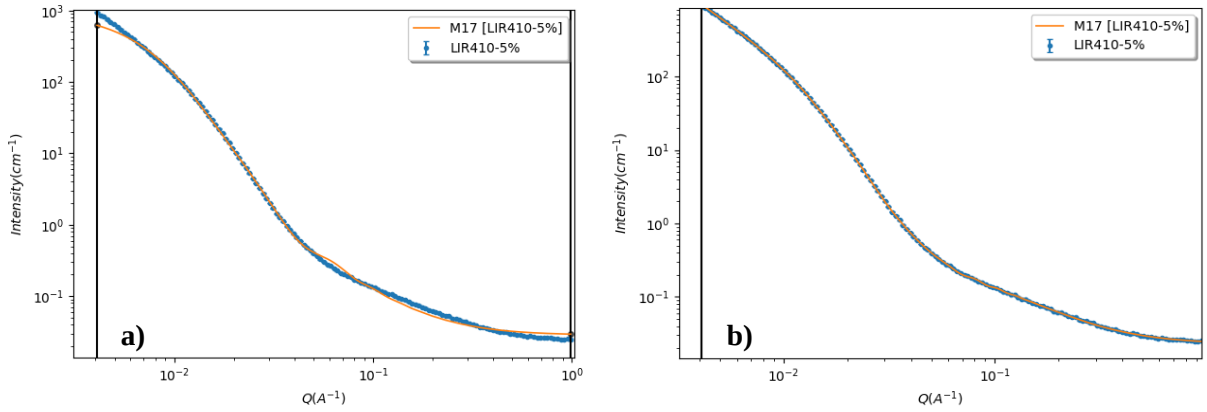

Fig.4.6: a) poly-micelle model, b) Guinier-poly_micelle multiply model.

Poly (ethylene glycol)-based amphiphilic such as LIR410-g-PEG are widely employed in drug-delivery applications due to their hydrophilic PEG corona, steric stabilisation, and ability to form micellar structures with hydrophobic cores. PEGylation is well recognised for enhancing colloidal stability, suppressing protein adsorption, and prolonging circulation time, making these systems attractive carriers for hydrophobic drugs such as ibuprofen. To assess whether ibuprofen loading alters the structural organisation of LIR410-g-PEG micelles, SANS measurements were performed on 5% w/w polymer solutions in D_2O at 37 °C with ibuprofen concentrations of 0%, 0.1%, 0.25%, and 0.5% w/w.

To quantify the effect of ibuprofen loading on LIR410-g-PEG micelle structure, SANS observables were compared across ibuprofen concentrations of 0–0.5% w/w at a fixed polymer level of 5% w/w. The key parameters summarised in Table 4.6 provide initial insight into changes in aggregate size, micelle stability, and the emergence of clustering behaviour.

The Low-Q intensity (I (q = 0.004 $Å^{-1}$)) increases sharply upon ibuprofen addition, rising from ~948 cm^{-1} in the drug-free sample to over 1170 cm^{-1} at 0.1% w/w. This indicates the formation of larger aggregates or enhanced micelle–micelle association driven by hydrophobic drug loading. Although the intensity decreases slightly at higher drug levels (0.25–0.5% w/w), it remains well above the drug-free baseline, confirming persistent clustering behaviour (Figure 4.7).

In contrast, the mid-Q region (I (q = 0.010 $Å^{-1}$)) shows only modest changes across all concentrations, suggesting that local chain conformation and corona structure are largely preserved. The High-Q overlap further supports the stability of the PEG corona and indicates that ibuprofen primarily affects larger-length-scale organisation rather than local segmental packing.

The shift from a single-level Guinier–Porod model (0% w/w ibuprofen) to a two-level unified model for all drug-loaded samples reflects the emergence of hierarchical structures and the onset of clustering. This structural transition is consistent with the formation of larger assemblies while retaining compact micelle cores.

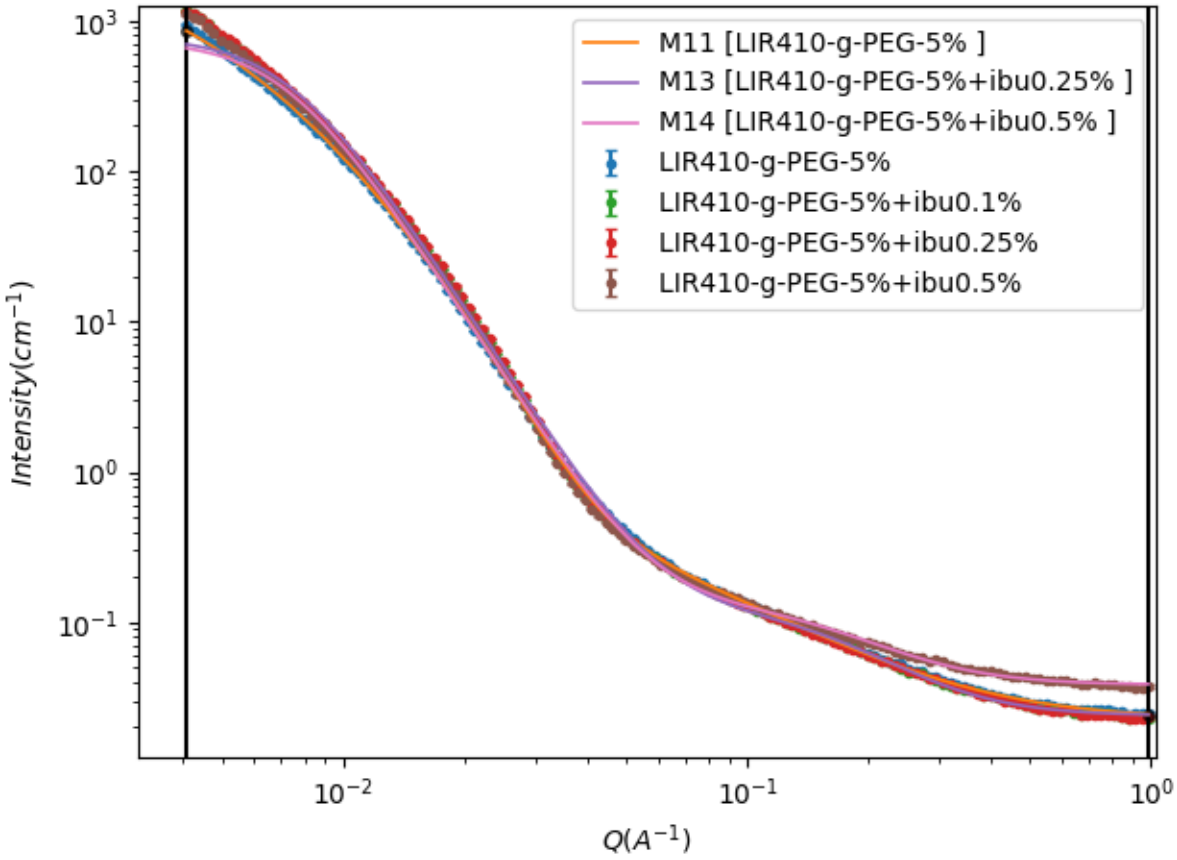

Fig.4.7: SANS intensity profiles of LIR410-g-PEG (5% w/w) at 37 °C with increasing ibuprofen concentrations (0–0.5% w/w). Experimental data (markers) and fitted model curves (lines) are shown. Low-q intensity remains stable across all drug loadings, indicating minimal clustering or aggregate growth. Mid- and high-q regions exhibit consistent slopes, confirming preserved micelle interface character and local chain conformation.

At low Q, the scattering intensity increases progressively with ibuprofen content, indicating the formation of larger aggregates or extended structures as drug loading rises. The strong upturn observed at 0.5% w/w ibuprofen is particularly indicative of weak inter-micellar clustering or loose network formation, a feature often associated with altered diffusion pathways and slower drug release (106).

In the mid-Q region, samples containing 0.25% and 0.5% w/w ibuprofen show a subtle change in slope, suggesting a transition toward denser or more compact internal domains. By contrast, the High-Q region overlaps closely for all samples, confirming that the local chain conformation and PEG corona structure remain largely unaffected by hydrophobic loading. This stability reflects the well-known steric resilience of PEG-based coronas, which maintain interface integrity even in the presence of core-modifying additives (158). To quantify the structural transitions observed in the scattering profiles, the poly-micelle–Guinier model was applied to LIR410-g-PEG systems at 5% w/w and 37 °C (Table 4.6).

The poly-micelle–Guinier hybrid model, which includes a core–corona form factor and a Guinier term for low-Q scattering from weak inter-micellar associations, captures these features (165). In the reported results, use the Guinier-Porod Rg to describe the "total package" (micelle + drug + PEG) and the Micelle Core Radius to describe where the Ibuprofen is actually sitting. If the Porod Exponent from GP model stays near 4, micelles have smooth, distinct surfaces; if it drops toward 2, PEG chains are likely very swollen and diffuse(166).

Table 4.6: Comparative SANS observables for LIR410-g-PEG (5% w/w, 37 °C) with varying ibuprofen concentrations(%w/w). The applied model for this data set is polymer-micelle-Guinier. Rg- Guinier is the total radius of the entire micelle, including the hydrated PEG shell, radius_core defines the radius of the hydrophobic inner region where Ibuprofen is encapsulated, Rg-PEG Corona the radius of gyration of a single PEG chain attached to the core.

Ibuprofen	Rg- Guinier (Å)	radius_core(Å)	Rg-PEG Corona(Å)	n_aggreg	χ2
0.00	83.6 ± 1.0	121.1 ± 0.6	12.7 ± 0.2	10.8 ± 3.0	2.1
0.10	106.4 ± 3.0	23.0 ± 3.4	41.8 ± 14.6	73.2 ± 38.9	19.4
0.25	94.6 ± 1.1	112. 7 ± 0.3	12.1 ± 0.1	19.3 ± 2.6	4.9
0.50	58.3 ± 0.7	54.2 ± 0.3	18.2 ± 0.3	6.6 ± 1.3	23.5

Core-Corona Relationship: Across the samples, the Rg of the PEG Corona remains relatively small (12–18Å, excluding the unstable 0.10%w/w sample), suggesting that the PEG chains are likely in a collapsed or "mushroom" conformation rather than an extended "brush" state(167, 168).

Fitting Limitations: The high χ2 values at 0.10 and 0.50%w/w confirm that Ibuprofen loading is not a linear process. The drug likely induces shape transitions (e.g., from spheres to cylinders) or polydispersity that a simple spherical core model cannot fully capture(169).

Optimal Loading: Based on the χ^2 and parameter stability, the 0.25 %w/w concentration represents the most successful incorporation of Ibuprofen into a stable, well-defined micellar structure.

4.1.5 Comparative Analysis of Ibuprofen Loading in IB-alt-MA-g-PEG, MA-alt-C_{18}-g-PEG, and LIR-PEG Micelles

Overview

The SANS datasets for IB-alt-MA-g-PEG, MA-alt-C_8-g-PEG, and LIR410-g-PEG at 5% w/w and 37 °C reveal distinct structural responses to ibuprofen incorporation. While all three polymers exhibit increased low-Q scattering with drug loading, reflecting enhanced aggregation or clustering, the nature and

progression of these changes differ significantly between systems. These differences highlight the influence of backbone chemistry, corona composition, and micelle stability on drug accommodation and release behaviour (106, 158).

4.1.6 Comparative Structural Behaviour

To directly compare the structural consequences of ibuprofen incorporation across the three polymer systems, the key SANS observables and fitted parameters are summarised in Table 4.7.

Table 4.7: Comparative Structural Behaviour of three studied polymers in presence of different drug concentrations.

Polymer system	Low-Q response	Mid-Q behaviour	High-Q behaviour	Core radius trend	Aggregation number trend	Interpretation
IB-alt-MA-g-PEG	Non-monotonic: strongest at 0.1% w/w ibu, weaker at 0.25–0.5% w/w	Stable slopes	Preserved interfaces	Decrease then recovery	Increase at 0.1% w/w, moderate at higher	Threshold clustering; depot-like behaviour at low drug, dispersed micelles at higher
MA-alt-C_{18}-g-PEG	Monotonic increase with drug loading	Slight slope changes at 0.25–0.5% w/w	Preserved interfaces	Decrease to 0.25%, recovery at 0.5% w/w	Doubling at 0.25%, elevated at 0.5% w/w	Progressive aggregation; structurally tolerant to higher drug loadings
PEG-g-LIR410	Unstable fluctuations: Max Rg at 0.10%; decrease at 0.50%w/w	Structural disruption at 0.10 & 0.50 %w/w	Poorly defined interfaces (High χ^2 >19)	Sharp collapse at 0.10 (23Å), recovery at 0.25 (113Å)	Extreme Spike at 0.10 (~73), stabilizes at 0.25 (~19)	Non-linear loading**:** Initial instability (0.10) precedes optimal drug-assisted packing (0.25). Excess drug (0.50) disrupts micellar integrity.

4.1.7 Implications for Drug Delivery

These results highlight the importance of tailoring drug-to-polymer ratios to the specific carrier system. IB-alt-MA-g-PEG requires careful optimisation to avoid non-monotonic clustering and ensure predictable

release. MA-alt-C_8-g-PEG tolerates higher drug loadings with progressive aggregation, favouring sustained release. LIR410-g-PEG achieves sustained release primarily through micelle population increases rather than core swelling, maintaining colloidal stability while slowing diffusion.

4.2 System B (ibuprofen 0.25% w/w): effect of polymer concentration

4.2.1 Effect of Polymer Concentration on Particle Size at Fixed Ibuprofen Loading

Varying IB-alt-MA-g-PEG concentrations in the presence of a fixed ibuprofen concentration (DLS)

To investigate the influence of polymer concentration on micelle formation and particle size at a fixed drug loading, dynamic light scattering (DLS) measurements were performed for IB-alt-MA-g-PEG systems containing 0.25% w/w ibuprofen and varying polymer concentrations (0.1–2.0% w/w).

As is shown in Figure 4.9, the particle size decreased sharply as IB-alt-MA-g-PEG concentration increased from 0.1% to 1.0% w/w, reaching a minimum at 1.0% w/w. This trend is consistent with the progressive self-assembly of surfactant molecules into micelles as the system approaches the critical micelle concentration (CMC). Below the CMC, surfactant monomers dominate, and particle size reflects loose aggregates or uncoated drug cores. As the concentration increases toward and beyond the CMC, micelle formation becomes more efficient, leading to smaller, more uniform particles.

At concentrations above 1.0% w/w, the particle size stabilises or slightly increases, suggesting saturation of micelle formation and possible onset of inter-micellar interactions or crowding effects. This behaviour aligns with previous reports on amphiphilic copolymer systems, where micelle size minimisation occurs near the CMC[2] (as is shown in Figure 4.8), followed by structural reorganisation at higher concentrations (170).

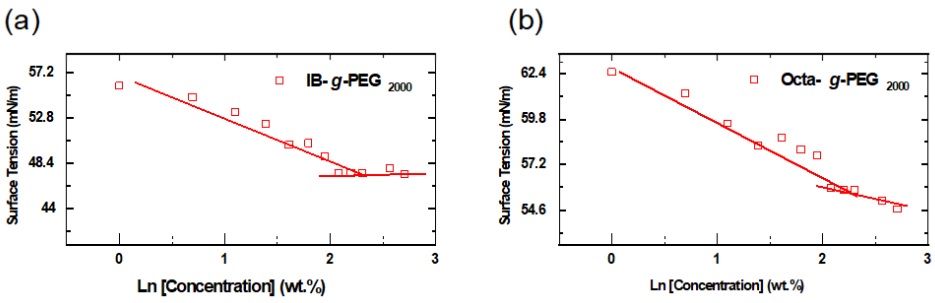

Fig 4.8: Surface tension measurements of grafted polymer-brine (undiluted seawater) droplet in air: (a) grafted PEG onto IB backbone, and (b) grafted PEG onto Octa backbone.

[2] The Figure (4.8) prepared by Dr. Wafaa Al Shatti, and I applied it hear under her authorization. https://specific-ikc.uk/wafaa-al-shatty/

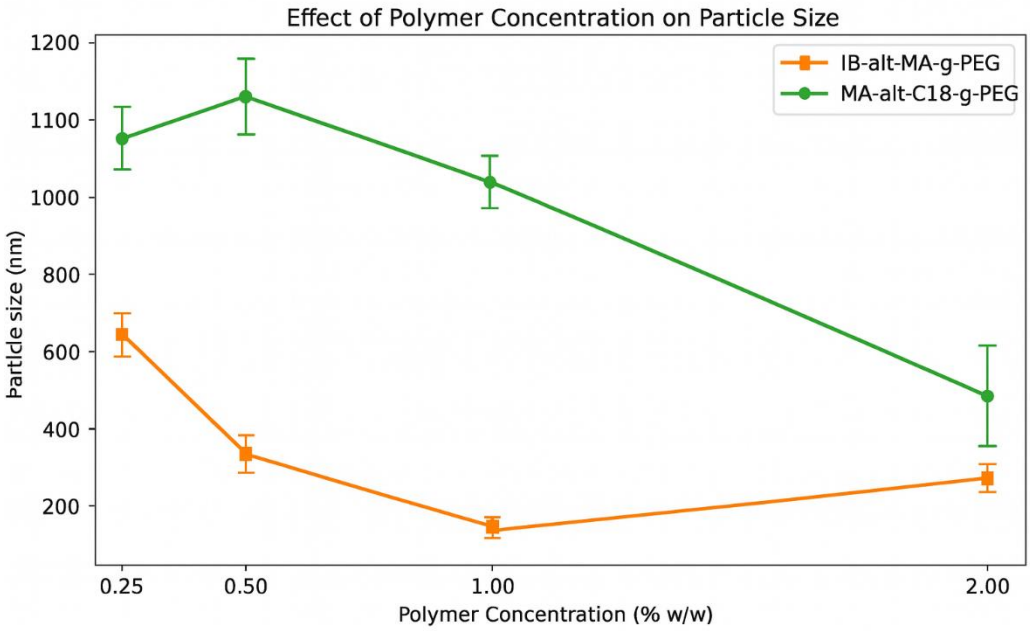

Fig.4.9: Effect of polymer concentration on particle size for two amphiphilic systems, highlighting architecture-dependent aggregation behaviour.

Both polymer systems exhibit concentration-dependent size transitions, though with distinct architectural signatures. IB-alt-MA-g-PEG displays a clear trend toward an optimal concentration for minimum size at 1.0% w/w; the particle size drops sharply from ~720 nm at 0.25% w/w to ~380 nm at 1.0% w/w. This is consistent with micelle compaction as the system approaches the critical micelle concentration (CMC), where improved packing yields more uniform assemblies. At higher concentrations (2.0% w/w), the size increases to ~470 nm, suggesting post-CMC swelling or emerging inter-micellar interactions.

In contrast, MA-alt-C_8-g-PEG maintains a relatively stable size profile at lower concentrations, with the first three data points (0.25% to 1.0% w/w) remaining within error of each other (ranging between ~1050 nm and ~1150 nm). This suggests a plateau in the aggregation state during initial assembly. A notable decrease to ~590 nm is only observed at 2.0% w/w, indicating that higher polymer content eventually promotes tighter packing or a transition to more compact structures. These contrasting behaviours highlight how polymer architecture governs the sensitivity of aggregation dynamics to concentration in drug delivery systems(158).

As shown in Figure 4.8, the IB-alt-MA-g-PEG formulations exhibit a clear trend where the particle size reaches a minimum at a specific concentration.

- The size initially decreases sharply from approximately 630 nm at 0.25% w/w to about 150 nm at 1.00% w/w. This initial reduction reflects increasingly efficient micelle formation and surfactant organization as the polymer concentration increases past the critical aggregation threshold.
- At low concentrations (0.25% and 0.50% w/w), loose aggregates or incomplete micelles likely dominate, resulting in larger particles and greater polydispersity.
- The size then slightly increases to around 270 nm at 2.00% w/w. This subtle upturn suggests that concentrations beyond the optimum (1.00% w/w) may lead to some degree of inter-micellar association or the formation of larger secondary structures.

The subsequent increase at 2.0% w/w may indicate post-CMC phenomena such as micelle swelling, inter-micellar interactions, or structural rearrangements due to excess surfactant. These transitions are commonly observed in amphiphilic copolymer systems and suggest that micelle morphology evolves with concentration beyond the CMC, though further characterisation (e.g., zeta potential or SANS) would be needed to confirm the underlying mechanisms(4-6, 83).

Varying IB-alt-MA-g-PEG concentrations in the presence of a fixed ibuprofen concentration (SANS)

To assess the influence of polymer concentration on drug-loaded micelles, SANS measurements were performed for IB-alt-MA-g-PEG at 0.25%, 0.5%, 1%, and 2% w/w in D_2O at 37 °C, each containing a fixed ibuprofen concentration of 0.25% w/w. This design isolates the effect of polymer concentration while maintaining constant drug loading, thereby clarifying how micelle population, aggregation number, and clustering evolve under constrained drug-to-polymer ratios. The SANS profiles in Figure 4.10 demonstrate the influence of polymer concentration on the structural organisation of IB-alt-MA-g-PEG systems containing a fixed ibuprofen concentration (0.25% w/w). All samples exhibit the characteristic decay in scattering intensity with increasing Q, typical of hierarchical structures in polymeric micellar systems.

At low Q, the sample with 0.25% w/w polymer shows the highest intensity, indicating the presence of larger aggregates or more extensive network formation compared to lower concentrations. This trend reflects increased interparticle correlations as polymer content rises, leading to enhanced scattering at larger length scales. The progressive increase in I ($q=0.004$ $Å^{-1}$) from 3.73 at 0.25% w/w to 100.0 at 2% w/w (Table 4.8) quantitatively confirms this clustering behaviour.

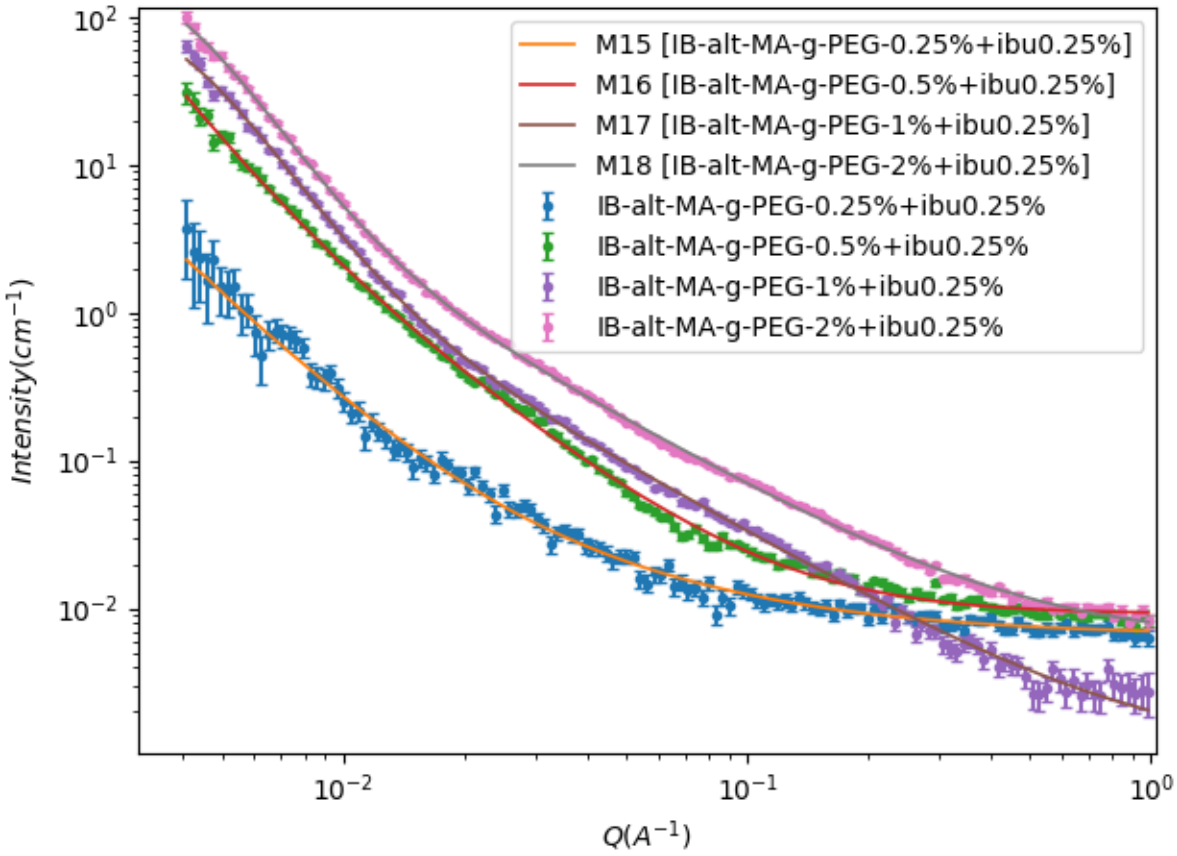

Fig.4.10: Scattering curves show a concentration-dependent effect: low polymer content yields larger aggregates, while higher concentrations produce smaller, more compact micelles.

In the mid-Q regime, slopes remain broadly similar across concentrations, suggesting that local micelle interface characteristics are preserved despite changes in aggregate size. At high Q, overlapping profiles indicate that chain conformation and corona structure remain stable, consistent with PEG-like steric protection of micelle cores (171). The combined analysis of Figure 4.9 and model fits (M5–M8) reveals that aggregate shape remains relatively consistent across polymer concentrations, likely Flexible cylinder. This is supported by smooth mid-Q decay and Porod slopes approaching 3–4, indicative of well-defined interfaces and compact micellar structures rather than loose networks (158).

As polymer concentration increases from 0.25% to 2% w/w (with ibuprofen fixed at 0.25% w/w), the low-Q intensity rises markedly, especially at 1% and 2%, suggesting the onset of interparticle correlations or weak clustering. This behaviour is typical of concentrated polymer solutions, where increased chain availability promotes micellar association and reduces hydration within aggregates (4-6, 83).

Despite these changes in aggregate size and connectivity, the high-Q region of the scattering curves converges across all samples. This indicates that the local chain conformation remains largely unaffected

by polymer concentration, and that the fundamental micelle structure is preserved. The constant ibuprofen level likely stabilises hydrophobic domains, but its influence appears secondary to polymer concentration in determining the overall scattering profile.

Table 4.8: Comparative SANS observables for IB-alt-MA-g-PEG at varying polymer concentrations(%w/w) with fixed ibuprofen (0.25% w/w, 37 °C). Two – Lorentzian and polymer-micelle models are applied in this table to compare with the previous section.

Polymer concentration(%w/w)	**Relevant parameters**				
Polymer - micelle	**radius_core(Å)**	**Rg(Å)**	**N_{agg}**		**χ^2**
0.25	198.0 ± 12.2	100.1 ± 58.1	11.4 ± 3.7		1.4
0.50	82.6 ± 3.3	290.7 ± 22.2	12.8 ± 0.7		2.7
Two-Lorentzian	**Lorentz length1(Å)**	**Lorentz length2(Å)**	**Lorentz exp1**	**Lorentz exp2**	**χ^2**
1.00	279.4 ± 25.9	197.1 ± 2.5	3.9 ± 0.3	1.5 ± 0.0	1.8
2.00	285.7 ± 28.9	12691 ± 4.9	4.1 ± 0.3	1.5 ± 0.0	3.0

Structural Interpretation of Parameters

1. Dilute Regime (0.25% – 0.50% w/w): Micellar Assembly

In the lower concentration range, the system is best described by a Polymer-micelle model(172).

- **Contraction of the Core:** As concentration increases from 0.25% to 0.50%, the radius_core drops significantly from ~198 Å to ~83 Å. This suggests that higher polymer density promotes a more compact, better-defined hydrophobic core.
- **Expansion of the Corona:** Conversely, the radius of gyration (Rg) nearly triples (100.1 Å to 290.7 Å). This indicates that while the core tightens, the polymer chains in the corona extend further into the solvent, likely due to increased steric repulsions between neighbouring chains as the aggregation number (N_{agg}) rises slightly from 11.4 to 12.8(173).

2. Semi-Dilute Regime (1.00% – 2.00% w/w): Network Formation

At 1.00% and above, the "micelle" description fails, necessitating a Two-Lorentzian model. This shift indicates the formation of a complex, interconnected network or a "mesh" rather than discrete particles(174).

- **Structural Length Scales:** The system exhibits two distinct correlation lengths. Lorentz length1 remains relatively stable (~280–285 Å), representing the primary mesh size or the distance between physical crosslinks.
- **Large-Scale Heterogeneity:** At 2.00%, Lorentz length2 explodes to ~12,691 Å. This suggests the emergence of massive, long-range structural fluctuations or the development of a macroscopic gel-like matrix.
- **Fractal Scaling:** The Lorentz exp1 values (~3.9 to 4.1) are near the Porod limit (4.0), indicating the presence of structures with very sharp, smooth interfaces. Meanwhile, Lorentz exp2 remains at 1.5, which is characteristic of Gaussian chains in a theta solvent, suggesting that the "links" between the large-scale structures remain flexible and polymeric in nature.

3. Model Fitting Quality

The χ^2 values remain relatively low (1.4 to 3.0), though the increase at 0.50% and 2.00% suggests these concentrations are near "tipping points" where the chosen models begin to struggle with the increasing structural complexity of the system.

Varying MA-alt-C_{18}-g-PEG concentrations in the presence of a fixed ibuprofen concentration (DLS)

In Figure 4.8, particle size changes with increasing MA-alt-C_{18}-g-PEG concentration in the presence of a fixed 0.25% w/w ibuprofen. Initially, particle size increases from ~1050 nm at 0.25% w/w to ~1150 nm at 0.5% w/w, suggesting enhanced aggregation and micelle swelling. This behaviour may reflect loose packing of amphiphilic chains and incomplete shielding of hydrophobic domains, leading to larger, more polydisperse structures.

As MA-alt-C_8-g-PEG concentration continues to rise, the particle size decreases steadily, reaching ~600 nm at 2.0% w/w. This downward trend likely indicates a transition from loosely packed aggregates to more compact micellar structures, driven by improved polymer–drug interactions and saturation of available hydrophobic sites (Scheme 4.2). The error bars suggest moderate variability, particularly at lower concentrations, consistent with unstable or transitional morphologies.

These data reflect a concentration-dependent restructuring of the polymer–drug system. Unlike IB-alt-MA-g-PEG, which shows a clear CMC-driven compaction phase(CMC was observed to be ~1.7 to 3 %w/w) followed by post-CMC swelling, MA-alt-C_8-g-PEG demonstrates initial aggregation before gradual size reduction(175). This contrast underscores the role of polymer architecture in determining aggregation dynamics and micelle evolution.

From a drug delivery perspective, IB-alt-MA-g-PEG can achieve sub-400 nm sizes at optimal concentration, but its tendency to swell at high polymer content may limit systemic use. In contrast, MA-alt-C_8-g-PEG remains above 600 nm even at 2.0% w/w, making it less suitable for intravenous administration but potentially useful for local or sustained-release applications. These findings align with previous reports on amphiphilic copolymers, where concentration-dependent morphology changes influence encapsulation efficiency and colloidal stability.

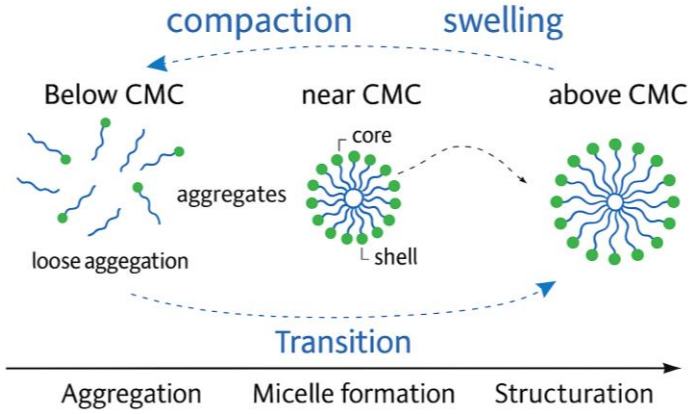

Scheme 4.2: Conceptual illustration of micelle morphology evolution with polymer concentration relative to the CMC. Below CMC: loose aggregates dominate. Near CMC: compact micelles form. Above CMC: micelle swelling and intermicellar interactions emerge, potentially compromising colloidal stability{Tawfik, 2020 #6}.

Varying MA-alt-C_{18}-g-PEG concentrations in the presence of a fixed ibuprofen concentration (SANS)

To investigate the effect of polymer concentration on micellar structure under constant drug loading, SANS measurements were performed at 0.25%, 0.5%, 1%, and 2% w/w MA-alt-C_8-g-PEG in D_2O at 37 °C, each containing 0.25% w/w ibuprofen. This design isolates the role of polymer content in modulating micelle population, corona hydration, and interparticle association.

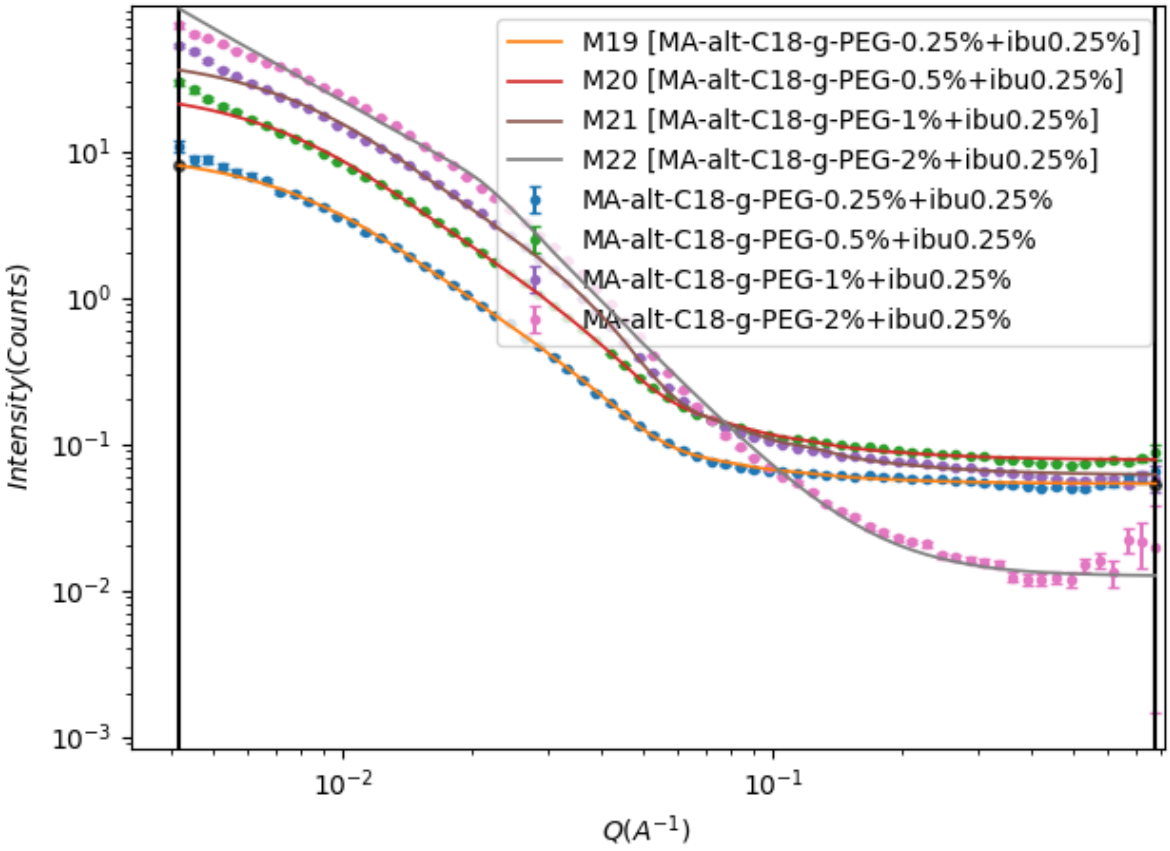

Fig.4.11: SANS intensity profiles for MA-alt-C_8 g-PEG micelles at fixed ibuprofen loading (0.25% w/w) and varying polymer concentrations (0.25–2% w/w). Increasing polymer content leads to higher low-Q intensity and model transitions from one-level to two-level fits, indicating progressive clustering and corona restructuring.

The scattering profiles in Figure 4.11 and the corresponding fit parameters confirm that MA-alt-C_8 -g-PEG micelles, loaded with 0.25% w/w Ibuprofen, transition from discrete spherical units to a hierarchically clustered network as polymer concentration increases.

Table 4.9: Comparative SANS observables for MA-alt-C_8 -g-PEG at varying polymer concentrations (%w/w) with fixed ibuprofen (0.25% w/w, 37 °C).

Polymer	**Rg (Å)**		**radius_core(Å)**	**n_aggreg**	**Best model**	**X^2**
0.25	124.3 ± 22.6		66.4 ± 7.2	6. 4 ± 2.4	Poly micelle	8.3
0.5	124.3 ± 22.6		66.4 ± 7.1	6. 4 ± 2.5	Poly micelle	8.3
1	Rg(guinier)	Rg (corona)	58.1 ± 0.8	4.5 ± 0.6	Poly-micelle_guinier	2.5
	49.7± 1.6	4.5 ± 0.3				
2	245.1 ± 2.1	88.1± 2.1	40.9 ± 0.9	10.4 ± 2.3	Poly-micelle_guinier	7.6

At Low Polymer Concentration (0.25%–0.5%) concentrations, the system is adequately described by a standard Polymer Micelle model ($X^2 = 8.3$). The micelles possess a hydrophobic core radius of 66.4 Å and a small aggregation number ($N_{agg} \sim 6.4$). The identical parameters across these two points suggest a stable, dilute regime where increasing the polymer does not yet force inter-micellar reorganization (176, 177).

The system reaches its most statistically reliable state ($X^2 = 2.5$) at 1%w/w concentration when transitioning to the Hybrid Poly-micelle–Guinier model. The core radius contracts to 49**.7** Å, and the aggregation number drops to 4.5. The emergence of the Guinier term (Total Rg = 58.1 Å) captures weak inter-particle associations, while the very small corona Rg (4.5 Å) suggests the PEG chains are in a highly collapsed, "mushroom" conformation at this concentration (178). At the highest concentration (2 % w/w), the micelles undergo significant drug-assisted growth and clustering. The aggregation number increases to 10.4, and the core radius expands to 88.1 Å. The massive jump in the Guinier Rg (245.1 Å) indicates that the micelles are no longer isolated but have formed large-scale clusters or a networked structure (171, 179).

The SANS profiles in Figure 4.10 and the corresponding model fits confirm that increasing MA-alt-C_8 -g-PEG concentration (0.25% to 2% w/w) induces a non-linear structural reorganization rather than a fundamental change in core-shell morphology. At low concentrations (0.25–0.5%), the system maintains discrete spherical micelles; however, at 1%, the transition to a multi-model Poly-micelle–Guinier model reveals an optimal structural state with refined core packing (Rg ~50 Å) and stabilized associations. At the highest concentration (2%), the significant increase in N_{agg} and the spike in Guinier Rg (~245 Å) indicate that while the underlying spherical architecture remains intact, the system transitions toward a hierarchically clustered network. These findings highlight the delicate balance between polymer solvation, Ibuprofen loading, and inter-particle effects in determining micellar stability and long-range organization.

4.2.2 Comparative Discussion: IB-alt-MA-g-PEG vs. MA-alt-C_{18}-g-PEG vs. LIR410-g-PEG (Fixed Ibuprofen Loading)

IB-alt-MA-g-PEG

SANS analysis confirms the presence of compact, spherical micelles with Porod slopes between 3 and 4, indicating well-defined interfaces. At a polymer concentration of 0.25% w/w, micelles are small and discrete, which typically favours rapid drug release. As the concentration increases (0.5–2%), the rise in Low-Q intensity reflects emergent clustering and inter-particle correlations. The aggregation behaviour is non-monotonic, peaking at intermediate concentrations before stabilizing, which suggests that release kinetics in this system are heavily influenced by the competitive balance between micellar stability and weak clustering.

MA-alt-C_{18}-g-PEG

This system exhibits a non-linear structural transition best captured by the multi model Poly-micelle–Guinier model.

- Aggregation and Growth: The aggregation number does not increase linearly; instead, it shifts from approximately 6.4 at low concentrations to a stabilized state of 4.5 at 1% w/w, before spiking to 10.4 at 2% w/w due to drug-assisted packing.
- Size Evolution: The Rg (Guinier) peaks at 1% w/w (~138 Å) due to optimal hydration and corona expansion, followed by contraction at 2% w/w (~115 Å) caused by crowding-induced compaction.
- Core Stability: The core radius fluctuates (from 66 Å to 50 Å and eventually 88 Å), indicating that Ibuprofen partitioning is concentration-dependent. At 2% w/w, the significant jump in both core size and total Rg (~245 Å) signifies the formation of a hierarchically clustered network.

LIR410-g-PEG

DLS data show moderate size redistribution rather than clustering. Hydrodynamic diameters increase with drug loading, reflecting more chains per micelle, but PEG coronas provide steric stabilisation that prevents extensive aggregation. Micelles remain discrete even at higher drug loadings, with drug accommodation occurring via population increase rather than corona expansion or clustering, consistent with PEGylated micelle behaviour.

4.3 Effect of pH on Formulation Behaviour

To evaluate the impact of environmental pH on micellar stability and particle size, DLS measurements were performed for ibuprofen-loaded formulations containing 5% w/w polymer and 0.25% w/w ibuprofen across a pH range of 3–14. This approach enables assessment of colloidal behaviour under physiologically and pharmaceutically relevant conditions, including acidic, neutral, and alkaline environments. The results provide insight into how polymer architecture influences pH responsiveness, micelle integrity, and

potential release dynamics. Figure 4.11 presents the particle size profiles for IB-alt-MA-g-PEG, MA-alt-C_8 -g-PEG, and LIR410-g-PEG systems under varying pH conditions.

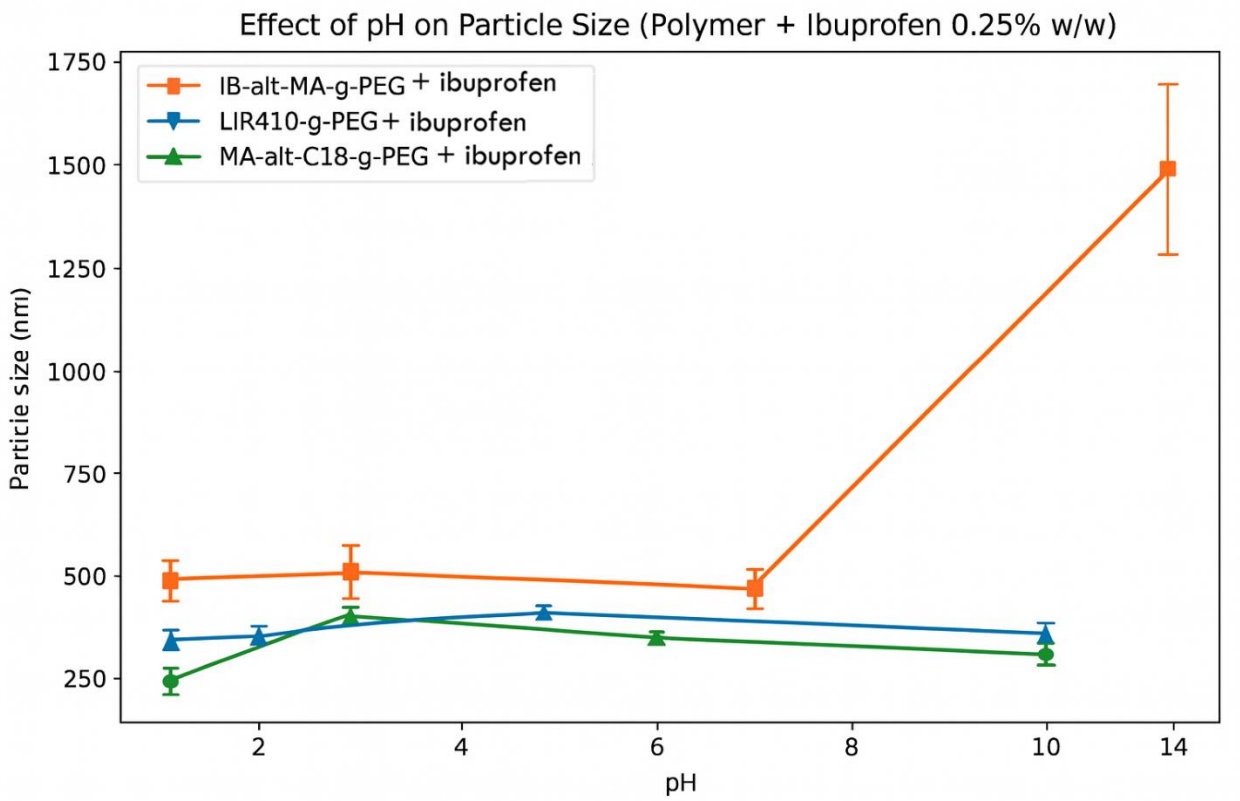

Fig.4.12: Effect of pH on particle size for polymer–ibuprofen formulations (0.25% w/w ibuprofen, 5% w/w polymer). IB-alt-MA-g-PEG shows a significant size increase at pH 14, while MA-alt-C_{18}-g-PEG and LIR410-g-PEG maintain stable particle sizes across the pH range, indicating differential pH sensitivity and colloidal stability.

IB-alt-MA-g-PEG exhibits a notable increase in particle size at pH 14, compared to the relatively stable sizes of 457 ± 31 nm, 467 ± 137 nm, and 403 ± 40 nm observed at pH 3, 5, and 9, respectively. This stability across acidic to near-neutral conditions suggests that limited ionization of the maleic anhydride groups preserves hydrophobic interactions and prevents excessive swelling. While the data at pH 14 suggests a transition toward larger assemblies, it is acknowledged that additional data points between pH 9 and 14 would be necessary to further clarify and confirm this observed trend. Nonetheless, the current results provide an initial indication of the system's sensitivity to highly alkaline environments.

At pH 14, particle size dramatically increased to 1656 ± 128.7 nm, suggesting significant aggregation and structural rearrangement. This behaviour is consistent with the hydrolysis of maleic anhydride units into maleate salts under strongly alkaline conditions, leading to increased chain ionisation, electrostatic repulsion, and possible bridging interactions that destabilise the micellar or aggregate structure. The large size increase may also indicate partial precipitation and formation of loose flocs. The IB polymer system

is pH-sensitive, remaining relatively stable in acidic and near-neutral environments but undergoing significant structural changes under highly alkaline conditions. This is important for formulation design, as extreme pH conditions (e.g., intestinal or cleaning environments) could compromise stability and drug delivery performance.

MA-alt-C_{18}-g-PEG maintains relatively stable particle sizes across the pH range, with only minor fluctuations. This indicates robust micelle formation and tolerance to both acidic and alkaline environments. The alternating maleic acid–octadecene architecture likely provides pH buffering capacity and structural resilience, preserving micelle integrity.

At pH 3, limited hydrolysis keeps anhydride groups protonated, preserving hydrophobic interactions but reducing electrostatic stabilisation. As pH increased to 5 and 8, particle size rose to 366 ± 18 nm and 333 ± 15 nm, respectively, with much lower variability. This indicates the formation of more uniform aggregates, likely due to partial hydrolysis of anhydride groups into carboxylates, introducing moderate charge repulsion while preserving hydrophobic domains. This balance promotes stable micelle-like structures.

At pH 12, particle size decreased slightly to 284.4 ± 8.8 nm, with the lowest variability. Under strongly alkaline conditions, extensive hydrolysis of anhydride groups to maleate salts occurs, increasing hydrophilicity and electrostatic repulsion. This likely leads to more compact, uniform aggregates or partial disassembly of larger clusters into smaller, stabilised particles.

Unlike IB, which showed dramatic size increase at high pH, the Ma system demonstrates greater adaptability and stability across the pH range, with no extreme aggregation even under alkaline conditions. This behaviour is attributed to the amphiphilic nature of Ma, where long hydrophobic octadecyl chains maintain core integrity, while ionizable anhydride groups modulate surface charge with pH. Such responsiveness is advantageous for controlled drug delivery, as it suggests Ma-based carriers can maintain colloidal stability in diverse physiological environments.

LIR410-g-PEG DLS data revealed that LIR410-g-PEG dispersions containing 0.25% w/w ibuprofen exhibit a non-linear response to pH variation. Under acidic conditions (pH 3–4), particle sizes remained relatively stable, with the smallest mean size observed at pH 4 (~324 nm). This behaviour suggests that near this pH the polymer–drug system achieves optimal electrostatic stabilisation, likely due to reduced ionisation of functional groups, which minimises interparticle repulsion and aggregation (180). At neutral pH (pH 7), particle size increased significantly to ~401 nm, representing a ~24% enlargement compared to pH 4. This increase may be attributed to enhanced ionisation of carboxylic groups in the polymer backbone, leading to greater hydration and swelling of micellar structures, or partial aggregation driven by charge screening in the presence of counter ions (181). Under strongly alkaline conditions (pH 12), particle size decreased again to ~340 nm, approaching values like those at acidic pH. This reduction likely reflects complete ionisation of polymer chains, which promotes electrostatic repulsion and partial

disassembly of aggregates. However, the higher variability observed at pH 12 indicates reduced structural stability under these conditions (6).

LIR410-g-PEG is a grafted copolymer of PEG2000, and the PEG chains impart hydrophilicity and steric stabilisation to the system[2] . This steric protection likely contributes to colloidal stability at extreme pH values, while the grafted hydrophobic segments enable association with ibuprofen. The observed pH sensitivity therefore reflects a delicate balance between hydrophobic association and electrostatic repulsion, strongly influenced by the ionisation state of the polymer backbone. Such behaviour has direct implications for drug release, as micelle swelling at neutral pH may favour sustained release, while dispersion under alkaline conditions could accelerate release kinetics (182, 183).

IB-alt-MA-g-PEG 5%w/w + ibuprofen 0.25%w/w (SANS)

To investigate the influence of pH on micellar architecture and drug encapsulation, SANS measurements were performed on IB-alt-MA-g-PEG formulations containing 5% w/w polymer and 0.25% w/w ibuprofen across four pH conditions: 3, 5, 8, and 12. These conditions span the protonation states of carboxylic acid groups (from hydrolyzed maleic anhydride residues), affecting micelle stability, corona hydration, and interparticle interactions. By applying advanced models including the elliptical cylinder, 2 Lorentzian + polymer-micelle, and cylinder-cylinder approaches, the data enable a detailed interpretation of pH-dependent structural rearrangements and their implications for drug encapsulation and release(184).

Figure 4.13 presents the SANS intensity profiles of IB-alt-MA-g-PEG formulations containing 5% w/w polymer and 0.25% w/w ibuprofen across the four pH conditions (3, 5, 8, and 12). These profiles highlight how scattering behavior evolves with pH, reflecting changes in micelle size, corona hydration, and interparticle interactions. The low-Q region captures clustering and aggregate formation (prominent at pH 3 and 5), while mid- and high-Q slopes provide insight into micelle compactness and interface definition. The curves demonstrate non-linear, phase-like transitions that require different analytical models at each pH.

[2] https://www.specialchem.com/adhesives/product/kuraray-kuraray-lir-410

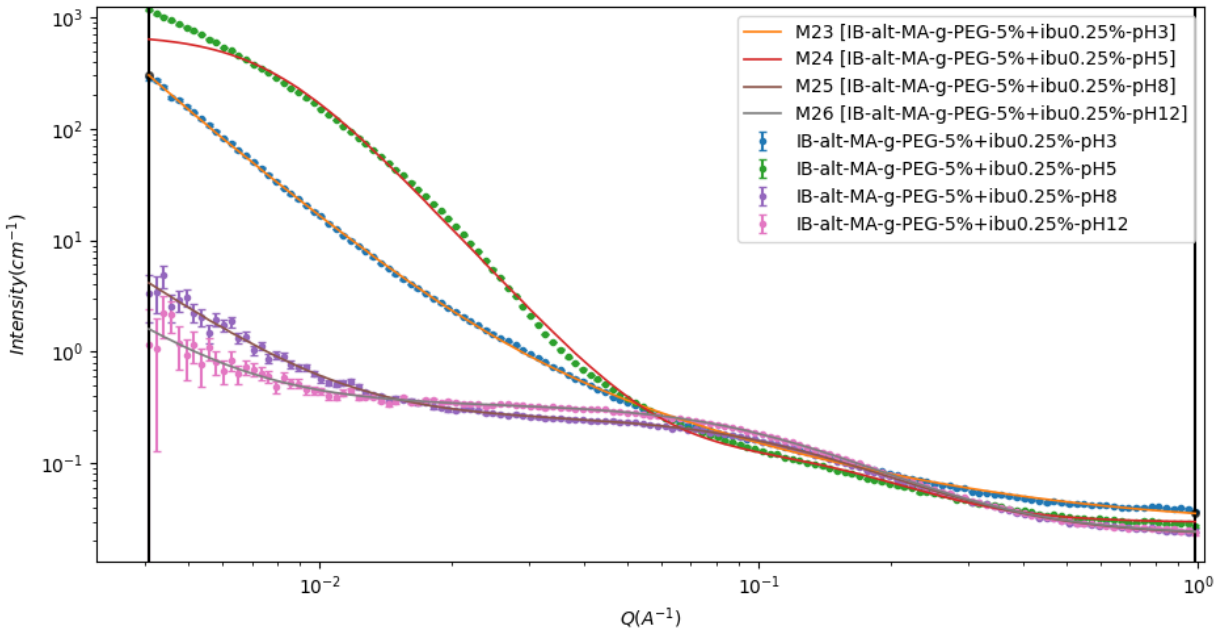

Fig.4.13: SANS intensity vs. Q for IB-alt-MA-g-PEG + 0.25% w/w ibuprofen at 5% w/w polymer concentration under different pH conditions. Symbols represent data points with error bars; lines indicate model fits where applicable. Data show large aggregates at low pH (high low-Q intensity) transitioning to smaller, more compact structures at high pH (reduced low-Q scattering).

The small-angle neutron scattering (SANS) data, characterized by the fitting parameters in Table 4.10, reveal a profound pH-dependent structural evolution of the IB-alt-MA-g-PEG system in the presence of ibuprofen. Progressive deprotonation of carboxylic acid groups drives a contraction from large, elongated nanostructures at low pH to much smaller, rigid cylindrical structures at high pH.

Table 4.10. SANS-derived parameters for IB-alt-MA-g-PEG (5% w/w) with 0.25% w/w ibuprofen across pH conditions. The applied models for pH 3 was Two-Lorentzian, for pH 5 was multimode from Two-Lorentzian and polymer-micelle, and finally for pH 8,12 was Cylinder- cylinder.

Model per pH	**Relevant parameters**			
elliptical_cylinder	**radius_minor(Å)**	**axis_ratio**	**length(Å)**	χ^2
pH 3	20.0 ± 0.0	1.5 ± 0.0	400.0 ± 0.0	8.2
2lor_polymer_micel	**radius_core(Å)**	**Rg(Å)**	**N_{agg}**	χ^2
pH 5	120.5 ± 0.2	10.9 ± 0.1	44.5 ± 3.1	21.6
Cylinder-Cylinder	**Length (Å)**	**Radius(Å)**		χ^2
pH 8	1.8 ± 0.9	16.7 ± 0.1		34.9
pH 12	54.1 ± 0.3	7.1 ± 0.03		8.6

At pH 3, the elliptical cylinder model indicates formation of elongated, stable core–shell aggregates (length 400 Å) in the acidic environment, consistent with protonated carboxylic groups favoring hydrophobic collapse (185). As pH increases to 5, partial ionization leads to swelling (larger core radius 120.5 Å, Nagg ≈ 44.5). At pH 8 and especially pH 12, the cylinder-cylinder model provides the best description, yielding compact cylindrical structures (notably at pH 12: radius 7.1 Å, length 54.1 Å, excellent fit $\chi^2 = 8.6$). The poorer fit at pH 8 ($\chi^2 = 34.9$, near-negligible length) suggests a transitional state before full stabilization of the cylindrical morphology under stronger alkaline conditions.

This overall contraction, from large elliptical cylinders (pH 3) to swollen micelles (pH 5) to small, rigid cylindrical nano-units (pH 12), demonstrates structural refinement and increased geometric uniformity with progressive ionization. This behavior contrasts with some carboxylic-acid-based systems that fully disassemble at high pH (186), but aligns with observations in hydrophobic-backbone graft copolymers where electrostatic repulsion compacts aggregates into shorter cylinders rather than promoting dispersion (187).

These structural changes significantly impact drug loading and release. The most favorable state for incorporating hydrophobic drugs like ibuprofen is at low pH (≤6), where stable, compact micelles and elliptical cylinders provide substantial hydrophobic cores (e.g., large internal volume at pH 3; sizable core at pH 5). This ensures effective partitioning, protection, and stability in acidic environments (e.g., gastric conditions).(38,49) At high pH (≥8), the shift to small cylinders reduces the available hydrophobic volume and may alter corona hydration, diminishing sustained loading capacity but enabling faster release kinetics (e.g., triggered disruption of larger assemblies or altered partitioning in alkaline sites like the intestines or

tumor microenvironment) (115, 134). Thus, the IB-alt-MA-g-PEG system offers promise as a pH-responsive delivery vehicle, with optimal loading at low pH and smart triggered release at high pH.

MA-alt-C_{18}-g-PEG 5%w/w + Ibuprofen 0.25%w/w (SANS)

While DLS highlights overall particle size trends, SANS provides deeper insight into micellar architecture, confirming how pH modulates core–corona dimensions and clustering behaviour.

The SANS profiles for MA-alt-C_8 -g-PEG with 5%w/w polymer and 0.25%w/w ibuprofen across pH levels 3, 5, 8, and 12 reveal significant structural changes in response to pH variation (Figure 4.14).

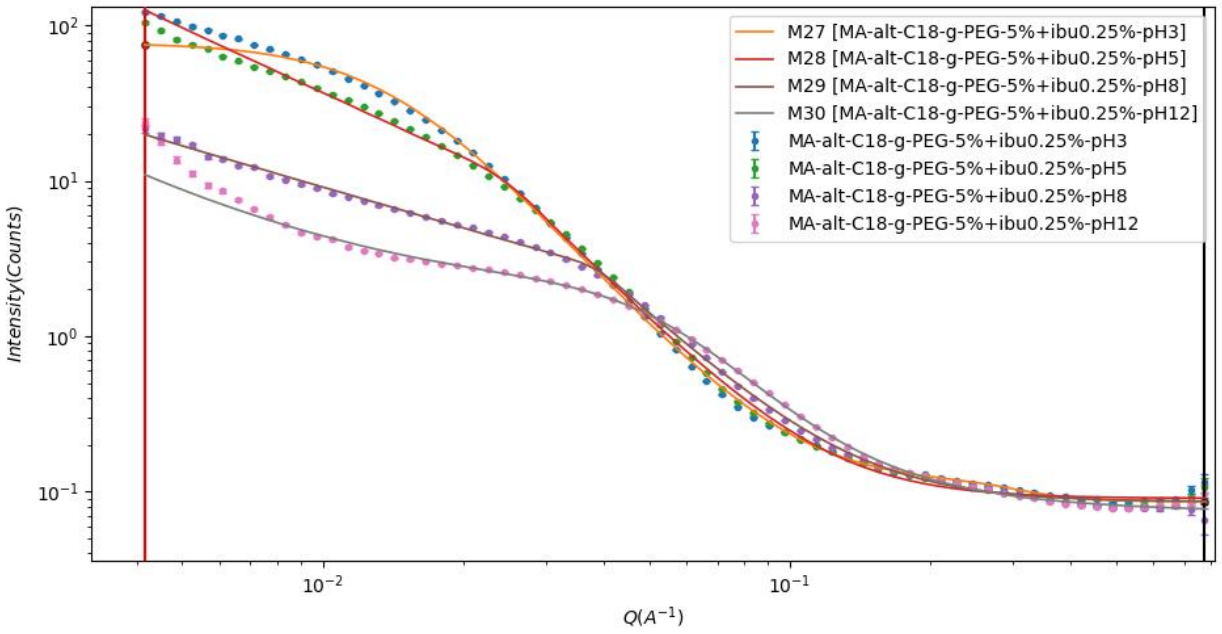

Fig.4.14: SANS intensity profiles for MA-alt-C_8 -g-PEG micelles (5% w/w polymer, 0.25% w/w ibuprofen) across pH 3, 5, 8, and 12. The profiles show a progressive shift from compact aggregates at acidic pH to dispersed micelles under alkaline conditions, with decreasing low-Q intensity and Porod slopes, consistent with reduced clustering and corona contraction.

Table 4.11. SANS-derived parameters for MA-alt-C_8-g-PEG (5% w/w) with 0.25% w/w ibuprofen across pH conditions. The multi model poly-micelle_guinier is applied for this dataset.

pH	Porod slope	Core radius (Å)	Rg (Å)	Rg corona (Å)	Aggregation number	X^2
3	~3.9	31.2±0.7	84.3±1.0	23.5±1.7	12.4±1.2	4.9
5	~3.8	30.7±0.6	76.5±1.8	24.8±1.5	12.9 ±1.2	3.9
8	~3.0	28.1±0.4	126.1±6.5	18.2±0.8	46.5±3.4	2.7
12	~2.9	27.1±0.3	46.3±14.4	18.5±1.6	2.2±0.8	2.1

The SANS profiles of MA-alt-C_{18}-g-PEG micelles loaded with ibuprofen reveal a transition from stable, well-defined spheres to a highly dispersed, low-aggregation state as pH increases. At pH 3 and 5, the system is characterized by compact, core-shell micelles with core radii of approximately 31 Å and sharp interfaces, evidenced by Porod slopes of ~3.8–3.9 (188, 189). The statistical reliability is high, with chi-squared values between 3.9 and 4.9, and a steady aggregation number of approximately 12.4–12.9. This indicates a robust micellar architecture where the ibuprofen is effectively sequestered within the core (190).

As the pH increases into the alkaline regime, the system undergoes a significant, non-monotonic structural reorganization. At pH 8, a distinct peak in the total radius of gyration (126.1 Å) and a sharp rise in the aggregation number to 46.5 suggest a transition toward drug-induced clustering or inter-micellar networking(144, 191). However, by pH 12, the aggregation number collapses to 2.2 and the core radius reaches its minimum of 27.1 Å. While the system reaches its most statistically optimal fit at this stage (chi-squared of 2.1), it possesses the lowest structural density. The Porod slope further drops to ~2.9, signalling a shift toward very diffuse, fractal-like interfaces (192). Unlike IB-alt-MA-g-PEG, which exhibits different morphological shifts, MA-alt-C_{18}-g-PEG maintains an underlying spherical architecture across the entire pH range. This adaptability is driven by the long hydrophobic octadecyl chains that preserve core integrity in acidic media, while the ionization of anhydride groups at higher pH modulates corona hydration and triggers dispersion (191). Functionally, this ensures robust drug protection and sustained release in acidic environments, while promoting triggered, rapid release at pH 12 as the micellar units disassemble into small, highly dispersed aggregates. The PEG coronas maintain colloidal stability through steric hindrance even as the aggregate population collapses (180, 193).

PEG-g-LIR-410 5%w/w + ibuprofen 0.25%w/w (SANS)

To gain deeper structural insight, SANS was employed to probe the core–corona dimensions, aggregation number, and interparticle interactions of LIR410-g-PEG micelles loaded with 0.25% w/w ibuprofen across pH 3–12. The fitted parameters are summarised in Table 4.12, and the corresponding scattering profiles are presented in Figure 4.15.

Table 4.12. SANS-derived parameters for LIR410-g-PEG (5% w/w) with 0.25% w/w ibuprofen across pH conditions. Poly-micelle and Poly-micelle_guinier models are applied.

pH	Porod slope	Core radius (Å)	Rg (Å)	Rg corona (Å)	N_{agg}	Interpretation	X^2
3	~3.9	111.2 ±0.4	95.9 ±1.2	12.9±1.2	18.9±2.4	Compact spherical micelles, moderate clustering	4.2
5	~3.8	99.8 ±0.1	229.5±1.7	-	22.1±0.1	Weak clustering, swollen corona, spherical shape	9.3
8	~3.1	99.7±0.2	186.6 ±0.1	-	14.4 ±0.2	Dispersed micelles, reduced hydration	53.1
12	~3.0	81.1±0.3	395.4±9.1	-	16.3±0.5	Highly dispersed, small spherical micelles	13.6

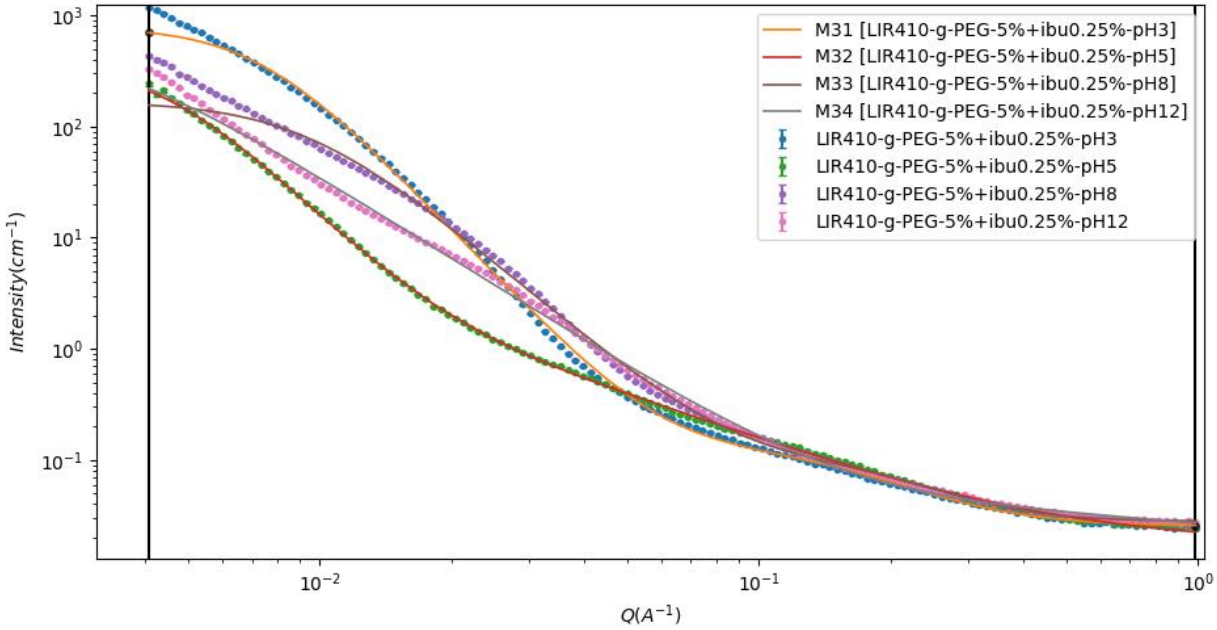

Fig.4.15: SANS intensity profiles for LIR410-g-PEG micelles (5% w/w polymer, 0.25% w/w ibuprofen) across pH 3, 5, 8, and 12. Experimental data (markers) are overlaid with model fits (lines). Low-Q intensity decreases markedly from acidic to alkaline pH, accompanied by reductions in Porod slope, core radius, Rg, and aggregation number, indicating a transition from moderately clustered, swollen-corona micelles to highly dispersed, small spherical micelles.

The SANS fitting results for LIR410-g-PEG micelles loaded with ibuprofen across pH 3–12 reveal a clear pH-sensitive modulation of micellar organisation while maintaining spherical morphology throughout (Table 4.12, Figure 4.15).

Acidic to Neutral Transition (pH 3–5) At pH 3, scattering intensity is highest (~437 cm^{-1}) and the system forms the most statistically reliable and well-defined structures. The Porod slope of ~3.9 confirms a sharp, smooth interface for these compact spherical micelles (194). As the pH increases to 5, the core radius slightly contracts (111.2 to 99.8 Å), while the Rg more than doubles (to 229.5Å)(195). This indicates a transition from discrete clustering to a state of weak clustering with a significantly swollen corona, likely driven by the partial deprotonation of the polymer backbone (196).

Alkaline Response (pH 8–12) At higher pH, the system becomes increasingly disordered, as evidenced by the high chi-squared values reaching up to 53.1. This transition is marked by a drop in the Porod slope to approximately 3.0–3.1, signalling a shift from smooth, well-defined surfaces to diffuse or fractal-like interfaces (104). By pH 12, the core radius reduces to its minimum of 81.1 Å, while the total radius of gyration spikes to 395.4 Å, indicating significant spatial expansion or long-range fluctuations. Furthermore, the aggregation number decreases from its peak of 22.1 at pH 5 to 16.3 at pH 12, suggesting that the micelles are breaking down into smaller, highly dispersed units with long-range spatial correlations rather than maintaining their original compact aggregate form (197).

Taken together, the SANS data establish a predictable transition from moderately clustered, swollen-corona micelles under acidic conditions to highly dispersed, small spherical micelles under alkaline conditions. PEG coronas confer steric stabilisation that preserves spherical architecture and suppresses clustering even when hydrophobic association is strong, while the ionisation state of the graft backbone modulates corona hydration and interparticle interactions (198). Functionally, this behaviour implies greater retention and potentially sustained release in mildly acidic environments, and accelerated release under alkaline conditions, with pH-robust colloidal stability across physiologically relevant regimes.

4.4 Comparative Analysis of IB-alt-MA-g-PEG, MA-alt-C_8-g-PEG, and PEG-g-LIR410 Micelles in the Presence of Ibuprofen

4.4.1 Structural Responses

The comparative evaluation of SANS and DLS parameters (Table 4.13) highlights distinct structural behaviour across the three micellar systems. IB-alt-MA-g-PEG micelles at concentrations between 0.25–2% w/w exhibit scattering intensities of 190–280 cm^{-1} at pH 3–5, with Porod slopes ~3.8–4.0 and aggregation numbers ranging from 6–15. These values confirm spherical morphology but reveal non-monotonic clustering, with weak interparticle correlations that vary with concentration and pH(199). In contrast, MA-alt-C_8-g-PEG micelles at 5%w/w concentration show intensities of 105–125 cm^{-1}, Porod slopes ~3.8–3.9, and aggregation numbers between 6–15, reflecting monotonic aggregation behaviour. Corona expansion is evident at mid pH (~5), followed by compaction under alkaline conditions, supporting predictable modulation of micellar organisation (182). LIR410-g-PEG micelles, also at 5% concentration, display higher intensities (242–437 cm^{-1}) with Porod slopes ~3.8–3.9 and aggregation

numbers ~9–16. These results confirm sterically stabilised spherical micelles, with moderate clustering under acidic conditions and dispersion under alkaline conditions, consistent with PEG-mediated steric protection (104).

Table 4.13. Summary of SANS/DLS parameters for IB-alt-MA-g-PEG, MA-alt-C_8-g-PEG, and LIR410-g-PEG micelles (5% w/w polymer, 0.25% w/w ibuprofen).

System	Porod slope	Core radius (Å)	R_g (Å)	Aggregation number(N_{agg})	Shape/Interpretation
IB-alt-MA-g-PEG	~3.0–4.1	~27–31	~46–126	~2–46	**Non-monotonic clustering/network expansion,** pH sensitive
MA-alt-C_8-g-PEG	~2.9–3.9	~27–31	~46–126	~2–46	**Non-monotonic aggregation/dispersion,** structurally tolerant spheres
LIR410-g-PEG	~3.8–3.9	~80-111	~96-395	14-22	Sterically stabilised spherical micelles, moderate clustering at acidic pH

4.4.2 Shape Evolution

- **IB-alt-MA-g-PEG**: extended large elliptical cylinders at low pH give way to swollen micelles at intermediate pH and then to short rigid cylindrical nanostructures at high pH. Increasing electrostatic repulsion from ionized carboxylic groups on the maleic anhydride backbone drives compaction into shorter more uniform cylinders (rather than swelling or full disassembly), while PEG grafts maintain solubility. This non-monotonic shape evolution (initial swelling followed by sharp contraction) highlights the system's unique response due to its graft architecture and hydrophobic isobutylene components.

- **MA-alt-C_{18}-g-PEG**: Demonstrates non-monotonic aggregation behavior across both concentration and pH gradients. The system reaches an optimal structural state at 1% w/w or pH 5, characterized by refined core packing and corona expansion. However, at higher concentrations (2–5% w/w) or extreme alkaline pH (12), the system undergoes significant reorganization, transitioning from clustered networks at pH 8 (N_{agg}~46) to highly dispersed, low-density aggregates at pH 12 (N_{agg}~ 2)(200).

- **LIR410-g-PEG**: Maintains a robust spherical morphology across all pH conditions, supported by strong steric stabilization from PEG coronas. At acidic pH, the system forms the largest and most well-defined core-shell structures (R_core ~ 111 Å). As pH increases, the core contracts while the total Rg spikes, indicating a shift toward highly dispersed micelles with significant long-range spatial fluctuations but no irreversible clustering.

4.4.3 Role of Drug pKa and pH on Drug Ionisation and Release from Micelles

In addition to the intrinsic pH-responsiveness of the polymeric micelles discussed above, the ionisation behaviour of ibuprofen itself plays a critical role in governing pH-dependent drug release. Ibuprofen is a weakly acidic non-steroidal anti-inflammatory drug with a reported pKa[2] of approximately 4.45–5.3 in aqueous media, depending on solvent composition and ionic strength (201). As a result, changes in environmental pH strongly modulate the balance between its unionised and ionised forms, directly affecting its solubility and affinity for hydrophobic micellar domains.

Below its pKa, ibuprofen exists predominantly in the unionised, hydrophobic form, favouring partitioning into the micellar core through hydrophobic and van der Waals interactions. This promotes efficient encapsulation and stabilisation within the core–shell assemblies. As the pH increases beyond the pKa, ibuprofen becomes progressively ionised, leading to increased aqueous solubility and reduced affinity for the hydrophobic core. This ionisation-driven shift favours diffusion of ibuprofen into the continuous phase and contributes to enhanced drug release.

Such behaviour has been well documented for weakly acidic drugs in amphiphilic micellar systems. In Pluronic–drug complexes, Alexander et al. demonstrated that increasing pH beyond the drug pKa resulted in partial or complete drug release accompanied by reductions in micelle aggregation number and structural integrity(202). While flurbiprofen was used in that study, the underlying mechanism, pKa-controlled ionisation of a weakly acidic NSAID, applies directly to ibuprofen and supports the interpretation of the present results.

Based on the structural trends observed in Chapter 3 and the pH-dependent release behaviour reported here, three non-mutually exclusive mechanisms can account for the enhanced release of ibuprofen at higher pH values:

1. **Polymer-driven pH sensitivity:**

   As shown in Chapter 3, ionisation of pendant functional groups within the polymer backbone at elevated pH leads to increased polymer solvation, micellar swelling, and partial destabilisation, facilitating drug release through increased permeability or micelle disassembly(180, 188).

2. **Ibuprofen ionisation-driven release:**

   At pH values above the pKa of ibuprofen, ionisation reduces hydrophobic interactions between the drug and the micellar core, favouring its partitioning into the aqueous phase. This mechanism is expected to be particularly significant near and above physiological pH(203).

3. **Combined polymer and drug effects:**

[2] National Center for Biotechnology Information (2026). PubChem Compound Summary for CID 3672, Ibuprofen, (+-)-. Retrieved January 23, 2026 from https://pubchem.ncbi.nlm.nih.gov/compound/Ibuprofen.

The most plausible explanation for the observed behaviour is a synergistic effect in which polymer pH-responsiveness and ibuprofen ionisation act concurrently. Polymer structural reorganisation weakens micellar confinement, while ibuprofen ionisation further diminishes drug–polymer affinity, together producing the pronounced pH-triggered release observed experimentally(204, 205).

Accordingly, the pH-dependent drug release behaviour described in this chapter should be interpreted as the combined consequence of polymer structural responsiveness and the pKa-controlled ionisation of ibuprofen. Explicit consideration of ibuprofen's pKa provides a more rigorous mechanistic framework for understanding release behaviour and strengthens the relevance of these findings for pH-responsive drug delivery applications(203, 206, 207).

4.4.4 Drug Delivery Perspective

The comparative analysis highlights distinct release strategies:

- **IB-alt-MA-g-PEG**: is well suited for sustained release in acidic environments and faster release at alkaline pH. At low pH (3), the large elongated elliptical cylinders (length ~400 Å) and associated aggregates provide a hydrophobic core and tortuous path that slow ibuprofen diffusion, supporting prolonged/depot-like release in acidic conditions.
- At high pH (8–12), the transition to small compact cylinders (radius ~7 Å, length ~54 Å at pH 12) reduces hydrophobic domain size and aggregation, enabling accelerated, diffusion-controlled release in alkaline sites (e.g., intestines).
- **MA-alt-C_{18}-g-PEG**: Offers highly tuneable, stimulus-responsive release. The non-monotonic behaviour allows for "triggered" release; specifically, the breakdown of the micellar structure at pH 12 (N_{agg} collapse to 2.2) promotes rapid drug unloading. Conversely, the stable spherical architecture at pH 3–5 ensures drug protection and sustained release in mildly acidic physiological sites.
- **LIR410-g-PEG**: Provides the most stable platform for systemic delivery. The high core volume at low pH maximizes drug loading capacity, while the steric stabilization ensures the carriers remain discrete in the bloodstream. The transition to a highly dispersed state at alkaline pH, marked by a Porod slope drop to ~3.0, suggests a mechanism for accelerated release through diffuse interfaces in targeted alkaline microenvironments.

4.5 Conclusion

The three grafted polymer systems display markedly different structural behaviours and colloidal responses when encapsulating ibuprofen, reflecting differences in backbone chemistry, hydrophobic content, and PEG steric stabilisation.

- **IB-alt-MA-g-PEG** is a highly pH-sensitive graft copolymer with excellent potential for controlled drug delivery. SANS data show progressive structural contraction with rising pH: large elongated elliptical cylinders at low pH (pH 3) resulted swollen micelles at pH 5 and small compact cylinders at high pH (pH 12). This enables sustained ibuprofen release in acidic environments (large hydrophobic domains and aggregates) and faster triggered release in alkaline conditions (reduced core size and aggregation). The system maintains good colloidal stability across pH 3–12, making it a promising platform for site-specific, pH-responsive nanocarriers.(105, 106, 180, 208).
- **MA-alt-C_{18}-g-PEG** tolerates the widest range of drug and polymer concentrations with progressive (mostly monotonic) structural adaptation — including core contraction and aggregation number increase at intermediate loadings, followed by partial clustering at the highest levels. It maintains good colloidal stability across a broad pH range without catastrophic changes, positioning it as the most promising system for sustained release with higher payload capacity(106, 182, 191).
- **LIR410-g-PEG** exhibits the highest colloidal robustness. It maintains hydrodynamic diameters in the 290–360 nm range across the broadest drug-loading window tested and shows only modest size/pH-induced changes. Strong PEG steric stabilisation minimises uncontrolled aggregation and polydispersity shifts, making it the preferred candidate for systemic intravenous delivery requiring reproducible nanoscale size and environmental stability(5, 104, 158).

In summary:

- IB-alt-MA-g-PEG → pH-responsive; suited for triggered or depot release in acidic settings
- MA-alt-C_{18}-g-PEG → highest concentration & loading tolerance; best for sustained release
- LIR410-g-PEG → most sterically stabilised; optimal for systemic applications

These complementary profiles demonstrate how backbone hydrophobicity, maleic anhydride content, chain flexibility, and PEG grafting density can be strategically adjusted to target specific administration routes, release kinetics, and physiological microenvironments. The combination 5% w/w polymer with 0.25% w/w ibuprofen provides a stable, reproducible baseline for subsequent release, cytotoxicity, and in-vivo studies.

Chapter 5

Conclusion and future works

This research set out to address one of the enduring challenges in pharmaceutical science: the effective delivery of hydrophobic drugs such as ibuprofen and oxaprozin. Their poor aqueous solubility and variable bioavailability limit therapeutic performance and complicate formulation. By focusing on amphiphilic grafted copolymers, IB-alt-MA-G-PEG, MA-alt-C_8-g-PEG, and PEG-g-LIR410, this study explored how polymer architecture, concentration, and environmental conditions shape micelle formation, stability, and drug-release behaviour.

Through a combination of Dynamic Light Scattering (DLS), Small-Angle Neutron Scattering (SANS), and complementary spectroscopic analyses, the work provided a detailed picture of how these systems behave at the nanoscale. DLS offered insight into hydrodynamic diameters and concentration-dependent size changes, while SANS revealed internal structural parameters such as core radius, radius of gyration, and aggregation number. Together, these techniques allowed a nuanced comparison of the three polymers under matched conditions.

The findings demonstrate that each polymer system offers distinct advantages. IB-alt-MA-G-PEG forms compact, near-spherical aggregates but shows non-monotonic clustering behaviour, with particle sizes increasing at intermediate concentrations before modest compaction at higher levels. Its moderate pH sensitivity, combined with an intermediate temperature response, characterised by an increase up to 35 °C followed by partial reorganisation, suggests suitability for depot-like release applications where slower diffusion and controlled structural rearrangement are advantageous. MA-alt-C_8-g-PEG displayed more predictable monotonic aggregation, with corona expansion at mildly acidic pH and compaction under alkaline conditions. Its reproducible shifts in aggregation number support concentration- and pH-tuned sustained release, making it a versatile candidate for controlled delivery. PEG-g-LIR410 consistently maintained spherical morphology and steric stabilisation across all conditions. DLS showed a monotonic decrease in particle size with increasing concentration, while SANS confirmed moderate clustering at acidic pH and dispersion at alkaline pH. The PEG corona provided steric stabilisation, preventing excessive aggregation and ensuring colloidal stability, positioning PEG-g-LIR410 as particularly suitable for systemic delivery.

Taken together, these results confirm that micelle stability, corona hydration, and clustering behaviour are tightly coupled to drug-release kinetics. More broadly, they highlight how polymer design—balancing hydrophobic and hydrophilic segments, controlling corona chemistry, and introducing PEGylation—can be strategically leveraged to tailor micelle carriers for specific therapeutic contexts. IB-alt-MA-G-PEG is most appropriate for local depot release, MA-alt-C_8-g-PEG for sustained release tuned by concentration and pH, and PEG-g-LIR410 for robust systemic delivery.

Overall, LIR410-g-PEG displayed the most pronounced and predictable thermoresponsiveness, MA-alt-C_8-g-PEG remained essentially thermoresistant within the studied range, and IB-alt-MA-g-PEG showed intermediate behaviour with a temperature-dependent increase up to 35 °C followed by partial recovery at higher temperatures. These differences highlight the dominant influence of backbone hydrophobicity and graft architecture on thermal behaviour. While the concentration discrepancy precludes direct quantitative comparison, the trends are sufficiently distinct to guide polymer selection:

LIR410-g-PEG for applications requiring thermal modulation, MA-alt-C_8-g-PEG for systems demanding high thermal stability, and IB-alt-MA-g-PEG for cases where an intermediate, partially temperature-responsive behaviour is advantageous.

5.1 Limitations and Outlook

While this study has provided valuable insights into the aggregation behaviour and drug-delivery potential of IB-alt-MA-G-PEG, MA-alt-C_8-g-PEG, and LIR410-g-PEG micelles, several limitations should be acknowledged. First, the work relied primarily on in vitro scattering techniques (DLS and SANS), which, although powerful for structural characterisation, cannot fully replicate the complexity of biological environments. The absence of drug-release kinetics experiments means that the structural behaviours observed here were interpreted as proxies for release potential rather than being directly validated against release profiles. Similarly, in vivo pharmacokinetic and biodistribution studies were beyond the scope of this thesis, limiting the ability to confirm how pH- and concentration-dependent behaviours translate into therapeutic outcomes.

Another limitation lies in the variability of DLS measurements, particularly for MA-alt-C_8-g-PEG, where large error bars indicate inconsistent aggregation behaviour. Although DLS can also provide polydispersity indices (PDI), these were not considered here. This omission represents a limitation, as PDI offers insight into size distribution. However, complementary SANS analyses provided more detailed structural information, mitigating this limitation. While SANS offered nanoscale resolution, further orthogonal methods such as zeta potential analysis, cryo-TEM, or flow imaging microscopy would strengthen confidence in the observed trends. Additionally, the study focused on ibuprofen and oxaprozin as model drugs, which, while representative of hydrophobic NSAIDs, may not capture the full diversity of drug–polymer interactions relevant to other therapeutic classes.

Despite these limitations, the thesis establishes a robust comparative framework for understanding how polymer architecture influences micelle behaviour. The findings provide a foundation for future work that integrates drug-release assays, in vivo validation, and advanced imaging techniques, ensuring that the structural insights gained here can be translated into practical therapeutic applications.

5.2 Future Work

While this thesis has provided a comprehensive structural and functional comparison of three amphiphilic copolymers, several avenues remain open for further exploration. Future studies should investigate multi-responsive micelles that respond not only to pH but also to reactive oxygen species, enzymatic activity, or temperature, enabling multi-modal release in complex biological environments (209). Hybrid nanocarriers that combine polymer–lipid or polymer–inorganic components could offer enhanced targeting and imaging capabilities (210). In vivo pharmacokinetic and biodistribution studies are essential to validate how the concentration- and pH-dependent behaviours observed here translate into therapeutic efficacy, particularly in tumour and inflamed tissue microenvironments (104).

There is also scope to tailor micelle formulations to patient-specific microenvironments, aligning with the growing emphasis on personalized nanomedicine(211). Gene delivery represents another promising direction, with MA-alt-C_{18}-g-PEG and PEG-g-LIR410 systems offering stability and tunability for nucleic acid encapsulation (210). Finally, sustainable synthesis routes for amphiphilic copolymers should be pursued to reduce environmental impact while maintaining performance, reflecting the broader move toward green chemistry in pharmaceutical development.

5.3 Suggested research

Building on these promising results, several directions are recommended:

1. **In Vitro Drug Release Studies**
    - Conduct release kinetics experiments under simulated physiological conditions (e.g., gastric and intestinal fluids).
    - Use UV-Vis spectroscopy or HPLC to monitor ibuprofen release over(212).
2. **Cytotoxicity and Biocompatibility Testing**
    - Perform cell viability assays (MTT, LDH) to assess safety.
    - Evaluate hemocompatibility and immunogenicity for systemic(213).
3. **Cellular Uptake and Targeting**
    - Use fluorescently labelled micelles to study uptake via confocal microscopy or flow cytometry.
    - Investigate passive targeting (EPR effect) and active targeting with ligands (folate, peptides)(214).
4. **In Vivo Pharmacokinetics and Biodistribution**
    - Test formulations in animal models to assess circulation time, organ distribution, and bioavailability.
    - Compare LIR410-g-PEG and MA-alt-C_8-g-PEG for tumour accumulation or intestinal absorption(215).
5. **Polymer Engineering and Optimisation**
    - Vary hydrophobic chain length, grafting density, or molecular weight.
    - Introduce stimuli-responsive linkers (pH-cleavable, redox-sensitive)(216).

6. **Multi-Drug Encapsulation**
    - Explore co-encapsulation of hydrophobic and hydrophilic drugs for combination therapies.
    - Study drug–drug interactions within micelles and their impact on(217).
7. **Long-Term Stability and Shelf-Life**
    - Assess physical and chemical stability under storage conditions.
    - Monitor particle size, PDI, and drug retention over time(218).
8. **Scale-Up and Formulation Development**
    - Investigate scalable synthesis methods for polymer micelles.
    - Develop injectable formulations suitable for clinical translation(219).

5.4 Final Remarks

This thesis demonstrates that amphiphilic copolymers can be rationally designed to overcome the limitations of hydrophobic drug delivery. By integrating DLS and SANS analyses, it has provided a robust comparative framework for understanding how IB-alt-MA-g-PEG, MA-alt-C_8-g-PEG, and PEG-g-LIR410 behave under different conditions and how these behaviours translate into drug-release strategies. The work underscores the versatility of polymeric micelles in modern nanomedicine and lays the foundation for future innovations in responsive, patient-tailored drug delivery systems.

Ultimately, integrating structural characterisation with functional assays and clinical translation will ensure that amphiphilic copolymers advance beyond laboratory models into practical therapeutic applications.

Appendix

Appendix A — SasView Workflow, q Range Guidance, and Fit Report Templates

A.1 Overview and Provenance

This appendix documents the exact steps used in SasView so examiners can reproduce fits and verify model selection. Archived files include:

- Raw and masked 1D I(q) data
- SasView project or parameter files
- Exported fit reports (text/PDF)
- Residual plots
- Post-processing scripts used to compute derived quantities (e.g., aggregation number, Nagg)

A.2 Definitions and Recommended q Ranges

- Instrument q range (measured): Full dataset range. Example (IB-alt-MA-g-PEG 0.1%): qmin = 0.00408 $Å^{-1}$, qmax = 0.985 $Å^{-1}$.
- Low q (Guinier region): Probes overall size. Use only where Guinier criterion holds ($q \cdot Rg \leq 1.3$). If the Guinier knee lies below qmin, treat Rg as a lower bound.
- Mid q region: Contains form factor features (oscillations, shoulders) revealing internal structure (core–shell contrast, shell thickness). Typically, 0.02–0.2 $Å^{-1}$.
- High q (Porod region): Probes surface/local structure. Use $q \geq 0.3$ $Å^{-1}$ (rightmost 20–30% of data) to estimate Porod exponent and incoherent background.

Rules of thumb:

- Guinier fits: Select leftmost points until curvature appears; verify $q \cdot Rg \leq 1.3$.
- Porod fits: Perform log–log linear regression on high q tail after background subtraction.
- Model fits: Choose q window containing relevant features (e.g., sphere oscillations in mid q).

A.3 Small Angle Neutron Scattering (SANS)

Small-Angle Neutron Scattering (SANS) measurements were performed on the SANS2D beamline at the ISIS Neutron and Muon Source (UK) to characterise the internal structure of micellar formulations. Samples were prepared in quartz cells with a path length of 1–2 mm and measured at room temperature. Deuterated water (D_2O) was used as the solvent to enhance contrast between micellar components and the background.

A collimated beam of cold neutrons was directed through the samples, and scattering was detected at small angles to probe differences in scattering length density (SLD) between the hydrophobic core, hydrophilic shell, and solvent. Multiple detector distances and neutron wavelengths were employed to cover a broad q-range, enabling resolution of both core and shell regions (Figure A.1).

Raw scattering data were corrected for background, transmission, and detector efficiency, and subsequently reduced to one-dimensional scattering profiles (intensity vs. q) for model fitting and structural analysis.

This experiment took place in ISIS Neutron and Muon Source, located at the STFC Rutherford Appleton Laboratory in Oxfordshire, which is a globally recognised research facility specialising in physical and

life sciences. All samples were prepared again, but this time they used D_2O and all lids were kept closed with parafilm to avoid unwanted interaction with oxygen. Then, after overnight magnet stirring, samples were transferred to the SANS2D and exposed to radiation.
All signals were stored in a folder and sent to us for analysis in SasView.

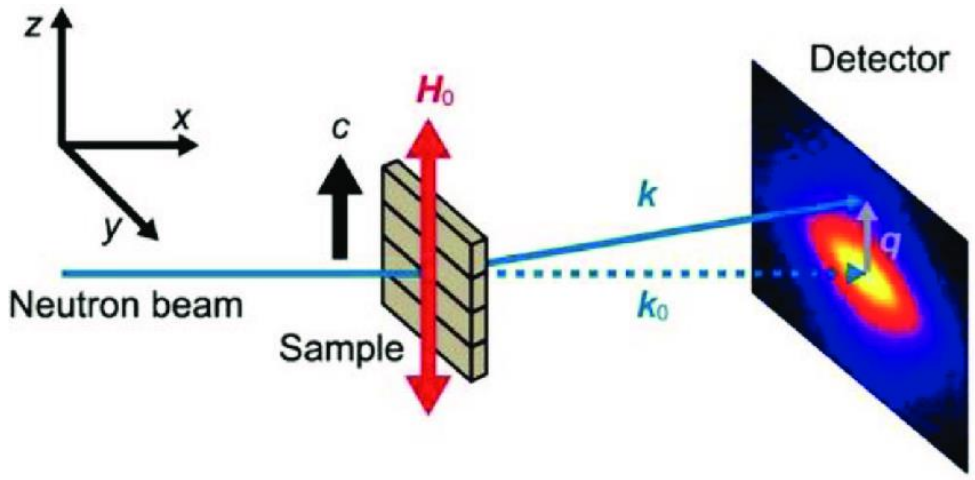

Fig A.1: Schematic of SANS experimental setup [3]. Reprinted with permission. Copyright 2016 Nature Publishing Group(220).

The scattering wave vector (Ks) and the incident wave vector (Ki) define the angle between them, denoted as 2θ. Mathematically, the magnitude of the scattering vector q is expressed as:

$$q = \frac{4\pi}{\lambda}\sin\theta$$

where λ is the neutron wavelength and θ is half the angle between Ks and Ki. The unit of q is typically $Å^{-1}$ or nm^{-1}. In real space, q can also be represented as:

$$q = \frac{2\pi}{d}$$

where d is the interplanar spacing in the crystal. For a more comprehensive explanation, readers are encouraged to consult specialised literature(220).

The scattering intensity I(q) is calculated as

$$I(Q) = \frac{A}{Q^n} + \frac{C}{1+(Q\xi)^m} + \text{background}$$

The first term describes Porod scattering from clusters (exponent = n), and the second term is a Lorentzian function describing scattering from polymer chains (exponent = m). This second term characterises polymer/solvent interactions and therefore the thermodynamics. The two multiplicative factors, A and C, and the two exponents n and m, are used as fitting parameters (Respectively, porod_scale, lorentz_scale,

porod_exp, and lorentz_exp in the parameter list). The remaining parameter ξ (*cor_length* in the parameter list) is a correlation length for the polymer chains. Note that when m=2, this functional form becomes the familiar Lorentzian function. Some interpretation of the values of A and C may be possible depending on the values of m and n.

A.4 SasView Procedure

- Import data: File → Load 1D data → select reduced I(q). Verify units (q in $Å^{-1}$, I in cm^{-1}).
- Masking/trimming: Mask detector edges/outliers; trim noisy extremes.
- Background estimation: Inspect high q region (e.g., 0.3–0.9 $Å^{-1}$). Compute weighted average of I(q) to estimate flat incoherent background B. Example: IB-alt-MA-g-PEG 0.1% → B ≈ 0.02035 cm^{-1}.
- Guinier check: Plot ln[I(q)] vs q^2 for leftmost points. Fit linear region only if Guinier criterion holds. If not, report Rg lower bound.
- Model testing: Load candidate models, set initial guesses/bounds, fix or tightly bound background, choose weighting (σ if present, otherwise $1/\sigma^2$), fit over appropriate q range. Inspect parameters, uncertainties, residuals. Save reports and plots.
- Model selection: Compare reduced χ^2, residuals, parameter plausibility, and consistency with DLS/chemistry. Prefer simpler or chemically consistent models if fits are comparable.
- Post processing: Export best fit parameters and covariance matrix. Compute derived quantities (sphere radius R = $\sqrt{(5/3)}\cdot$Rg, Nagg) with error propagation. Archive outputs.

A.5 Initial Guesses and Bounds

- Background: Set to high q average; bound ±10–20% if not fixed.
- Guinier–Porod (Beaucage): Rg start 350–600 Å; Porod exponent start 2.0–3.0; bounds Rg [50, 5000] Å; s [0.5, 6].
- Debye (Gaussian coil): Rg start 400–800 Å; bounds [50, 5000] Å.
- Flexible cylinder: Persistence length 20–50 Å; contour length 1000–10000 Å; cross section radius 5–20 Å.
- Sphere/Core–Shell Sphere: Seed radius from Guinier Rg ($R \approx \sqrt{(5/3)}\cdot Rg$); otherwise 50–70 Å.
- Two Lorentzian: Correlation lengths ξ_1 ~ 10–50 Å, ξ_2 ~ 100–1000 Å.

A.6 Data Preprocessing

- File import and masking: Load reduced 1D I(q) files; mask detector edges and remove obvious outliers.
- Background estimation: Estimate a flat incoherent background from the high q tail (q ≈ 0.3–0.9 $Å^{-1}$). For IB-alt-MA-g-PEG 0.1%, B ≈ 0.02035 cm^{-1}; fixed or tightly bounded during fits.

- q range trimming: Retain full measured q range (0.00408–0.985 $Å^{-1}$); select subranges for specific fits (Guinier, Porod, mid q model checks).

Guinier Check and Limits

- Guinier validity: Use criterion $q \cdot Rg \leq 1.3$. If no Guinier knee is visible at q_min, report lower bound: $Rg \geq 1.3/q\_min$. For IB-alt-MA-g-PEG 0.1%, q_min = 0.00408 $Å^{-1}$ → $Rg \geq 319$ Å.
- Practical Guinier fit: Attempt ln[I(q)] vs q^2 fits only where Guinier condition holds; otherwise treat Rg as bound.

A.7 Model Selection Strategy

Decision tree:

- If a clear Guinier plateau exists → use Guinier → test sphere/core–shell or Guinier–Porod.
- If low q shows power law scaling → prefer Guinier–Porod or Debye (Gaussian coil).
- If mid q indicates semiflexible behaviour → test flexible cylinder.
- If broad low q intensity and hierarchical structure appear → test two Lorentzian / correlation length models.

Model comparison criteria:

- Reduced χ^2
- Residual structure
- Parameter uncertainties and covariance
- Physical plausibility (e.g., R_g consistent with q range)
- Reproducibility across replicates

A.8 Practical SasView Settings and Initial Guesses

- Weighting: Use experimental uncertainties if available; otherwise use $1/\sigma^2$ or default SasView weighting.
- Background: Fix or tightly bound near high q estimate (e.g., 0.02035 cm^{-1} for IB-alt-MA-g-PEG 0.1%).
- Guinier–Porod: Rg start 350–600 Å; Porod exponent start 2.0–3.0.
- Debye (Gaussian coil): R_g start 400–800 Å; allow background ±10–20%.
- Flexible cylinder: Persistence length 20–50 Å; contour length sufficient for R_g in hundreds of Å; cross section radius a few Å–nm.
- Bounds and convergence: Use physically reasonable bounds; inspect covariance and parameter limits after fitting.

Notes on Two-Term Scattering Function

The first term describes Porod scattering from clusters (exponent = n), and the second term is a Lorentzian function describing scattering from polymer chains (exponent = m). This second term characterises polymer/solvent interactions and therefore the thermodynamics. The two multiplicative factors, A and C, and the two exponents n and m, are used as fitting parameters (porod_scale, lorentz_scale, porod_exp, lorentz_exp). The remaining parameter ξ (cor_length) is a correlation length for the polymer chains. When m = 2, the second term becomes the familiar Lorentzian function. Interpretation of A and C may be possible depending on the values of m and n.

A.8 Fit Report Template

Table A.1 — Fit summary (example: IB-alt-MA-g-PEG 0.1%)

Model	q fit range ($Å^{-1}$)	Background (cm^{-1})	Parameters (best ± err)	Notes
Guinier–Porod	0.00408–0.2	0.02035 (fixed)	R_g lower bound ≥ 319 Å	No clear Guinier knee
Debye coil	0.0055–0.02	0.02035 (±10%)	R_g = 227 Å (weakly constrained)	Driven to upper bound
Two Lorentzian	0.00408–0.3	0.02035 (fixed)	ξ = …; ξ = …	Preferred if residuals minimal

Record for each dataset:

- q ranges used
- Background estimate
- Parameter values ± errors
- Reduced χ^2
- Residual plots and covariance matrices
- Derived quantities (sphere radius, N_{agg}) with assumptions stated

A.9 Notes on Models Used in This Work

- Guinier–Porod: applied to MA-alt-C_{18}-g-PEG and LIR410-g-PEG micelles, capturing overall size and Porod slope for compact spherical aggregates.
- Debye coil: tested for IB-alt-MA-g-PEG to probe coil-like behaviour; fits often weakly constrained, reported cautiously.
- Sphere/Core–Shell Sphere: used where mid-q oscillations suggested discrete micelles; provided radius and shell thickness estimates.
- Flexible cylinder: explored for LIR410-g-PEG under conditions suggesting elongated structures; persistence length and contour length parameters reported.

- Two Lorentzian: preferred for IB-alt-MA-g-PEG in D_2O, capturing correlation lengths of diffuse domains and clustering behaviour.

A.10 Reproducibility Checklist

- SasView version and platform
- Raw filenames and acquisition metadata (wavelength, detector distance, exposure time)
- Mask file and trimming details
- Exact q ranges used
- Initial guesses and bounds
- Weighting scheme
- Exported fit reports and covariance matrices
- Post-processing scripts with README

Appendix B — SANS2D Experiment and SasView Analysis Guide

B.1 SasView User Guide for SANS Data Analysis

SasView is an open-source application for analysing small-angle scattering data (SANS/SAXS), enabling users to fit experimental data to theoretical models and extract structural parameters.

Workflow:

1. Install SasView (sasview.org).
2. Launch and load 1D SANS data (.txt, .h5, .xml).
3. Select appropriate model (Core–Shell Sphere, Guinier–Porod, Debye coil, Flexible cylinder, Two Lorentzian).
4. Set parameters (core radius, shell thickness, SLDs, volume fraction).
5. Fit model using non-linear least squares. Inspect χ^2 and residuals.
6. Export results (parameters, plots, reports).

Tips:

- Use contrast variation (D_2O/H_2O) for better visibility.
- Fit multiple datasets together for comparative studies (e.g., pH, concentration).
- Use log–log plots to visualise low-q and high-q regions.

B.2 Python workflow

Here is the Python workflow that reads reduced 1D SANS files, subtracts the background, and extracts key parameters such as Guinier radius R_g, Porod exponent, and correlation lengths.

```
import numpy as np
import pandas as pd
import matplotlib.pyplot as plt
from scipy.stats import linregress

# === Load SANS file ===
# Assumes columns: q, I(q), error, (optional extra)
def load_sans_file(filename):
    data      =      np.loadtxt(filename,      comments=['#','SANS2D','Workspace'],
usecols=(0,1,2))
    q, Iq, err = data[:,0], data[:,1], data[:,2]
    return q, Iq, err

# === Background subtraction ===
def subtract_background(q, Iq, high_q_range=(0.3,0.9)):
    mask = (q >= high_q_range[0]) & (q <= high_q_range[1])
    B = np.average(Iq[mask])
    Iq_corr = Iq - B
    return Iq_corr, B

# === Guinier fit ===
def guinier_fit(q, Iq_corr, qmax=0.02):
    mask = (q <= qmax) & (Iq_corr > 0)
    lnI = np.log(Iq_corr[mask])
    slope, intercept, r, p, se = linregress(q[mask]**2, lnI)
    Rg = np.sqrt(-slope) if slope < 0 else None
    return Rg, slope, intercept

# === Porod fit ===
def porod_fit(q, Iq_corr, qmin=0.3):
    mask = (q >= qmin) & (Iq_corr > 0)
    lnI = np.log(Iq_corr[mask])
    lnq = np.log(q[mask])
    slope, intercept, r, p, se = linregress(lnq, lnI)
    porod_exp = -slope
    return porod_exp, slope, intercept

# === Example usage ===
if __name__ == "__main__":
    q, Iq, err = load_sans_file("IB-BB-2%-d-THF_merged_1D.txt")
    Iq_corr, B = subtract_background(q, Iq)

    Rg, slope_g, intercept_g = guinier_fit(q, Iq_corr)
    porod_exp, slope_p, intercept_p = porod_fit(q, Iq_corr)

    print(f"Background B ≈ {B:.5f} cm⁻¹")
    print(f"Guinier Rg ≈ {Rg:.1f} Å (if valid)")
    print(f"Porod exponent ≈ {porod_exp:.2f}")

    # Plot corrected data
    plt.loglog(q, Iq_corr, 'o', label="Corrected I(q)")
    plt.xlabel("q (Å⁻¹)")
    plt.ylabel("I(q) (cm⁻¹)")
    plt.legend()
    plt.show()
```

What this code does

- **Loads** reduced 1D SANS file (skips headers).
- **Subtracts background** using the weighted average of the high-q tail.
- **Guinier fit**: linear regression of ln[I(q)] vs q^2 in the low-q region.
- **Porod fit**: slope of ln[I(q)] vs ln(q) in the high-q region.
- **Outputs** background, Guinier radius, and Porod exponent.
- **Plots** corrected scattering curve for quick inspection.

Appendix C — Dynamic Light Scattering (DLS) Sample Preparation and SOP

C.1 Overview

This appendix documents the procedures used to prepare polymer–drug micelle samples for DLS analysis, the rationale for solvent and temperature selection, and the standard operating procedure (SOP) followed on the Malvern Zetasizer instrument. The aim is to ensure reproducibility and transparency in the measurement of hydrodynamic size and polydispersity.

Dynamic Light Scattering (DLS), also known as Photon Correlation Spectroscopy (PCS), measures the translational diffusion of particles in solution. The diffusion coefficient is converted to hydrodynamic diameter, providing insights into particle size and conformation. This technique is widely applied to evaluate micellar systems, confirm nanoscale particle formation, and assess stability.

Concentration limits are critical:

- **>1% w/w** in cuvette → multiple scattering, inaccurate readings.
- **<0.001% w/w** → weak signals.

Careful dilution and baseline stability checks were therefore essential. Samples showing multimodal distributions or abnormal scattering were re-prepared to maintain data integrity (221).

C.2 Sample Preparation

Solvent and buffer selection

- Ultrapure water (18.2 MΩ·cm) for baseline measurements.
- D_2O for contrast matching experiments aligned with SANS.
- Buffers: acetate (pH 4.5–5.5), phosphate (pH 7.0–7.4), Tris (pH 8.0–8.5).
- Ionic strength varied between low salt (≤10 mM) and physiological (~150 mM NaCl).

Polymer and drug handling

- Polymer stocks prepared at 1–2% w/w, equilibrated 12–24 h for micelle formation.

- Ibuprofen dissolved in minimal ethanol or neutralised NaOH before addition.
- Target drug loadings: 0.10–0.50% w/w.
- Gentle stirring and dialysis used to remove cosolvent.

Clarification

- Filtration through 0.45 μm syringe filters (PTFE/PES) unless aggregates disrupted.
- Degassing by brief sonication to eliminate bubbles.

Concentration selection

- Screening: 0.10%, 0.25%, 0.50% w/w polymer.
- Drug loading at 0.25% w/w prioritised for balance of compactness and stability.

Cuvettes and cleanliness

- Disposable polystyrene cuvettes for aqueous samples.
- Quartz cuvettes for elevated temperatures or organic traces.
- Rinsed with DI water → ethanol → DI water, dried with filtered air.
- Solvent blanks measured to confirm cleanliness.

C.3 SOP Design for Malvern Zetasizer

Instrument settings

- Measurement angle: backscatter (173°).
- Equilibration: 120–300 s per measurement.
- Temperature: 25 °C baseline; 37 °C physiological; 20–45 °C thermoresponsive screening.
- Replicates: 10 runs per sample.
- Automatic attenuation enabled.
- Viscosity and refractive index entered according to solvent/buffer composition.

Workflow steps

1. Prepare polymer–drug solution at target pH and ionic strength.
2. Load cuvette carefully, avoiding bubbles.
3. Measure solvent blank to confirm baseline.
4. Select SOP parameters (temperature, runs, attenuation, viscosity, RI).
5. Acquire data: cumulant analysis (Z average, PDI), distribution analysis (multimodal behaviour).
6. Review quality metrics: count rate stability, correlogram intercept, PDI thresholds.
7. Export raw autocorrelation data, cumulant fits, distribution tables.

8. Record metadata: sample ID, SOP name, instrument serial number, date/time, solvent, buffer, pH, ionic strength, temperature.

C.4 Data Processing and Interpretation

Core outputs

- Z average hydrodynamic diameter (Dh).
- Polydispersity index (PDI).
- Intensity, number, and volume distributions.

Quality criteria

- Count rate stability within ±10%.
- Autocorrelation function (ACF) intercept ≥0.9.
- PDI ≤0.2 narrow; 0.2–0.4 moderate; >0.4 broad/multimodal.

Cross validation

- DLS results compared with SANS parameters (core radius, Rg, aggregation number).
- Full PDF reports archived (intensity, number, volume distributions).

C.5 Practical Notes

- Residual cosolvent (e.g., ethanol) can inflate Dh → dialysis or buffer exchange recommended.
- Dust and bubbles are common artefacts → rigorous cleaning and gentle handling essential.
- Incorrect viscosity inputs skew Dh → solvent viscosity must match measurement temperature.
- Avoid aggregation during filtration → low-speed centrifugation may be used as alternative.

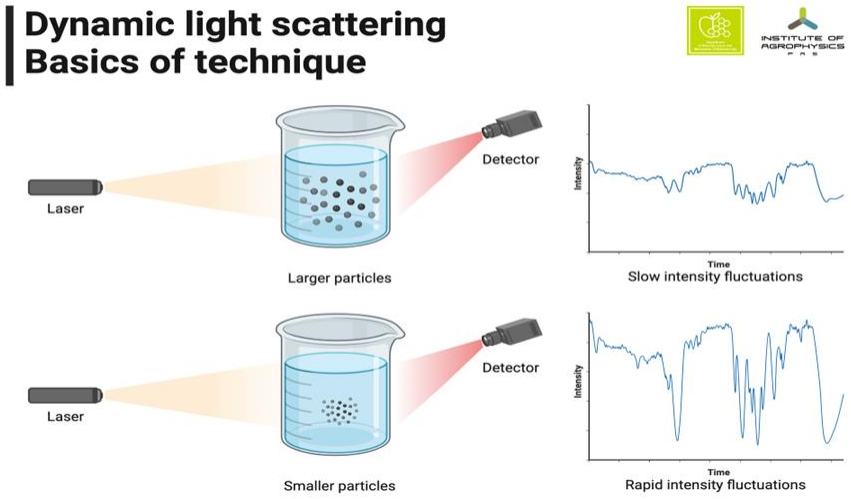

Fig C.1: The method that DLS uses to get data[2] . [5]

C.6 Dynamic Light Scattering (DLS) Data Output and Processing

To illustrate how DLS data were obtained and processed (Figure C.1), representative reports from the Malvern Zetasizer instrument are included. In this study, DLS measurements were restricted to the determination of hydrodynamic diameters (Dh). Although DLS can also provide polydispersity indices (PDI), these were not considered here. Instead, distributional and structural characteristics were assessed using Small Angle Neutron Scattering (SANS) and model fitting with SasView and Python scripts, which offered more detailed and reproducible insights into micelle morphology, aggregation number, and core–shell dimensions. This methodological choice reflects a focus on size as a primary screening parameter, with structural heterogeneity addressed through complementary scattering analyses.

Perspectives on DLS Output

The Zetasizer reports provide three complementary perspectives on particle size distribution:

- Intensity distribution Particle size is reported based on the relative intensity of scattered light. Larger particles scatter disproportionately more light, so intensity distributions are often dominated by rare large aggregates.
- Number distribution By applying Mie theory and instrument algorithms, intensity data are converted into an estimated number distribution. This reduces the bias toward large particles and highlights the most abundant species in solution.

[2] https://www.biorender.com/template/dynamic-light-scattering [5]

- Volume distribution A further transformation provides the relative contribution of each size class to the total sample volume. This is useful for correlating with drug loading capacity, since larger micelles contribute more volume per particle.

Representative Dataset

A dataset from the IB-alt-MA-g-PEG + drug 1 formulation illustrates how DLS output is structured and interpreted:

- Sample ID: IB-alt-MA-g-PEG + drug 1
- Date measured: 19 November 2024
- SOP used: *Tamara – IB.sop*
- Z-average hydrodynamic diameter (Dh): 268.7 nm
- Standard deviation: 3.35 nm (narrow distribution)
- Derived count rate: 21,228 kcps (strong scattering, good sample quality)

a)

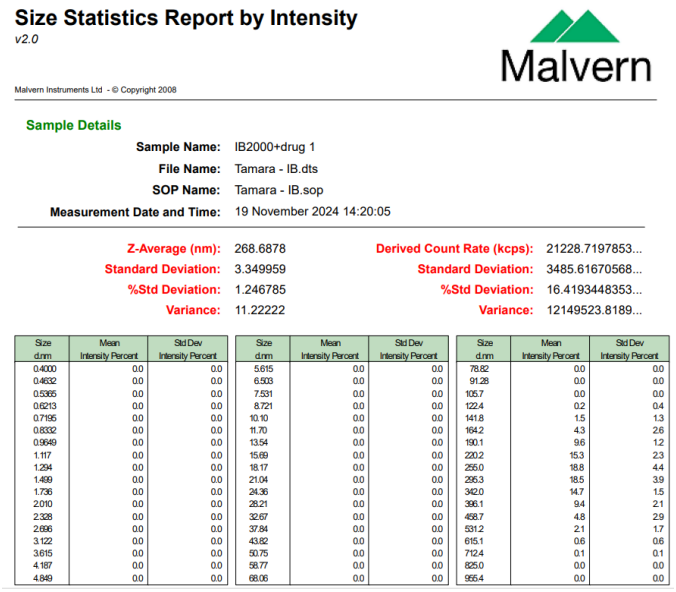

Size Statistics Report by Intensity

v2.0

Malvern

Malvern Instruments Ltd. - © Copyright 2008

Sample Details

Sample Name:	IB2000+drug 1
File Name:	Tamara - IB.dts
SOP Name:	Tamara - IB.sop
Measurement Date and Time:	19 November 2024 14:20:05

Z-Average (nm):	268.6878	**Derived Count Rate (kcps):**	21228.7197853...
Standard Deviation:	3.349959	**Standard Deviation:**	3485.61670568...
%Std Deviation:	1.246785	**%Std Deviation:**	16.4193448353...
Variance:	11.22222	**Variance:**	12149523.8189...

Size d.nm	Mean Intensity Percent	Std Dev Intensity Percent	Size d.nm	Mean Intensity Percent	Std Dev Intensity Percent	Size d.nm	Mean Intensity Percent	Std Dev Intensity Percent
0.4000	0.0	0.0	5.615	0.0	0.0	78.82	0.0	0.0
0.4632	0.0	0.0	6.503	0.0	0.0	91.28	0.0	0.0
0.5365	0.0	0.0	7.531	0.0	0.0	105.7	0.0	0.0
0.6213	0.0	0.0	8.721	0.0	0.0	122.4	0.2	0.4
0.7195	0.0	0.0	10.10	0.0	0.0	141.8	1.5	1.3
0.8332	0.0	0.0	11.70	0.0	0.0	164.2	4.3	2.6
0.9649	0.0	0.0	13.54	0.0	0.0	190.1	9.6	1.2
1.117	0.0	0.0	15.69	0.0	0.0	220.2	15.3	2.3
1.294	0.0	0.0	18.17	0.0	0.0	255.0	18.8	4.4
1.499	0.0	0.0	21.04	0.0	0.0	295.3	18.5	3.9
1.736	0.0	0.0	24.36	0.0	0.0	342.0	14.7	1.5
2.010	0.0	0.0	28.21	0.0	0.0	396.1	9.4	2.1
2.328	0.0	0.0	32.67	0.0	0.0	458.7	4.8	2.9
2.696	0.0	0.0	37.84	0.0	0.0	531.2	2.1	1.7
3.122	0.0	0.0	43.82	0.0	0.0	615.1	0.6	0.6
3.615	0.0	0.0	50.75	0.0	0.0	712.4	0.1	0.1
4.187	0.0	0.0	58.77	0.0	0.0	825.0	0.0	0.0
4.849	0.0	0.0	68.06	0.0	0.0	955.4	0.0	0.0

b)

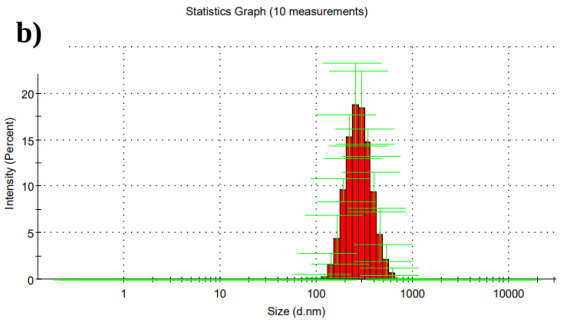

Fig. C.2: Representative DLS Output for IB-alt-MA-g-PEG + ibuprofen Formulation. a) Tabulated intensity-based size distribution showing particle diameters (d.nm), mean intensity percentages, and standard deviations across size bins. Larger particles dominate the intensity signal due to their higher scattering power. b) Logarithmic plot of intensity (%) versus particle size (d.nm), highlighting the peak around 100–300 nm where micelle populations are most prevalent. Error bars represent ±1 standard deviation across 10 measurements.

Intensity distribution: This representation is dominated by larger particles due to their disproportionate scattering power. In this sample, the intensity curve showed peaks around 295.3 nm, contributing over 12% of the total intensity, while smaller micelles in the 190–255 nm range contributed cumulatively over 50%. This suggests a mixed population with some larger aggregates present.

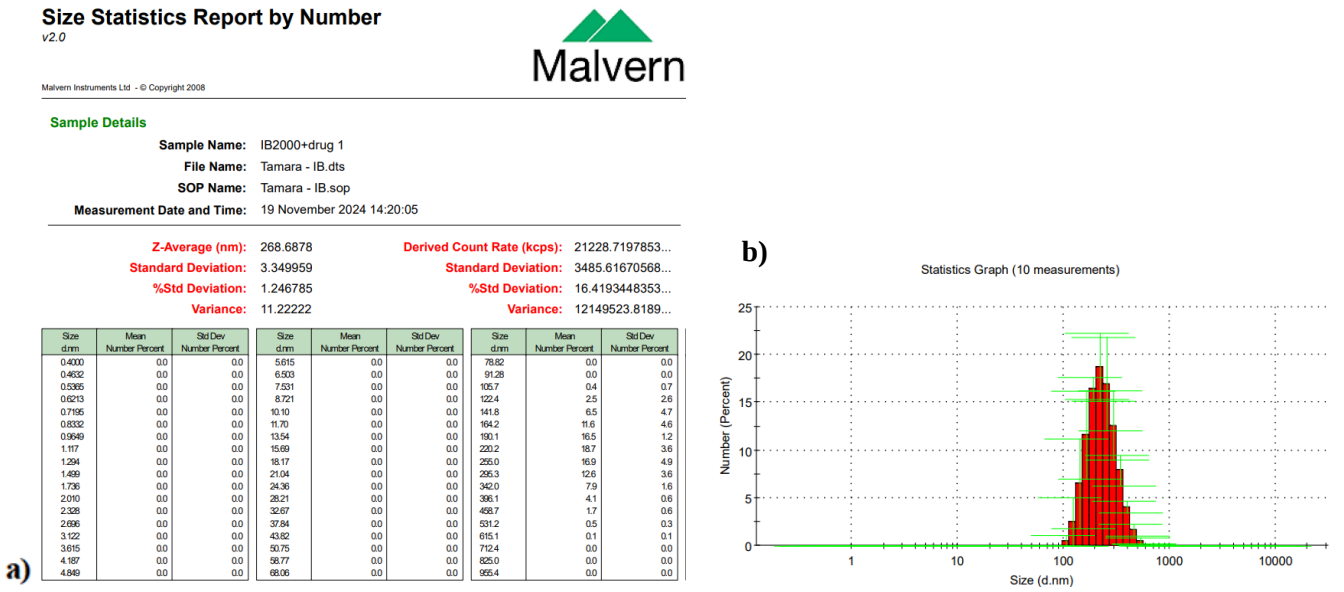

Fig. C.3: DLS Number-Based Size Distribution for IB-alt-MA-g-PEG + ibuprofen. a) Tabulated number distribution showing particle diameters (d.nm), mean number percentages, and standard deviations across size bins. This representation corrects for intensity bias and highlights the most abundant micelle population. b) Logarithmic plot of number (%) versus particle size (d.nm), with a clear peak around 100–220 nm, indicating the dominant micelle size range. Error bars represent ±1 standard deviation across 10 measurements.

Number distribution: The number-based curve revealed that most micelles were in the 190–255 nm range, with the highest number percentage (~18.7%) at 220.2 nm. This distribution corrects for the bias of larger particles and reflects the dominant population in solution. The presence of particles above 300 nm was minimal in number, despite their strong intensity signal.

a)

Size Statistics Report by Volume
v2.0

Malvern

rern Instruments Ltd. - © Copyright 2008

Sample Details

Sample Name:	IB2000+drug 1
File Name:	Tamara - IB.dts
SOP Name:	Tamara - IB.sop
Measurement Date and Time:	19 November 2024 14:20:05

Z-Average (nm):	268.6878	**Derived Count Rate (kcps):**	21228.7197853...
Standard Deviation (nm):	3.349959	**Standard Deviation (kcps):**	3485.61670568...
%Std Deviation:	1.246785	**%Std Deviation:**	16.4193448353...
Variance:	11.22222	**Variance:**	12149523.8189...

Size d.nm	Mean Volume Percent	Std Dev Volume Percent	Size d.nm	Mean Volume Percent	Std Dev Volume Percent	Size d.nm	Mean Volume Percent	Std Dev Volume Percent
0.4000	0.0	0.0	5.615	0.0	0.0	78.82	0.0	0.0
0.4632	0.0	0.0	6.503	0.0	0.0	91.28	0.0	0.0
0.5365	0.0	0.0	7.531	0.0	0.0	105.7	0.0	0.1
0.6213	0.0	0.0	8.721	0.0	0.0	122.4	0.4	0.4
0.7195	0.0	0.0	10.10	0.0	0.0	141.8	1.3	1.0
0.8332	0.0	0.0	11.70	0.0	0.0	164.2	3.5	1.3
0.9649	0.0	0.0	13.54	0.0	0.0	190.1	7.2	0.6
1.117	0.0	0.0	15.69	0.0	0.0	220.2	11.9	2.2
1.294	0.0	0.0	18.17	0.0	0.0	255.0	15.8	3.9
1.499	0.0	0.0	21.04	0.0	0.0	295.3	17.6	3.9
1.736	0.0	0.0	24.36	0.0	0.0	342.0	16.5	1.7
2.010	0.0	0.0	28.21	0.0	0.0	396.1	12.7	2.0
2.328	0.0	0.0	32.67	0.0	0.0	458.7	7.7	3.3
2.696	0.0	0.0	37.84	0.0	0.0	531.2	3.7	2.5
3.122	0.0	0.0	43.82	0.0	0.0	615.1	1.4	1.2
3.615	0.0	0.0	50.75	0.0	0.0	712.4	0.3	0.4
4.187	0.0	0.0	58.77	0.0	0.0	825.0	0.0	0.1
4.849	0.0	0.0	68.06	0.0	0.0	955.4	0.0	0.0

b)

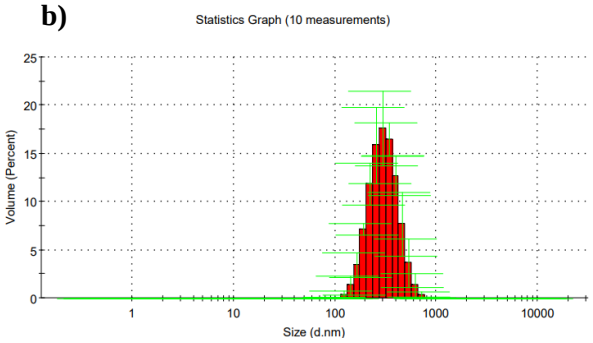

Fig.C.4: DLS Volume-Based Size Distribution for IB-alt-MA-g-PEG + ibuprofen. a) Tabulated volume distribution showing particle diameters (d.nm), mean volume percentages, and standard deviations across size bins. This representation reflects the relative contribution of each size class to the total sample volume, which is relevant for drug-loading capacity. b) Logarithmic plot of volume (%) versus particle size (d.nm), with a peak around 255–295 nm, indicating micelles with the greatest volumetric contribution. Error bars represent ±1 standard deviation across 10 measurements.

Volume distribution: Volume-based data showed that micelles around 255–295 nm contributed most to the total sample volume, consistent with their larger size and encapsulation potential. This is particularly relevant for drug delivery, where volume may correlate with payload capacity.

C.7 Data extraction and analysis:

The Zetasizer software provides comprehensive data analysis, exporting tabulated values for size (nm), mean percentage, and standard deviation across each distribution. Key metrics are the Z-average hydrodynamic diameter (Dh) and the Polydispersity Index (PDI), both derived from the cumulant analysis of the autocorrelation function to report average size and assess sample heterogeneity, respectively. Derived count rates (kcps) are simultaneously recorded to monitor sample quality and scattering intensity. For detailed interpretation, intensity distributions are specifically utilized to identify rare, large aggregates, while the number and volume distributions help determine the primary micelle population. All relevant values are cross-checked, where appropriate, against parameters from Small-Angle Neutron Scattering (SANS) measurements, such as core radius, radius of gyration (R_g), and aggregation number, to ensure consistency between hydrodynamic and structural characterizations. Including these raw reports demonstrates the workflow from instrument output to processed data. It also highlights the importance of interpreting DLS results cautiously: intensity distributions can exaggerate the presence of large

aggregates, while number and volume distributions provide a more realistic view of the micelle population.

Appendix D — Fourier-Transform Infrared (FTIR) Spectroscopy

D.1 Overview and Instrumentation

Fourier-transform infrared (FTIR) spectroscopy was employed to investigate chemical interactions between polymer and drug components, confirm functional group presence, and assess formulation stability. FTIR provides spectral fingerprints by measuring the absorption of infrared radiation across a range of wavenumbers, typically 4000–500 cm^{-1}.

Measurements were performed using a standard FTIR spectrometer equipped with a Michelson interferometer, a DTGS detector, and a KBr beam splitter (Figure D.1). Samples were prepared as thin films or dispersions, depending on solubility and formulation type. The interferogram generated by the modulated IR beam was processed via Fast Fourier Transform (FFT) to yield transmittance spectra (%T vs. wavenumber).

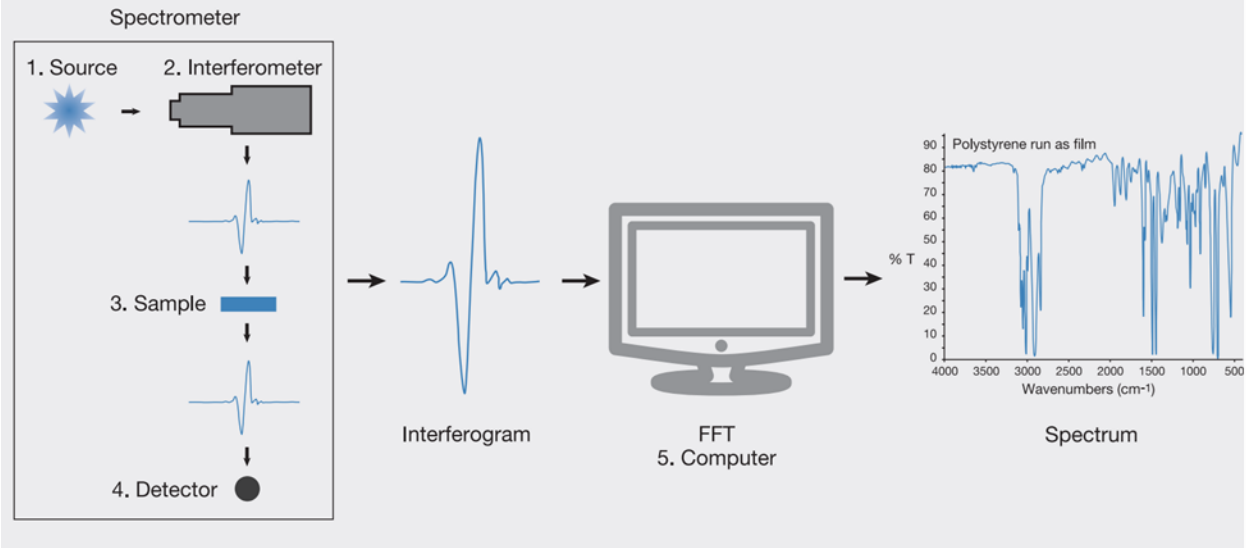

Fig.D.1: FTIR operation: light from the source passes through an interferometer and the sample, producing an interferogram at the detector, which is converted into a spectrum via Fast Fourier Transform (FFT)[1].

D.2 Measurement Workflow

The FTIR process follows five key stages (see Figure D.1):

1. **Source** — emits broadband infrared radiation.
2. **Interferometer** — modulates the IR beam using a moving mirror.
3. **Sample** — absorbs specific wavelengths corresponding to molecular vibrations.
4. **Detector** — records the transmitted or reflected light.
5. **Computer** — applies FFT to convert the interferogram into a usable spectrum.

Spectra were collected in the range 4000–500 cm^{-1}, with a resolution of 4 cm^{-1} and 32 scans per sample. Background spectra were recorded prior to each run and subtracted automatically.

D.3 Sample Preparation

- **Polymers and micelles** were cast as thin films or freeze-dried and pressed into KBr pellets.
- **Ibuprofen** was measured both as a pure compound and within polymer–drug formulations.
- **Solvent traces** were minimized by drying under vacuum or nitrogen flow.
- **Film uniformity** was confirmed visually and by baseline stability in the spectrum.

D.4 Data Interpretation

FTIR spectra were analysed to identify characteristic peaks corresponding to:

- C=O stretching (carboxylic acid, ester) near 1700 cm^{-1}
- O–H stretching (hydrogen bonding) near 3200–3600 cm^{-1}
- C–H stretching (alkyl chains) near 2800–3000 cm^{-1}
- C–O stretching (ethers, esters) near 1000–1300 cm^{-1}

Comparative analysis between pure ibuprofen, polymer-only, and polymer–drug formulations revealed peak shifts, broadening, or intensity changes, indicating possible hydrogen bonding, encapsulation, or chemical interactions.

D.5 Representative Spectrum

A sample spectrum from Polystyrene run as film is shown in Figure D.2. The x-axis represents wavenumbers (cm^{-1}) and the y-axis shows % transmittance. Key peaks were annotated and compared to literature values for validation.

Appendix E — Prepared Sample Photographs

This appendix presents photographic documentation of the polymer–drug micelle samples prepared for experimental analysis. These images serve as visual records of sample appearance, clarity, and homogeneity before measurement. They were taken immediately after preparation, ensuring consistency with the conditions described in Appendices C and D.

Each image captures the physical appearance of micelle dispersions across varying polymer concentrations and drug loadings. Labels on the vials indicate formulation details, including polymer type, concentration (% w/w), and drug content. These records support reproducibility by allowing examiners to verify sample clarity, homogeneity, and labeling accuracy.

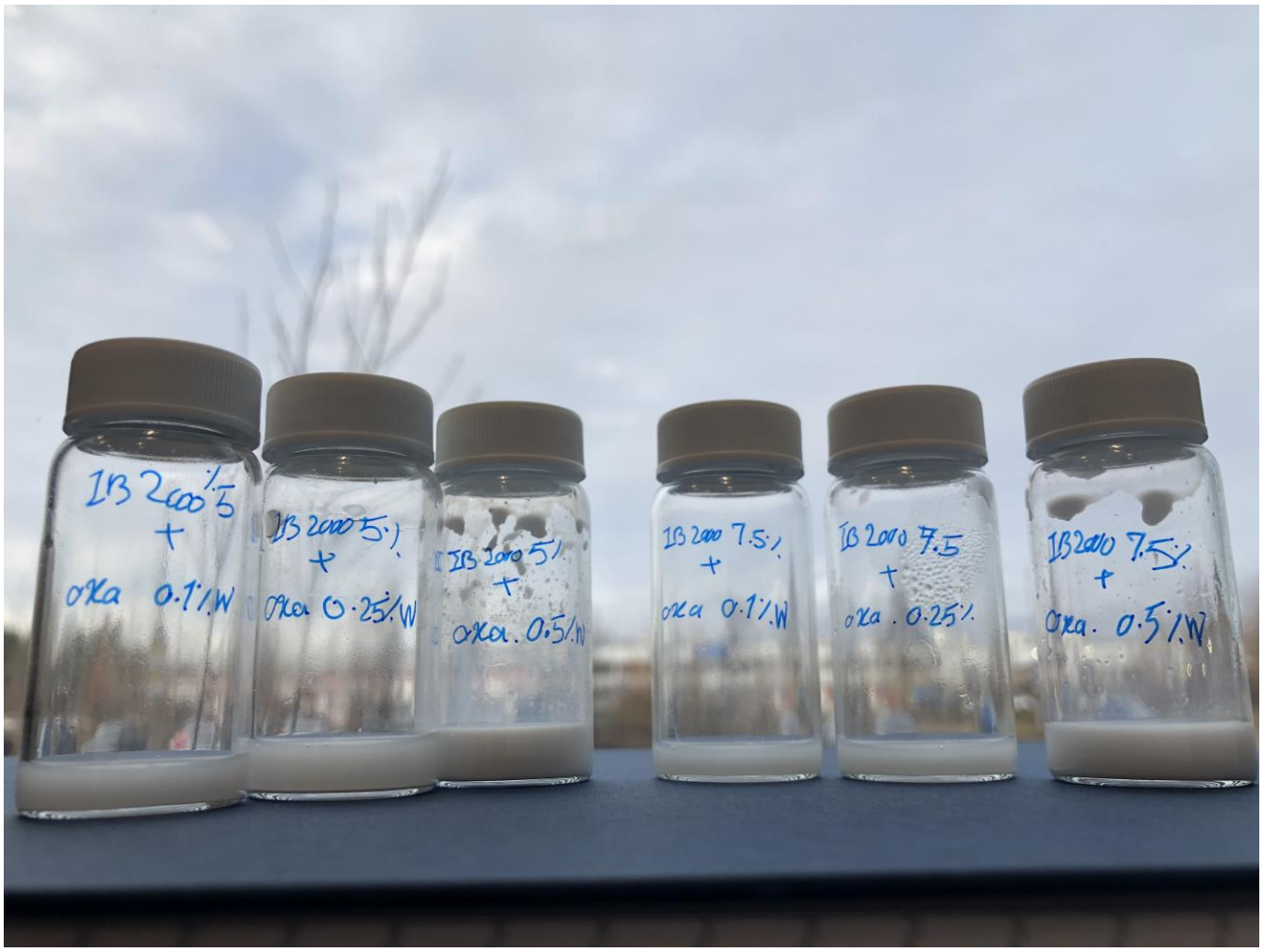

Fig. E.1: six formulations of IB-alt-MA-g-PEG combined with oxaprozin (Oxa) at 5% and 7.5% w/w polymer concentrations, with drug loadings of 0.1%, 0.25%, and 0.5% w/w. All samples were stored in sealed vials and photographed under ambient light conditions.

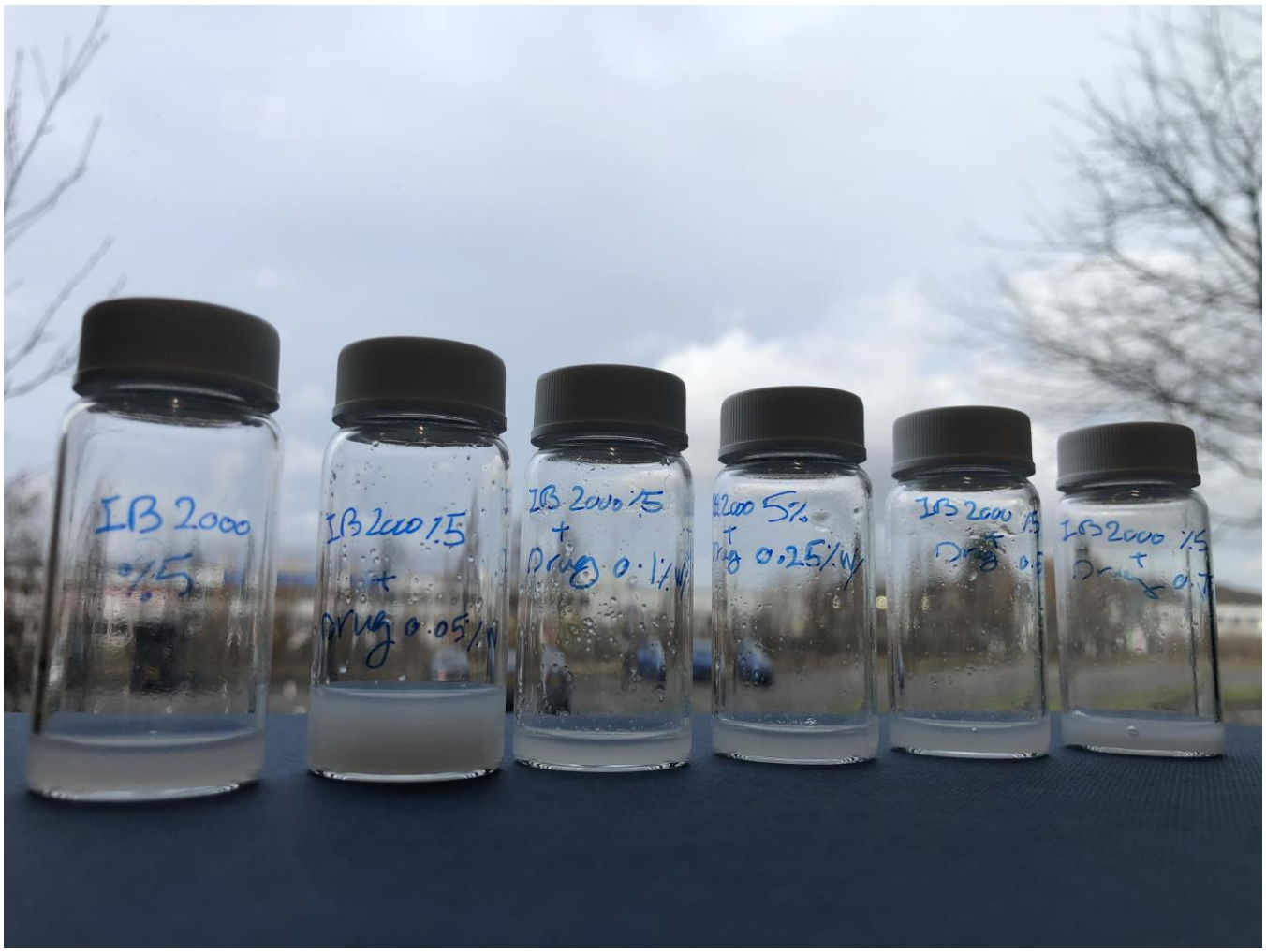

Fig. E.2: Second series of samples at 5% w/w polymer concentration, with increasing ibuprofen loadings from 0.05% to 0.75% w/w. Variations in turbidity suggest concentration-dependent aggregation or solubility effects.

Fig. E.3: Four samples of MA-alt-C_{18}-g-PEG 5% with ibuprofen at 0.25% w/w, prepared at different pH values (pH 3, 5, 8, and 12). These images illustrate pH-dependent solubility and micelle appearance.

Fig. E.4: shows a separate pH screening series for MA-alt-C_{18}-g-PEG at 2% w/w, with pH values ranging from 3 to 12. These samples were used to assess micelle stability and visual clarity across acidic, neutral, and basic conditions.

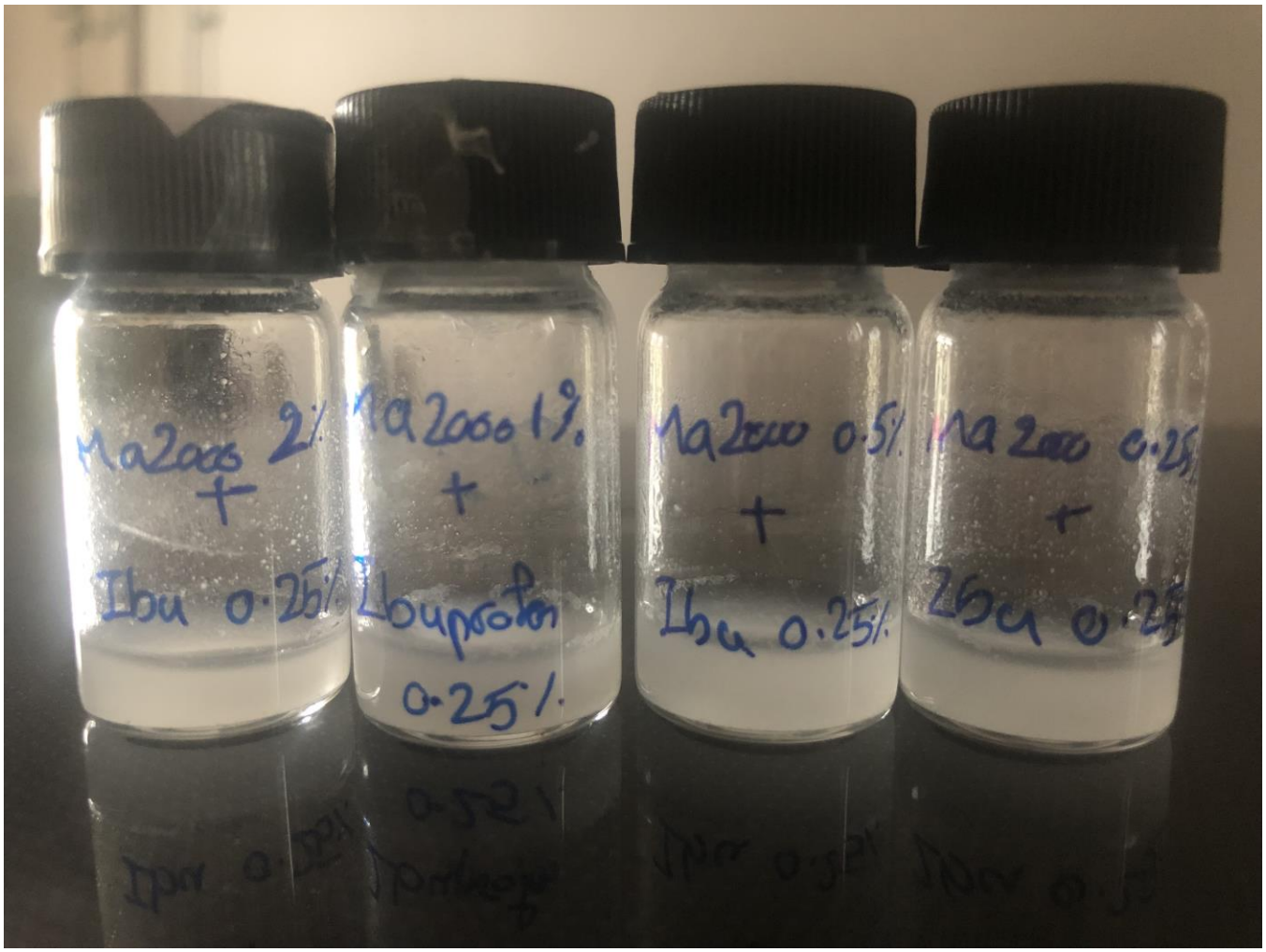

Fig. E.5: Four formulations of MA-alt-C_{18}-g-PEG with ibuprofen at 0.25% w/w, across polymer concentrations from 0.25% to 2%, highlighting concentration-dependent turbidity and solubility effects.

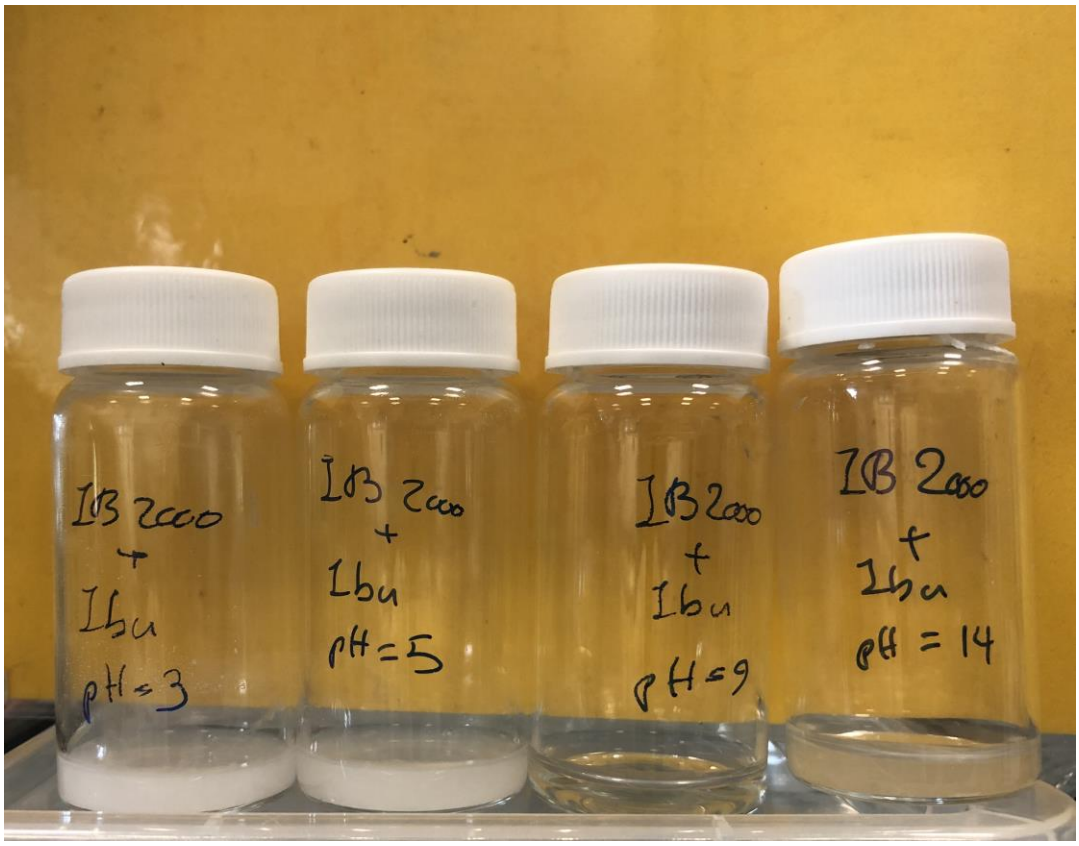

Fig. E.6: pH-dependent solubility study for IB-alt-MA-g-PEG with ibuprofen 0.25% w/w at fixed drug loading, across pH values of 3, 5, 9, and 14. Visible differences in clarity and precipitation suggest strong pH sensitivity.

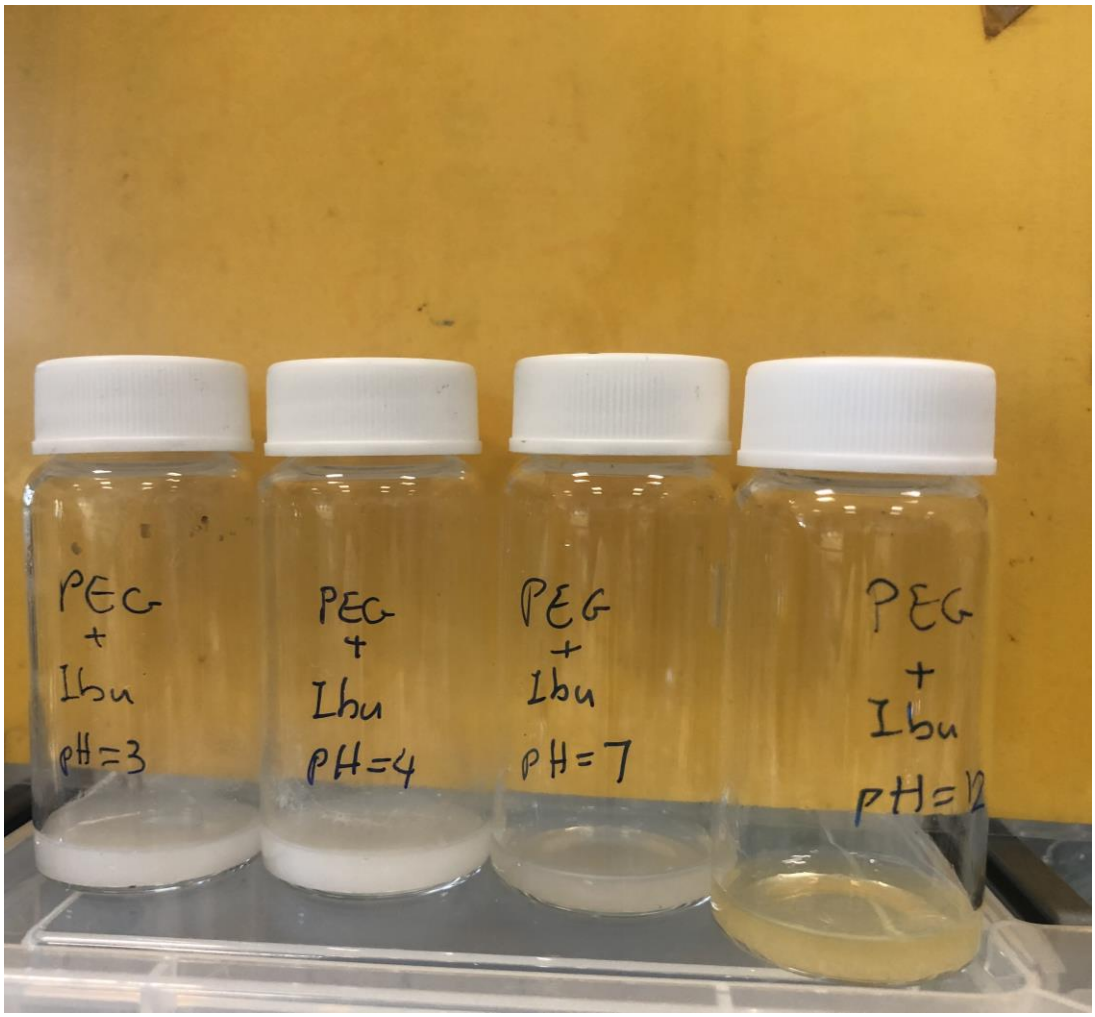

Fig. E.7: LIR410-g-PEG + ibuprofen 0.25% w/w, pH series (3, 4, 7, 12), showing sedimentation at high pH.

Bibliography

1. Schittny A, Huwyler J, Puchkov M. Mechanisms of increased bioavailability through amorphous solid dispersions: a review. Drug delivery. 2020;27(1):110–27.
2. Karbasi AB, Barfuss JD, Morgan TC, Collins D, Costenbader DA, Dennis DG, et al. Sol-moiety: Discovery of a water-soluble prodrug technology for enhanced oral bioavailability of insoluble therapeutics. Nature Communications. 2024;15(1):8487.
3. Desantis F, Miotto M, Di Rienzo L, Milanetti E, Ruocco G. Spatial organization of hydrophobic and charged residues affects protein thermal stability and binding affinity. Scientific Reports. 2022;12(1):12087.
4. Jain A, Bhardwaj K, Bansal M. Polymeric micelles as drug delivery system: recent advances, approaches, applications and patents. Current Drug Safety. 2024;19(2):163–71.
5. Sang-Cheol C, Dae-Il Y, Sung-Chul K, Eun-Seok P. A polymeric micellar carrier for the solubilization of biphenyl dimethyl dicarboxylate. Archives of pharmacal research. 2003;26(2):173–81.
6. Vambhurkar G, Jain N, Srinivasarao DA, Famta P, Singh SB, Srivastava S. Drug solubilization and drug release from polymeric micelles. Polymeric Micelles: Principles, Perspectives and Practices: Springer; 2023. p. 87–109.
7. Hari SK, Gauba A, Shrivastava N, Tripathi RM, Jain SK, Pandey AK. Polymeric micelles and cancer therapy: an ingenious multimodal tumor-targeted drug delivery system. Drug Delivery and Translational Research. 2023;13(1):135–63.
8. Dubey S, T D, Reddy DR, Rajou M. Development and Characterization of an Ibuprofen-Salicylic Acid Co-crystal with Improved Solubility. Journal of Pharmaceutical Innovation. 2025;20(2):67.
9. Bagwan JA, Adhav DU, Ade DD, Bhalerao DD, Avdhut MS. A review on solid dispersion technique for enhancing solubility of poorly soluble drugs. World Journal of Pharmaceutical Research. 2024;13(8):87–106.
10. Dugar RP, Gajera BY, Dave RH. Fusion method for solubility and dissolution rate enhancement of ibuprofen using block copolymer poloxamer 407. AAPS PharmSciTech. 2016;17(6):1428–40.
11. Naik J, Rajput R, Singh MK. Development and evaluation of ibuprofen loaded hydrophilic biocompatible polymeric nanoparticles for the taste masking and solubility enhancement. BioNanoScience. 2021;11(1):21–31.
12. Logacheva K, Gergelezhiu P, Raksha E, Savostina L, Arzumanyan G, Eresko A, et al. Vibrational spectroscopic features of ibuprofen and ketoprofen: IR and Raman spectroscopy combined with DFT calculations. Physics of Particles and Nuclei Letters. 2024;21(4):839–42.
13. Fernandes ARV. Enhancing the solubility of ibuprofen using biopolymers-based nanoencapsulation: Universidade de Coimbra (Portugal); 2016.
14. Li J, Wang Y, Yu D. Effects of additives on the physical stability and dissolution of polymeric amorphous solid dispersions: a review. AAPS PharmSciTech. 2023;24(7):175.
15. Shaikh Naziya V, Shinde Vaishnavi D, Shaikh Naziya V. AUTOMATED DRUG DISPENSING SYSTEM AND DEVICES.
16. Roy A, Das S, Saha S, Chaudhuri MG. Applications Of Nano Materials in Drug Delivery and Release Mechanism: A Review Exemplified With A Herbal Drug, Curcuma Longa, Its Potential In Different Disease Cure, Encapsulation With Different Nano Materials.
17. Clissold SP, Beresford R. Proquazone: A review of its pharmacodynamic and pharmacokinetic properties, and therapeutic efficacy in rheumatic diseases and pain states. Drugs. 1987;33(5):478–502.
18. Zhang Y, Wu Y, Du H, Li Z, Bai X, Wu Y, et al. Nano-drug delivery systems in oral cancer therapy: recent developments and prospective. Pharmaceutics. 2023;16(1):7.
19. Lopes-de-Araujo J, Neves A, Gouveia V, Moura C, Nunes C, Reis S. Oxaprozin-Loaded Lipid Nanoparticles towards Overcoming NSAIDs Side-Effects. Pharmaceutical research. 2016;33(2).

20. Davies NM. Clinical Pharmacokinetics of Oxaprozin. Clinical Pharmacokinetics. 1998;35(6):425–36.
21. Rainsford KD, Omar H, Ashraf A, Hewson AT, Bunning RAD, Rishiraj R, et al. Recent pharmacodynamic and pharmacokinetic findings on oxaprozin. InflammoPharmacology. 2002;10(3):185–239.
22. Babić MM, Antić KM, Vuković JSJ, Božić BĐ, Davidović SZ, Filipović JM, et al. Oxaprozin/poly (2-hydroxyethyl acrylate/itaconic acid) hydrogels: morphological, thermal, swelling, drug release and antibacterial properties. Journal of Materials Science. 2015;50(2):906–22.
23. Lopes-de-Araújo J, Neves AR, Gouveia VM, Moura CC, Nunes C, Reis S. Oxaprozin-Loaded Lipid Nanoparticles towards Overcoming NSAIDs Side-Effects. Pharmaceutical Research. 2016;33(2):301–14.
24. Babić MM, Antić KM, Vuković JSJ, Božić BĐ, Davidović SZ, Filipović JM, et al. Oxaprozin/poly(2-hydroxyethyl acrylate/itaconic acid) hydrogels: morphological, thermal, swelling, drug release and antibacterial properties. Journal of Materials Science. 2015;50(2):906–22.
25. Selvaraj C, Singh SK. Computational and Experimental Binding Interactions of Drug and β-Cyclodextrin as a Drug-Delivery Vehicle. Nanomaterials: Evolution and Advancement towards Therapeutic Drug Delivery (Part II): Bentham Science Publishers; 2021. p. 151–93.
26. Alshehri S, Alqarni M, Namazi NI, Naguib IA, Venkatesan K, Mosaad YO, et al. Design of predictive model to optimize the solubility of Oxaprozin as nonsteroidal anti-inflammatory drug. Scientific Reports. 2022;12(1):13106.
27. de Araújo JPL. Oxaprozin-loaded lipid nanoparticles towards overcoming NSAIDs side-effects: Universidade do Porto (Portugal); 2014.
28. Mehra S, Singh V, Gupta G, Srivastava A, Sharma SN. Experimental analysis of methylammonium and Formamidinium-based halide perovskite properties for optoelectronic applications. Heliyon. 2023;9(11).
29. Ugrinović V, Marković M, Božić B, Panić V, Veljović Đ. Poly (methacrylic acid) hydrogels crosslinked by poly (ethylene glycol) diacrylate as pH-responsive systems for drug delivery applications. Hemijska industrija. 2023;77(4):235–49.
30. Miranda G, Santos V, Bessa J, Teles Y, Yahouédéhou S, Goncalves M, et al. Inclusion complexes of non-steroidal anti-inflammatory drugs with cyclodextrins: a systematic review. Biomolecules 2021; 11: 361. s Note: MDPI stays neutral with regard to jurisdictional claims in published …; 2021.
31. Hashmi AR, Sekar M, Zahra F, Molugulu N, Wong LS. Advanced Drug Delivery Strategies to Overcome Solubility and Permeability Challenges: Driving Biopharmaceutical Advancements Toward Commercial Success. ACS omega. 2025.
32. Shelke PS, SU W, Suryawanshi R, Tushar B. A review on solubility enhancement technique.
33. Sagane R, Erande K. Review On Methods Of Solubility Enhancement Of BCS Class II Drugs. INTERNATIONAL JOURNAL OF PHARMACEUTICAL SCIENCES. 2024;2(1):64–76.
34. Bajpai YK, Singh S, Bisht V, Butola K, Awasthi A, Kumar S. BCS class II drug & its solubility enhancement: A review. J Res Appl Sci Biotechnol. 2022;1(5):48–58.
35. Ajaz SA, Majaz Q, Kalam I, Shaikh A, Shaikh M, Ayyaj P. Solubility Enhancement of BCS Class 2 Drugs by Solid Dispersion Technique. Research Journal of Pharmaceutical Dosage Forms and Technology. 2024;16(3):215–20.
36. SIVANATHAN G, RAJAGOPAL S, MAHADEVASWAMY G, ANGAMUTHU G, DHANDAPANI NV. PHARMACEUTICAL NANOCRYSTALS: AN EXTENSIVE OVERVIEW. Int J App Pharm. 2024;16(6):1–9.
37. Pathomthongtaweechai N, Muanprasat C. Potential Applications of Chitosan-Based Nanomaterials to Surpass the Gastrointestinal Physiological Obstacles and Enhance the Intestinal Drug Absorption. Pharmaceutics. 2021;13(6).
38. Urso R, Blardi P, Giorgi G. A short introduction to pharmacokinetics. European review for medical and pharmacological sciences. 2002;6:33–44.
39. Loftsson T, Brewster ME. Pharmaceutical applications of cyclodextrins: basic science and product development. Journal of Pharmacy and Pharmacology. 2010;62(11):1607–21.

40. Rathore C, Hemrajani C, Sharma AK, Gupta PK, Jha NK, Aljabali AAA, et al. Self-nanoemulsifying drug delivery system (SNEDDS) mediated improved oral bioavailability of thymoquinone: optimization, characterization, pharmacokinetic, and hepatotoxicity studies. Drug Deliv Transl Res. 2023;13(1):292–307.
41. Aggarwal K, Joshi S, Jindal P, Patel P, Das Kurmi B. Solid Lipid Nanoparticles: An Innovative Drug Delivery System for Enhanced Bioavailability and Targeted Therapy. AAPS PharmSciTech. 2025;26(6):186.
42. Aitken P, Stanescu I, Playne R, Zhang J, Frampton CMA, Atkinson HC. An integrated safety analysis of combined acetaminophen and ibuprofen (Maxigesic (®) /Combogesic(®)) in adults. J Pain Res. 2019;12:621–34.
43. Sarabia-Vallejo Á, Caja MdM, Olives AI, Martín MA, Menéndez JC. Cyclodextrin inclusion complexes for improved drug bioavailability and activity: synthetic and analytical aspects. Pharmaceutics. 2023;15(9):2345.
44. Onyeji C. Cyclodextrin complexes: utility in improving drug bioavailability and other applications. Bioequivalence & Bioavailability International Journal. 2018;2(2):000130.
45. Nicolaescu OE, Ionescu C, Samide A, Tigae C, Spînu CI, Oprea B. Advancements in Cyclodextrin Complexes with Bioactive Secondary Metabolites and Their Pharmaceutical Applications. Pharmaceutics. 2025;17(4):506.
46. Loftsson T. Increasing the cyclodextrin complexation of drugs and drug biovailability through addition of water-soluble polymers. Die Pharmazie. 1998;53(11):733–40.
47. Pereva S, Nikolova V, Sarafska T, Angelova S, Spassov T, Dudev T. Inclusion complexes of ibuprofen and β-cyclodextrin: Supramolecular structure and stability. Journal of Molecular Structure. 2020;1205:127575.
48. Vasconcelos T, Sarmento B, Costa P. Solid dispersions as strategy to improve oral bioavailability of poor water soluble drugs. Drug discovery today. 2007;12(23-24):1068–75.
49. Huang Y, Dai W-G. Fundamental aspects of solid dispersion technology for poorly soluble drugs. Acta Pharmaceutica Sinica B. 2014;4(1):18–25.
50. Baghel S, Cathcart H, O'Reilly NJ. Polymeric amorphous solid dispersions: a review of amorphization, crystallization, stabilization, solid-state characterization, and aqueous solubilization of biopharmaceutical classification system class II drugs. Journal of pharmaceutical sciences. 2016;105(9):2527–44.
51. Emami S, Siahi-Shadbad M, Adibkia K, Barzegar-Jalali M. Recent advances in improving oral drug bioavailability by cocrystals. BioImpacts: BI. 2018;8(4):305.
52. Patel PM. In-Vitro and In-Silico Evaluation of the Physical Stability and Solubilization Mechanisms of Naproxen-Nicotinamide Co-Crystals: Saint Joseph's University; 2023.
53. Bhatia M, Devi S. Co-crystallization: a green approach for the solubility enhancement of poorly soluble drugs. CrystEngComm. 2024;26(3):293–311.
54. Chettri A, Subba A, Singh GP, Bag PP. Pharmaceutical co-crystals: A green way to enhance drug stability and solubility for improved therapeutic efficacy. Journal of Pharmacy and Pharmacology. 2024;76(1):1–12.
55. Ishihara S, Hattori Y, Otsuka M, Sasaki T. Cocrystal formation through solid-state reaction between ibuprofen and nicotinamide revealed using THz and IR spectroscopy with multivariate analysis. Crystals. 2020;10(9):760.
56. Suresh K, Mehta T, Thakrar V, Sharma RG. Innovative Strategies in Generic Drug Development: The Role of Polymorph, Amorphous, Pseudopolymorph, and Cocrystal Solid Forms. Crystal Growth & Design. 2025;25(4):1282–92.
57. Atre P, Rizvi SA. Advances in Oral Solid Drug Delivery Systems: Quality by Design Approach in Development of Controlled Release Tablets. BioChem. 2025;5(2):9.
58. Haghighizadeh A, Mahdavi H, Rajabi O. Continuous and size-controlled preparation of ibuprofen nanosuspension by antisolvent crystallization method using hollow fiber membrane. Journal of Pharmaceutical Innovation. 2023;18(1):195–204.

59. Borba PAA, Pinotti M, de Campos CEM, Pezzini BR, Stulzer HK. Sodium alginate as a potential carrier in solid dispersion formulations to enhance dissolution rate and apparent water solubility of BCS II drugs. Carbohydrate polymers. 2016;137:350–9.
60. Mehvar R. The relationship among pharmacokinetic parameters: effects of altered kinetics on the drug plasma concentration-time profiles. American Journal of Pharmaceutical Education. 2004;68:NN1.
61. Benet LZ, Kroetz D, Sheiner L, Hardman J, Limbird L. Pharmacokinetics: the dynamics of drug absorption, distribution, metabolism, and elimination. Goodman and Gilman's the pharmacological basis of therapeutics. 1996;3:e27.
62. Fernandes GJ, Kumar L, Sharma K, Tunge R, Rathnanand M. A review on solubility enhancement of carvedilol—a BCS class II drug. Journal of Pharmaceutical Innovation. 2018;13(3):197–212.
63. Negi A, Nimbkar S, Moses J. Engineering Inhalable Therapeutic Particles: Conventional and Emerging Approaches. Pharmaceutics 2023, 15, 2706. 2023.
64. Li M, Guo Q, Zhong C, Zhang Z. Multifunctional cell membranes-based nano-carriers for targeted therapies: a review of recent trends and future perspective. Drug delivery. 2023;30(1):2288797.
65. Prasad D, Jain A, Garad S. Oral delivery of poorly soluble drugs. Poorly Soluble Drugs: Jenny Stanford Publishing; 2017. p. 149–210.
66. Kleiner LW, Wright JC, Wang Y. Evolution of implantable and insertable drug delivery systems. Journal of controlled release. 2014;181:1–10.
67. Mehandole A, Walke N, Mahajan S, Aalhate M, Maji I, Gupta U, et al. Core–shell type lipidic and polymeric nanocapsules: the transformative multifaceted delivery systems. AAPS PharmSciTech. 2023;24(1):50.
68. Patnaik A, Jena GK, Patra CN. Recent Advancements and Patent Search on Polymeric Nanoparticles. BioNanoScience. 2023;13(4):1463–9.
69. Elbana E, Elzayat AM, Abdelrazek E, Abou-Saleh RH. Chitosan micro/nanobubbles: novel chemical structure and characterization. 2024.
70. Solanki N, Dureja H. Polymeric nanoparticles-based drug delivery systems for anticancer therapy. Recent Advances in Pharmaceutical Innovation and Research: Springer; 2023. p. 499–515.
71. GUDE S. Exploring innovative drug delivery systems for the targeted treatment and rehabilitation of individuals affected by narcotics and psychotropic substances: a multidisciplinary approach in pharmaceutics. Translational and Regulatory Sciences. 2024;6(3):72–83.
72. Lewis A, Heaysman C. Biomedical applications of hydrogels: poly (vinyl alcohol)-based hydrogels for embolotherapy and drug delivery. 2012.
73. Fratila DN, Virvescu DI, Luchian I, Hancianu M, Baciu ER, Butnaru O, et al. Advances and Functional Integration of Hydrogel Composites as Drug Delivery Systems in Contemporary Dentistry. Gels. 2024;10(10):661.
74. Zhou Y, Wang P, Wan F, Zhu L, Wang Z, Fan G, et al. Further improvement based on traditional nanocapsule preparation methods: a review. Nanomaterials. 2023;13(24):3125.
75. Liu Y, Yang G, Zou D, Hui Y, Nigam K, Middelberg AP, et al. Formulation of nanoparticles using mixing-induced nanoprecipitation for drug delivery. Industrial & engineering chemistry research. 2019;59(9):4134–49.
76. Dima Ş, Dima C, Iordăchescu G. Encapsulation of functional lipophilic food and drug biocomponents. Food Engineering Reviews. 2015;7(4):417–38.
77. Luo X, Su P, Zhang W, Raston CL. Microfluidic devices in fabricating nano or micromaterials for biomedical applications. Advanced Materials Technologies. 2019;4(12):1900488.
78. Abd Ellah NH, Abouelmagd SA. Surface functionalization of polymeric nanoparticles for tumor drug delivery: approaches and challenges. Expert opinion on drug delivery. 2017;14(2):201–14.
79. Verma VS, Pandey A, Jha AK, Badwaik HKR, Alexander A, Ajazuddin. Polyethylene glycol–based polymer-drug conjugates: novel design and synthesis strategies for enhanced therapeutic efficacy and targeted drug delivery. Applied Biochemistry and Biotechnology. 2024;196(10):7325–61.

80. Wang Z, Ye Q, Yu S, Akhavan B. Poly ethylene glycol (PEG)‐based hydrogels for drug delivery in cancer therapy: a comprehensive review. Advanced healthcare materials. 2023;12(18):2300105.
81. Brewer K, Gundsambuu B, Facal Marina P, Barry SC, Blencowe A. Thermoresponsive poly (ε-caprolactone)-poly (ethylene/propylene glycol) copolymers as injectable hydrogels for cell therapies. Polymers. 2020;12(2):367.
82. Biswas A, Kumar S, Choudhury AD, Bisen AC, Sanap SN, Agrawal S, et al. Polymers and their engineered analogues for ocular drug delivery: enhancing therapeutic precision. Biopolymers. 2024;115(4):e23578.
83. Aguilar M, García-Fernández L, López-Donaire M, Parra F, Rojo L, Rodriguez G, et al. Medical Devices and Preparative Medicine: Polymer Drug Application. Concise Encyclopedia of Biomedical Polymers and Polymeric Biomaterials. 2017:789–826.
84. Rossier B, Jordan O, Allémann E, Rodriguez-Nogales C. Nanocrystals and nanosuspensions: an exploration from classic formulations to advanced drug delivery systems. Drug Delivery and Translational Research. 2024;14(12):3438–51.
85. Hassan A, Khan JA, Nasir F, Shabir H, Hannan PA, Ullah R, et al. Synthesis, Characterization, and Stability Optimization of Ibuprofen Cocrystals Employing Various Hydrophilic Polymers. Current Pharmaceutical Design. 2025;31(11):873–83.
86. Todd PA, Brogden RN. Oxaprozin: a preliminary review of its pharmacodynamic and pharmacokinetic properties, and therapeutic efficacy. Drugs. 1986;32(4):291–312.
87. Rainsford K. Ibuprofen: pharmacology, efficacy and safety. Inflammopharmacology. 2009;17(6):275–342.
88. Foster LJR. PEGylation and bioPEGylation of polyhydroxyalkanoates: synthesis, characterisation and applications. Biopolymers. 2010:243–56.
89. Bitounis D, Fanciullino R, Iliadis A, Ciccolini J. Optimizing druggability through liposomal formulations: new approaches to an old concept. International Scholarly Research Notices. 2012;2012(1):738432.
90. Loyer P, Cammas-Marion S. Natural and synthetic poly (malic acid)-based derivates: a family of versatile biopolymers for the design of drug nanocarriers. Journal of drug targeting. 2014;22(7):556–75.
91. Shivalkar S, Ranjan S, Sahoo AK. Polymeric nanocomposites: synthesis, characterization, and recent applications. Nanomaterials: advances and applications. 2023:267–95.
92. Kumar A, Kulkarni PS, Samui A. Polyethylene glycol grafted cotton as phase change polymer. Cellulose. 2014;21(1):685–96.
93. Abou Bakr MS, Salem YY, Mohamed TM. Controlled and targeted drug delivery using smart nanovectors. International journal of drug discovery and pharmacology. 2023;2(1):84.
94. Isloor AM, Ganesh B, Isloor SM, Ismail A, Nagaraj H, Pattabi M. Studies on copper coated polysulfone/modified poly isobutylene alt-maleic anhydride blend membrane and its antibiofouling property. Desalination. 2013;308:82–8.
95. Guan W, Ma Y, Ding S, Liu Y, Song Z, Liu X, et al. The technology for improving stability of nanosuspensions in drug delivery. Journal of Nanoparticle Research. 2022;24(1):14.
96. Sarkar P, DAS S, MAJEE SB. Solid dispersion tablets in improving oral bioavailability of poorly soluble drugs. Int J Curr Pharm Res. 2022;14(2):15–20.
97. Viegas C, Patrício AB, Prata JM, Nadhman A, Chintamaneni PK, Fonte P. Solid lipid nanoparticles vs. nanostructured lipid carriers: a comparative review. Pharmaceutics. 2023;15(6):1593.
98. Patil AS, Kamat SS, Birkodi SU, Kokatanur U, Masareddy RS, Dandagi PM. Fabrication of polyisobutene based matrix patches for transdermal delivery of atenolol. Research Journal of Pharmacy and Technology. 2023;16(5):2085–90.
99. Popescu I, Suflet DM, Pelin IM, Chitanu GC. Biomedical applications of maleic anhydride copolymers. Rev Roum Chim. 2011;56(3):173–88.

100. Jin Z, Du L, Zhang C, Sugiyama Y, Wang W, Palui G, et al. Modification of poly (maleic anhydride)-based polymers with H2N–R nucleophiles: Addition or substitution reaction? Bioconjugate chemistry. 2019;30(3):871–80.
101. Chao S, Zhang Y, Cheng S, Shao X, Liu S, Lu W, et al. Ibuprofen-loaded ZnO nanoparticle/polyacrylonitrile nanofibers for dual-stimulus sustained release of drugs. ACS Applied Nano Materials. 2023;6(7):5535–44.
102. Stern T. Deciphering the Triple-Peak COC Stretching FTIR Absorbance Consistently Occurring in Semicrystalline PEG. Polymers. 2025;17(16):2199.
103. Chiu H-C, Hu C-H, Chern C-S. Preparation and characterization of amphiphilic poly (ethylene glycol) graft copolymers. Polymer journal. 1999;31(6):535–41.
104. Kotta S, Aldawsari HM, Badr-Eldin SM, Nair AB, Yt K. Progress in polymeric micelles for drug delivery applications. Pharmaceutics. 2022;14(8):1636.
105. Popescu I, Prisacaru AI, Suflet DM, Fundueanu G. Thermo- and pH-sensitivity of poly(N-vinylcaprolactam-co-maleic acid) in aqueous solution. Polymer Bulletin. 2014;71(11):2863–80.
106. Salamanca CH, Yarce CJ, Zapata CA, Giraldo JA. Relationship between the Polymeric Ionization Degree and Powder and Surface Properties in Materials Derived from Poly(maleic anhydride-alt-octadecene). Molecules. 2018;23(2):320.
107. Sawant RR, Torchilin VP. Polymeric Micelles: Polyethylene Glycol-Phosphatidylethanolamine (PEG-PE)-Based Micelles as an Example. In: Grobmyer SR, Moudgil BM, editors. Cancer Nanotechnology: Methods and Protocols. Totowa, NJ: Humana Press; 2010. p. 131–49.
108. Yusa S-i. Development and application of pH-responsive polymers. Polymer Journal. 2022;54(3):235–42.
109. Hammouda B. A new Guinier-Porod model. Journal of Applied Crystallography. 2010;43(4):716–9.
110. Castelletto V, Hamley I, English RJ, Mingvanish W. SANS and rheology study of aqueous solutions and gels containing highly swollen diblock copolymer micelles. Langmuir. 2003;19(8):3229–35.
111. Singh P. Small-angle scattering techniques (SAXS/SANS). Membrane Characterization: Elsevier; 2017. p. 95–111.
112. Larison T, Pingali SV, Stefik M. New approach for SANS measurement of micelle chain mixing during size and morphology transitions. Soft Matter. 2023;19(19):3487–95.
113. D'Errico G. NMR of liquid crystals and micellar solutions. 2013.
114. Kim JO. Polymer micelles with cross-linked ionic cores for delivery of doxorubicin: University of Nebraska Medical Center; 2010.
115. Tea L, Willner L, Waldorf C, Matsarskaia O, Schweins R, Förster S, et al. Surface Charged Polymeric Micelles— A Tunable Model System Studied by SANS. Macromolecules. 2024;57(12):5818–30.
116. Bharatiya B, Wlodek M, Harniman R, Schweins R, Mantell J, Wang G, et al. Solution and interfacial self-assembly of Bacillus subtilis bacterial lipoteichoic acid (LTA): nanoclustering, and effects of Ca 2+ and temperature. Nanoscale. 2022;14(34):12265–74.
117. Doublier J-L, Garnier C, Renard D, Sanchez C. Protein–polysaccharide interactions. Current opinion in Colloid & interface Science. 2000;5(3-4):202–14.
118. Endo H, Mihailescu M, Monkenbusch M, Allgaier J, Gompper G, Richter D, et al. Effect of amphiphilic block copolymers on the structure and phase behavior of oil–water-surfactant mixtures. The Journal of chemical physics. 2001;115(1):580–600.
119. Brisson ER, Worthington MJ, Kerai S, Müllner M. Nanoscale polymer discs, toroids and platelets: a survey of their syntheses and potential applications. Chemical Society Reviews. 2024;53(4):1984–2021.
120. Tondock F, Nash D, Hudziak C, Ludwig K, Weinhart M. Design and synthesis of amphiphilic statistical copolymers forming unimeric micelles with thermoresponsive behaviour in the physiological range. Polymer Chemistry. 2025;16(19):2216–31.

121. Li Z, Feng H, Jin L, Zhang Y, Tian X, Li J. Polymeric micelle with pH-induced variable size and doxorubicin and siRNA co-delivery for synergistic cancer therapy. Applied Nanoscience. 2020;10(6):1903–13.
122. Oh S-T, Jeong Y-W, Kim S-S, Ryu S-W. Synthesis of poly(isobutylene-alt-maleic anhydride)-based water-soluble binders and their electrochemical properties. Ionics. 2022;28(9):4303–10.
123. Zhang S, Srivastava A, Li W, Rijpkema SJ, Carnevale V, Klein ML, et al. Molecular Engineering of pH-Responsive Anchoring Systems onto Poly (ethylene glycol) Corona. Journal of the American Chemical Society. 2023;145(19):10458–62.
124. Yuan Y, Tan W, Mi Y, Wang L, Qi Z, Guo Z. Effect of Hydrophobic Chain Length in Amphiphilic Chitosan Conjugates on Intracellular Drug Delivery and Smart Drug Release of Redox-Responsive Micelle. Marine Drugs. 2024;22(1):18.
125. Zhou XX, Jin L, Qi RQ, Ma T. pH-responsive polymeric micelles self-assembled from amphiphilic copolymer modified with lipid used as doxorubicin delivery carriers. Royal Society open science. 2018;5(3):171654.
126. Yin X, Stöver HD. Thermosensitive and pH-sensitive polymers based on maleic anhydride copolymers. Macromolecules. 2002;35(27):10178–81.
127. Wu X. Polymer grafting onto cellulose 2023.
128. Rätzsch M. Alternating maleic anhydride copolymers. Progress in polymer science. 1988;13(4):277–337.
129. Dai K, Olsen BD. Accelerated small angle neutron scattering algorithms for polymeric materials. Soft Matter. 2025;21(41):8060–77.
130. Kuyler GC, Barnard E, Cunningham RD, Sibariboyi S, White L, Wessels I, et al. Amphiphilic Copolymers and Their Role in the Study of Membrane Proteins. The Journal of Physical Chemistry Letters. 2025;16:5784–99.
131. Nishimura T, Hatatani Y, Ando M, Sasaki Y, Akiyoshi K. Single-component nanodiscs via the thermal folding of amphiphilic graft copolymers with the adjusted flexibility of the main chain. Chemical Science. 2022;13(18):5243–51.
132. Matsunaga T, Sakai T, Akagi Y, Chung U-i, Shibayama M. SANS and SLS studies on tetra-arm PEG gels in as-prepared and swollen states. Macromolecules. 2009;42(16):6245–52.
133. Lee A, Lundberg P, Klinger D, Lee BF, Hawker CJ, Lynd NA. Physiologically relevant, pH-responsive PEG-based block and statistical copolymers with N, N-diisopropylamine units. Polymer chemistry. 2013;4(24):5735–42.
134. Yoshida T, Lai TC, Kwon GS, Sako K. pH-and ion-sensitive polymers for drug delivery. Expert opinion on drug delivery. 2013;10(11):1497–513.
135. Gvozdeva Y, Staynova R. pH-Dependent drug delivery systems for ulcerative colitis treatment. Pharmaceutics. 2025;17(2):226.
136. Sun S, Cui Y, Yuan B, Dou M, Wang G, Xu H, et al. Drug delivery systems based on polyethylene glycol hydrogels for enhanced bone regeneration. Frontiers in bioengineering and biotechnology. 2023;11:1117647.
137. Price DL, Fernandez-Alonso F. Neutron scattering-magnetic and quantum phenomena: Elsevier; 2015.
138. Di Corato R, Quarta A, Piacenza P, Ragusa A, Figuerola A, Buonsanti R, et al. Water solubilization of hydrophobic nanocrystals by means of poly (maleic anhydride-alt-1-octadecene). Journal of Materials Chemistry. 2008;18(17):1991–6.
139. Mazİ H, SurmelİHİNdİ B. Temperature and Ph-sensıtıve Super absorbent Polymers based on Modıfied Maleıc Anhydrıde. Journal of Chemical Sciences. 2021;133(1):10.
140. Fan H, Li Y, Yang J, Ye X. Effect of hydrophobic chain length on the stability and guest exchange behavior of shell-sheddable micelles formed by disulfide-linked diblock copolymers. The Journal of Physical Chemistry B. 2017;121(41):9708–17.

141. Scheidelaar S, Koorengevel MC, van Walree CA, Dominguez JJ, Dörr JM, Killian JA. Effect of polymer composition and pH on membrane solubilization by styrene-maleic acid copolymers. Biophysical journal. 2016;111(9):1974–86.
142. Metze FK, Sant S, Meng Z, Klok H-A, Kaur K. Swelling-activated, soft mechanochemistry in polymer materials. Langmuir. 2023;39(10):3546–57.
143. Thakur A, Wanchoo R, Singh P. Structural parameters and swelling behavior of pH sensitive poly (acrylamide-co-acrylic acid) hydrogels. Chemical and Biochemical Engineering Quarterly. 2011;25(2):181–94.
144. Perumal S, Atchudan R, Lee W. A Review of Polymeric Micelles and Their Applications. Polymers. 2022;14(12):2510.
145. Polat H, Eren MC, Polat M, Koss KM, Polat OK. Comparative Stability of Synthetic and Natural Polymeric Micelles in Physiological Environments: Implications for Drug Delivery. Pharmaceutics. 2025;17(11):1439.
146. Das A, Prévost S, Gradzielski M. Positional Correlation Length-Induced Morphological Transformation of Interpolyelectrolyte Complexes (IPECs) Made of Polysaccharides: The Role of Molar Charge Ratio. Macromolecules. 2025;58(19):10763–77.
147. McCauley PJ. Understanding Self-assembly and Flow Heterogeneities in Poloxamer Wormlike Micelles: University of Minnesota; 2023.
148. Angelico R, Colombo C, Di Iorio E, Brtnický M, Fojt J, Conte P. Humic substances: from supramolecular aggregation to fractal conformation—is there time for a new paradigm? Applied Sciences. 2023;13(4):2236.
149. Khairuldin DBM. Properties of Surfactants: University of Bristol; 2024.
150. Rosario AJ, Ma B. Stimuli-responsive polymer networks: Application, design, and computational exploration. ACS Applied Polymer Materials. 2024;6(23):14204–28.
151. Aleemardani M, Trikić MZ, Green NH, Claeyssens F. Elastomeric, bioadhesive and pH-responsive amphiphilic copolymers based on direct crosslinking of poly (glycerol sebacate)-co-polyethylene glycol. Biomaterials Science. 2022;10(24):7015–31.
152. Cespi M, Bonacucina G, Tiboni M, Casettari L, Cambriani A, Fini F, et al. Insights in the rheological properties of PLGA-PEG-PLGA aqueous dispersions: Structural properties and temperature-dependent behaviour. Polymer. 2021;213:123216.
153. Chakravarthy RD, Sahroni I, Wang C-W, Mohammed M, Lin H-C. Temperature-induced nanostructure transition for supramolecular gelation in water. ACS nano. 2023;17(12):11805–16.
154. Hishida M, Kanno R, Terashima T. Hydration State on Poly (ethylene glycol)-Bearing Homopolymers and Random Copolymer Micelles: In Relation to the Thermoresponsive Property and Micellar Structure. Macromolecules. 2023;56(18):7587–96.
155. Nunziata G, Limiti E, Aramini D, Nava M, Moretti L, Rainer A, et al. pH-Thermo Dual-Responsive Polymeric Nanoparticles for Women's Health: Dual Action Against Cervical and Ovarian Cancer Cells. ACS Applied Materials & Interfaces. 2025.
156. Rajan R, Ahmed S, Sharma N, Kumar N, Debas A, Matsumura K. Review of the current state of protein aggregation inhibition from a materials chemistry perspective: special focus on polymeric materials. Materials Advances. 2021;2(4):1139–76.
157. Garzón LC, Martínez F. Temperature Dependence of Solubility for Ibuprofen in Some Organic and Aqueous Solvents. Journal of Solution Chemistry. 2004;33(11):1379–95.
158. Kabedev A, Bergström CAS, Larsson P. Molecular dynamics study on micelle-small molecule interactions: developing a strategy for an extensive comparison. Journal of Computer-Aided Molecular Design. 2023;38(1):5.
159. Akiba I, Sakurai K. Characterizing block-copolymer micelles used in nanomedicines via solution static scattering techniques. Polymer journal. 2021;53(9):951–73.
160. Han W, Liu F, Liu G, Li H, Xu Y, Sun S. Research progress of physical transdermal enhancement techniques in tumor therapy. Chemical Communications. 2023;59(23):3339–59.

161. Mineiro R, Albuquerque T, Neves AR, Santos CR, Costa D, Quintela T. The role of biological rhythms in new drug formulations to cross the brain barriers. International Journal of Molecular Sciences. 2023;24(16):12541.
162. Kriplani P, Guarve K. Transdermal drug delivery: A step towards treatment of cancer. Recent Patents on Anti-Cancer Drug Discovery. 2022;17(3):253–67.
163. Taib MNAM, Osman S, Solihat NN, Arnata IW, Sartika D, Jamal T, et al. Advances in lignin and lignin-based composites in biomedical applications. Biomaterials Science. 2026.
164. Tincu C-E, Andrițoiu CV, Popa M, Ochiuz L. Recent advancements and strategies for overcoming the blood–brain barrier using albumin-based drug delivery systems to treat brain cancer, with a focus on glioblastoma. Polymers. 2023;15(19):3969.
165. Quintero-Marquina G, Segovia G, Oestreicher V, Lamas D, Huck-Iriart C. Quick assessment of a Small-Angle Scattering data using Guinier-Porod model: Introducing the correlative size. 2025.
166. Toth SH, Stoica AD, Sevcencu C. Redesigning Ibuprofen for Improved Oral Delivery and Reduced Side Effects. Bioconjugate Chemistry. 2025;36(5):893–913.
167. Dubey R, Shende P. Potential of brush and mushroom conformations in biomedical applications. Chemical Papers. 2024;78(12):6873–89.
168. Fujii S. Polymeric core-crosslinked particles prepared via a nanoemulsion-mediated process: from particle design and structural characterization to in vivo behavior in chemotherapy. Polymer Journal. 2023;55(9):921–33.
169. Lodge TP, Seitzinger CL, Seeger SC, Yang S, Gupta S, Dorfman KD. Dynamics and equilibration mechanisms in block copolymer particles. ACS polymers Au. 2022;2(6):397–416.
170. Roy T, Padhi S. A Meticulous Focus on the Determination of Critical Micelle Concentration Employing Fluorescence Spectroscopy. Journal of Fluorescence. 2025:1–15.
171. Yang S, Sattari A, Han D, Lodge TP. Fragmentation Kinetics of Block Copolymer Micelles: Effect of Core and Corona Block Lengths. Macromolecules. 2024;57(17):8298–305.
172. Lafleche F, Durand D, Nicolai T. Association of adhesive spheres formed by hydrophobically end-capped PEO. 1. Influence of the presence of single end-capped PEO. Macromolecules. 2003;36(4):1331–40.
173. Nikkhah SJ, Sammalkorpi M. Single core and multicore aggregates from a polymer mixture: A dissipative particle dynamics study. Journal of Colloid and Interface Science. 2023;635:231–41.
174. Langevin D. Complexation of oppositely charged polyelectrolytes and surfactants in aqueous solutions. A review. Advances in colloid and interface science. 2009;147:170–7.
175. Tecilla P, Scrimin P. Assessing Hydrolytic Activity of Surfactant-Based Nanozymes: Methodological and Kinetic Considerations. Nanomaterials. 2026;16(2):106.
176. Gupta S, Lodge TP. Effect of Changing Interfacial Tension on Fragmentation Kinetics of Block Copolymer Micelles. Macromolecules. 2023;56(5):2137–48.
177. Gupta S, Liberman L, Lodge TP. Role of Distance from Equilibrium in the Fragmentation Kinetics of Block Copolymer Micelles. Macromolecules. 2023;56(13):4874–83.
178. Ishkhanyan H, Ziolek RM, Barlow DJ, Lawrence MJ, Poghosyan AH, Lorenz CD. NSAID solubilisation promotes morphological transitions in Triton X-114 surfactant micelles. Journal of Molecular Liquids. 2022;356:119050.
179. Singh D, Singh L. A Pioneering Review on Quantitative Analysis of the Effect of Macromolecular Crowding on Drug Transport and Release: Current Implications. Journal of Macromolecular Science, Part B. 2025;64(8):902–16.
180. Singh J, Nayak P. pH‐responsive polymers for drug delivery: trends and opportunities. Journal of polymer science. 2023;61(22):2828–50.
181. Lei M, Huang W, Jin Z, Sun J, Zhang M, Zhao S. Effect of molecular structure and ionization state on aggregation of carboxymethyl chitosan: A molecular dynamics study. Carbohydrate Polymers. 2022;297:119993.

182. Aliabadi A, Hasannia M, Vakili-Azghandi M, Araste F, Abnous K, Taghdisi SM, et al. Synthesis approaches of amphiphilic copolymers for spherical micelle preparation: application in drug delivery. Journal of Materials Chemistry B. 2023;11(39):9325–68.
183. Jain A, Bhardwaj K, Bansal M. Polymeric Micelles as Drug Delivery System: Recent Advances, Approaches, Applications and Patents. Curr Drug Saf. 2024;19(2):163–71.
184. Jones MC, Cavalcanti LP, Smith GN, Dalgliesh R, Euston SR, Vilela F, et al. Self-sorting and co-assembly control in multicomponent supramolecular hydrogels with dual monomer and polymer statistical distribution. Communications Chemistry. 2025;8(1):265.
185. Liao M, Gong H, Liu H, Shen K, Ge T, King S, et al. Combination of a pH-responsive peptide amphiphile and a conventional antibiotic in treating Gram-negative bacteria. Journal of colloid and interface science. 2024;659:397–412.
186. Cen J, Hou M, Hu J, Liu S. Advanced Synthesis, Structural Characterization, and Functional Applications of Precision Polymers. Chemistry–A European Journal. 2024;30(56):e202401911.
187. Filice S, Scuderi V, Scalese S. Sulfonated pentablock copolymer (NexarTM) for water remediation and other applications. Polymers. 2024;16(14):2009.
188. Beach MA, Nayanathara U, Gao Y, Zhang C, Xiong Y, Wang Y, et al. Polymeric nanoparticles for drug delivery. Chemical Reviews. 2024;124(9):5505–616.
189. Menath J. Self-Assembly of Colloidal Surface Structures: Dissertation, Erlangen, Friedrich-Alexander-Universität Erlangen-Nürnberg …; 2024.
190. Almeida M. Stimuli-responsives polymer and fatty acids nanostructures: Université Paris-Est Créteil Val-de-Marne-Paris 12; 2024.
191. Kockelmann J, Zentel R, Nuhn L. Post‐Polymerization Modifications to Prepare Biomedical Nanocarriers with Varying Internal Structures, their Properties and Impact on Protein Corona Formation. Macromolecular Chemistry and Physics. 2023;224(24):2300199.
192. Liu Y, Chen X, Liu X, Guan W, Lu C. Aggregation-induced emission-active micelles: synthesis, characterization, and applications. Chemical Society Reviews. 2023;52(4):1456–90.
193. Bag S, Ghosh S, Paul S, Khan MEH, De P. Styrene‐Maleimide/Maleic Anhydride Alternating Copolymers: Recent Advances and Future Perspectives. Macromolecular Rapid Communications. 2021;42(23):2100501.
194. Giridhar S, Murthy HA. Advances in Controlled Drug Delivery Using Grafted Copolymer. Graft Copolymers of Polysaccharides for Drug Delivery Systems: Apple Academic Press; 2025. p. 201–35.
195. Cen J, Hou M, Liu S. Discrete polyethylene glycol derivatives as a potent impetus for next-generation biomedicines. Giant. 2023;15:100169.
196. Wong CK, Lai RY, Stenzel MH. Polymersomes with micellar patches. Journal of Colloid and Interface Science. 2024;671:449–56.
197. Singh K, Wychowaniec JK, Edwards-Gayle CJ, Reynaud EG, Rodriguez BJ, Brougham DF. Structure-dynamics correlations in composite PF127-PEG-based hydrogels; cohesive/hydrophobic interactions determine phase and rheology and identify the role of micelle concentration in controlling 3D extrusion printability. Journal of Colloid and Interface Science. 2024;660:302–13.
198. Pavon Regaña C. POLYMER COMPOSITION AND FUNCTIONAL EFFECTS OF THE SPECIES-SPECIFIC BIOMOLECULAR CORONA FORMATION ON NPs. 2025.
199. García-Gallego S, Ottaviani M. Micellar Nanocarriers. 2024.
200. Andrew EC, Maduabuchi MV, Grace EA, Chidera AC, Pauline ON, Benjamin OK, et al. Preparation and In Vitro Evaluation of Ibuprofen Microspheres Using Ionic Gelation Method. Mathews Journal of Pharmaceutical Science. 2024;8(3):1–13.
201. Meloun M, Bordovská S. Benchmarking and validating algorithms that estimate p K a values of drugs based on their molecular structures. Analytical and Bioanalytical Chemistry. 2007;389(4):1267–81.
202. Alexander S, De Vos WM, Castle TC, Cosgrove T, Prescott SW. Growth and shrinkage of pluronic micelles by uptake and release of flurbiprofen: variation of pH. Langmuir. 2012;28(16):6539–45.

203. Yamin M, Ghouri ZK, Rohman N, Syed JA, Skelton A, Ahmed K. Unravelling pH/pKa influence on pH-responsive drug carriers: Insights from ibuprofen-silica interactions and comparative analysis with carbon nanotubes, sulfasalazine, and alendronate. Journal of Molecular Graphics and Modelling. 2024;128:108720.
204. Schmaljohann D. Thermo-and pH-responsive polymers in drug delivery. Advanced drug delivery reviews. 2006;58(15):1655–70.
205. Ge Z, Liu S. Functional block copolymer assemblies responsive to tumor and intracellular microenvironments for site-specific drug delivery and enhanced imaging performance. Chemical Society Reviews. 2013;42(17):7289–325.
206. Inamdar SN, Ahmed K, Rohman N, Skelton AA. Novel p K a/DFT-Based Theoretical Model for Predicting the Drug Loading and Release of a pH-Responsive Drug Delivery System. The Journal of Physical Chemistry C. 2018;122(23):12279–90.
207. Rizwan M, Yahya R, Hassan A, Yar M, Azzahari AD, Selvanathan V, et al. pH sensitive hydrogels in drug delivery: Brief history, properties, swelling, and release mechanism, material selection and applications. Polymers. 2017;9(4):137.
208. Aizik G, Choi W, Ostertag-Hill CA, Torre M, Kohane DS. Injectable Microparticle-Nanoliposome Hydrogel for Extended Release of Small Hydrophilic Molecules. ACS nano. 2025;19(41):36342–52.
209. Song X, Yang F, Ji R, Yang B, Lv Y, Wei Z. ROS-responsive polymeric micelles with aggregation-induced emission effects for drug delivery and cellular imaging. New Journal of Chemistry. 2024;48(12):5186–98.
210. Haladjova E, Rangelov S. Application of Polymeric Micelles for Drug and Gene Delivery. Pharmaceutics. 2024;16(5):646.
211. Delivery ND, Patkari K, Dwivedi J, Mahajan H. Indian Journal of Novel Drug Delivery ISSN 0975-5500.
212. Abbasnezhad N, Zirak N, Champmartin S, Shirinbayan M, Bakir F. An overview of in vitro drug release methods for drug-eluting stents. Polymers. 2022;14(13):2751.
213. Malehmir S, Esmaili MA, Khaksary Mahabady M, Sobhani-Nasab A, Atapour A, Ganjali MR, et al. A review: hemocompatibility of magnetic nanoparticles and their regenerative medicine, cancer therapy, drug delivery, and bioimaging applications. Frontiers in Chemistry. 2023;11:1249134.
214. Mishra K. Folate Receptor-Targeted Polymeric Micellar Nanocarriers as Drug Delivery Systems: The University of Akron; 2021.
215. Li Y, Gao S, Jiang H, Ayat N, Laney V, Nicolescu C, et al. Evaluation of physicochemical properties, pharmacokinetics, biodistribution, toxicity, and contrast-enhanced cancer MRI of a cancer-targeting contrast agent, MT218. Investigative Radiology. 2022;57(10):639–54.
216. Patra D, Basheer B, Shunmugam R. pH-responsive materials: properties, design, and applications. Stimuli-Responsive Materials for Biomedical Applications: ACS Publications; 2023. p. 145–79.
217. Aslam S, Rehman M, ud Din F. 6 Combination Therapies and Multi-Drug Delivery Systems. Electrospraying and Electrospinning in Drug Delivery.188.
218. González-González O, Ramirez IO, Ramirez BI, O'Connell P, Ballesteros MP, Torrado JJ, et al. Drug stability: ICH versus accelerated predictive stability studies. Pharmaceutics. 2022;14(11):2324.
219. Tewari AK, Upadhyay SC, Kumar M, Pathak K, Kaushik D, Verma R, et al. Insights on development aspects of polymeric nanocarriers: the translation from bench to clinic. Polymers. 2022;14(17):3545.
220. Dwivedi D, Lepková K. SAXS and SANS Techniques for Surfactant Characterization: Application in Corrosion Science. Application and Characterization of Surfactants. 2017.
221. Stetefeld J, McKenna SA, Patel TR. Dynamic light scattering: a practical guide and applications in biomedical sciences. Biophys Rev. 2016;8(4):409–27.